

8-1-2024

Effects of Climate Change on (Semi)-Arid Ecosystems in the Southwestern United States

Charlotte Van Der Nagel

Follow this and additional works at: <https://digitalscholarship.unlv.edu/thesesdissertations>



Part of the [Environmental Sciences Commons](#), [Geology Commons](#), [Hydrology Commons](#), and the [Terrestrial and Aquatic Ecology Commons](#)

Repository Citation

Van Der Nagel, Charlotte, "Effects of Climate Change on (Semi)-Arid Ecosystems in the Southwestern United States" (2024). *UNLV Theses, Dissertations, Professional Papers, and Capstones*. 5151. <https://digitalscholarship.unlv.edu/thesesdissertations/5151>

This Dissertation is protected by copyright and/or related rights. It has been brought to you by Digital Scholarship@UNLV with permission from the rights-holder(s). You are free to use this Dissertation in any way that is permitted by the copyright and related rights legislation that applies to your use. For other uses you need to obtain permission from the rights-holder(s) directly, unless additional rights are indicated by a Creative Commons license in the record and/or on the work itself.

This Dissertation has been accepted for inclusion in UNLV Theses, Dissertations, Professional Papers, and Capstones by an authorized administrator of Digital Scholarship@UNLV. For more information, please contact digitalscholarship@unlv.edu.

EFFECTS OF CLIMATE CHANGE ON (SEMI)-ARID ECOSYSTEMS IN THE
SOUTHWESTERN UNITED STATES

By

Charlotte van der Nagel

Bachelor of Science – Earth Science
Vrije Universiteit Amsterdam
2018

Master of Science – Hydrology
Vrije Universiteit Amsterdam
2020

A dissertation submitted in partial fulfillment
of the requirements for the

Doctor of Philosophy – Geoscience

Department of Geoscience
College of Sciences
The Graduate College

University of Nevada, Las Vegas
August 2024

June 13, 2024

This dissertation prepared by

Charlotte van der Nagel

entitled

Effects of Climate Change on (Semi)-Arid Ecosystems in the Southwestern United States

is approved in partial fulfillment of the requirements for the degree of

Doctor of Philosophy – Geoscience
Department of Geoscience

Henry Sun, Ph.D.
Examination Committee Chair

Michael Nicholl, Ph.D.
Examination Committee Member

Hannes Bauser, D.Sc
Examination Committee Member

Matthew Lachniet, Ph.D.
Examination Committee Member

Deena Hannoun, Ph.D.
Examination Committee Member

Dale Devitt, Ph.D.
Graduate College Faculty Representative

Alyssa Crittenden, Ph.D.
*Vice Provost for Graduate Education &
Dean of the Graduate College*

ABSTRACT

Climate change is considered amongst the most severe threats to terrestrial and aquatic ecosystems globally. Ecosystems in the southwestern United States have specifically been impacted by intense drought conditions since 2000. Higher temperatures combined with altered precipitation stresses many ecosystems; however, ecosystem specific responses to such stressors may vary. Here, the effects of climate change on semi-arid ecosystems are analyzed for some of the most vulnerable ecosystems in the southwestern United States: lacustrine, riparian, and dryland ecosystems.

Lakes and reservoirs in arid environments often serve as drinking water sources and recreational areas where high water quality is essential. Climate change may decrease water quality by shifting phytoplankton community structures to favor bloom forming and toxin producing species. In this chapter, I analyzed phytoplankton community compositions in Lake Mead, Nevada-Arizona, to detect trends in past communities and create predictive models for future communities. Results indicated stable community structures, apart from restricted shallow locations where temperature or phosphorus had increased. This study highlights the current buffering capacity of large, oligotrophic reservoirs to maintain stable phytoplankton communities even in the presence of environmental change, but also highlights potential rapid community shifts once this capacity is passed.

Riparian ecosystems are generally believed to be buffered from drought as many trees are phreatophytes with roots extending to groundwater. Recent observations of regional riparian woodland dieback and mortality suggest this ecosystem might be more vulnerable to climate change than previously believed. Understanding drivers of the mortality is important as riparian woodlands harvest high biodiversity, improve water quality, and aid in flood control. In this chapter, I studied riparian woodlands at sites in California, Nevada, Arizona, and New Mexico to construct a conceptual model explaining the timing, regionality, and local occurrences of mortality through a sequence of extreme hydrological events:

intensified drought and flooding. Drought can reduce shallow root activity, affecting the ability of riparian trees to deal with high groundwater levels during wet periods.

Dryland ecosystems cover approximately 40 percent of the Earth's surface and contain various vegetation patterns. Patterns may emerge prior to the ecosystem reaching its tipping point, after which rapid shift in ecosystem states occurs which can lead to desertification. It is therefore important to understand drivers of pattern formation. In this chapter, I studied soil moisture as driver of vegetation patterns created by the western harvester ant, *Pogonomyrmex occidentalis*. Patterns increased soil moisture inside the ant created vegetation pattern by reducing moisture lost through transpiration. The vegetation pattern can disappear following increases in aridity and ant colony mortality, which decreases plant and animal diversity, making the ecosystem more vulnerable to change.

ACKNOWLEDGEMENT

The research presented in this dissertation would not have been possible without the dedication, intellectual, emotional, and financial support of numerous individuals and organizations. First, I would like to thank my advisor Dr. Henry Sun for introducing me to the multi-disciplinary research conducted at the Desert Research Institute (DRI). I acknowledge the countless hours you spent helping your students improve as scientists and appreciate the opportunity you have provided me to grow professionally by allowing me to maintain my internship at SNWA throughout my Ph.D. You were an integral part even before I started my Ph.D. journey by facilitating me to visit DRI as a visiting scholar back in 2020. During this time, I was finishing up my master's degree from the Netherlands and conducted eco-hydrological research in Nevada as part of my thesis. Without the support of Dr. Sun, Jonathan (JJ) Smith (Bureau of Land Management (BLM), Las Vegas) and Boris Poff (BLM, Las Vegas), I would not have visited Las Vegas in 2020, and consequently would have never applied for a Ph.D. position at UNLV/DRI. So, thank you for replying to my email back in 2019; you have changed my life and future for the better.

Part of the research presented in this study would not have been possible without the intellectual and financial support of Dr. Deena Hannoun and Dr. Todd Tietjen from the Southern Nevada Water Authority (SNWA). Over the last two years, Dr. Deena Hannoun has stepped up as my unofficial Ph.D. advisor, aiding me in improving my statistical, coding, and numerical modeling skills. Thank you for always being available and going through the loops to obtain funding to cover my stipend and tuition. Not only did I obtain many important skills through this internship, Dr. Hannoun and Dr. Tietjen also introduced me to various professional organizations, encouraged me to attend and present at multiple conferences, and apply (successfully) for many scholarships. I am incredibly grateful for all the opportunities you have provided, and I am sure I would not have found such a good job without this experience.

This dissertation would not have been possible without the financial support of numerous organizations. I would like to thank Dr. Henry Sun and the BLM for providing my first semester of funding, and their efforts in trying to extend this funding. I would like to thank SNWA (Dr. Deena Hannoun, Dr. Todd Tietjen, and staff) for the effort you have taken to re-allocate a previously disbursed grant to cover my stipend and tuition in the second and third year of my Ph.D. I would like to thank DRI and its department's director Dr. Philippe Vidon for providing financial support to cover gaps in funding I encountered over the last three years. I would also like to thank various professional organizations for providing financial and professional support during my time at UNLV: Geological Society of Nevada, Nevada Water Reuse Association, California Lake Management Society, North American Lake Management Society, UNLV's College of Sciences, and particularly the Nevada Water Resources Association (NWRA) which has also facilitated to my personal and professional growth as student representative for Southern Nevada. I would furthermore like to thank UNLV's Graduate & Professional Student Association for funding travel grant applications to present my dissertation research at the National Water Quality Monitoring Conference in Virginia Beach, VA, and at the North American Lake Management Society's conference in Eerie, PA.

Lastly, I want to express my deepest appreciation of my friends and family, without whose love and support, this journey would have been impossible. Thank you to my parents, Ron and Cora van der Nagel, and my sister Sophie van der Nagel, for always being there for me, especially in the stressful period leading up to my departure to the United States. Thank you to my fiancée Zechariah Johnson; I could not have prayed for someone more understanding, supporting, and loving as a partner than you are. Last but not least; thank you Wookiee, for always being my best boy.

DEDICATION

To my parents, Ron and Cora van der Nagel, without whose unconditional love and support to my education, scientific curiosity, and wanderlust, none of this would have been possible. I love you.

TABLE OF CONTENTS

ABSTRACT.....	iii
ACKNOWLEDGEMENT	v
DEDICATION	vii
TABLE OF CONTENTS	viii
LIST OF TABLES	xii
LIST OF FIGURES	xiv
CHAPTER 1 - INTRODUCTION.....	1
CHAPTER 2 – LACUSTRINE ECOSYSTEMS.....	7
2.1 Abstract.....	7
2.2 Introduction.....	8
2.3 Material and methods.....	10
2.3.1 Study area.....	10
2.3.2 Data collection	12
2.3.2.1 Phytoplankton community structure and chlorophyll <i>a</i>	13
2.3.2.2 Water quality and hydrological data	13
2.3.3 Statistical analyses	14
2.3.3.1 Trend analysis.....	14
2.3.3.2 Variance and correlation analysis	15
2.3.3.3 Clustering	15
2.3.3.4 Machine learning.....	16
2.4. Results.....	17
2.4.1 Water quality parameters.....	17
2.4.2 Phytoplankton community structures and trends	20
2.4.2.1 Spatial variability of phytoplankton communities.....	20

2.4.3.2	Cluster analysis.....	21
2.4.3.3	Phytoplankton community structures and trends.....	23
2.4.4	Prediction of phytoplankton biovolume and major groups	25
2.5.	Discussion	28
2.5.1	Phytoplankton response to environmental stressors	28
2.5.2	Spatial variability in total phytoplankton biomass and community structure.....	29
2.5.3	Using machine learning to predict total and phytoplankton group biovolume.....	30
2.5.4	Broader implications.....	32
2.6.	Conclusion	33
2.7	References.....	34
2.8	Supplementary materials.....	41
CHAPTER 3 – RIPARIAN ECOSYSTEMS.....		60
3.1	Abstract.....	60
3.2	Introduction.....	61
3.3	Methods.....	62
3.3.1	Study location.....	62
3.3.2	Remote sensing	65
3.3.3	Statistical analyses	67
3.3.3.1	Trend analysis.....	67
3.3.3.2	Regression tree analysis	67
3.3.4	Topography and groundwater depth.....	69
3.3.5	Root distribution analysis.....	69
3.4	Results.....	70
3.4.1	Regionality and timing of riparian vegetation mortality	70
3.4.2	Climatic control.....	72
3.4.3	Groundwater fluctuations and topographic control on woodland mortality	76
3.4.4	Root distribution analysis.....	79
3.5	Discussion	81

3.5.1	Conceptual model.....	81
3.5.2	Timing die-off after a dry-wet cycle	83
3.5.3	Regionality of riparian woodland mortality	84
3.5.4	Topographic and human control on woodland mortality	84
3.5.5	Implications and broader impacts	85
3.6	Conclusion	86
3.7	References.....	88
3.8	Supplementary materials.....	94
CHAPTER 4 – DRYLAND ECOSYSTEMS		104
4.1	Abstract.....	104
4.2	Introduction.....	105
4.3	Methods.....	107
4.3.1	Study area.....	107
4.3.2	Field measurements.....	108
4.3.2.1	Soil texture.....	108
4.3.2.2	Soil moisture and temperature	109
4.3.2.3	Root area.....	110
4.3.3	Numerical simulations	110
4.3.4	Remote sensing	114
4.4	Results.....	115
4.4.1	Field measurements.....	115
4.4.1.1	Soil texture.....	115
4.4.1.2	Soil moisture and soil temperature	116
4.4.1.3	Root area.....	118
4.4.2	Numerical simulations	119
4.4.3	Remote sensing	123
4.5	Discussion	128
4.5.1	Threshold for vegetation gaps created by harvester ants	128
4.5.2.	Numerical modeling of moisture dynamics in ant circles.....	130

4.5.3	Soil temperature as alternative hypothesis for circle creation.....	132
4.5.4	Pattern persistence through vegetation change	133
4.5.5	Effects of threshold crossing and climate change	133
4.6	Conclusion	135
4.7	References.....	136
4.8	Supplementary materials.....	142
CHAPTER 5 - CONCLUSION		154
CURRICULUM VITAE		156

LIST OF TABLES

Table 2.1. Trend analysis of water quality parameters for Lake Mead monitoring stations.....	20
Table 2.2. Trends in total phytoplankton biovolume and cell abundance, and biovolume of Bacillariophyta, Chlorophyta, and Cyanophyta.	25
Table S2.1. Analysis of variance (ANOVA) for environmental and water quality parameters, showing the mean and standard deviation of all stations combined, along with the degrees of freedom (between groups, within groups) and the significance level.....	49
Table S2.2. Trends of biovolume of phytoplankton groups at various locations in Lake Mead using significance level of 0.05..	55
Table S2.3. Comparison of regression model performances to predict cyanobacteria biovolume.....	55
Table S2.4. Hyperparameters for each constructed model after optimization.....	56
Table S2.5. Model performance for all subsets of models trained with randomly selected input data and hyperparameters optimized.	56
Table S2.6. Predictor importance for each model constructed for cross-validation.	58
Table S3.1. Summary statistics and trend for NDVI of all study locations calculated for 1993-2023.....	96
Table S3.2. Drought and precipitation values associated with node 5 in the regression tree model, showing most years with large decreases in NDVI are accompanied by above average precipitation (110 mm).....	101
Table 4.1. Summary of meteorological data and soil hydraulic properties, listed in units as required by HYDRUS software.	113
Table 4.2. Spatial pattern analysis of active and abandoned circles.....	128
Table S4.1. Average grain size distribution for an ant circle and natural vegetation gap in annual and shrub dominated vegetation at the research site.....	143

Table S4.2. Gravimetric soil moisture during the growing season inside ant circles and natural vegetation gaps on shrub and annual dominated vegetation.	144
Table S4.3. Summary of meteorological data and vegetation and site-specific parameters, listed in units as required by HYDRUS software.	146
Table S4.4. Parameters for the Feddes water uptake reduction model and root distribution.	148

LIST OF FIGURES

Figure 2.1. Lake Mead, including inflows, outflows, basins, river arms, and sampling stations.....	12
Figure 2.2. Summary of water quality and hydrological parameters at Lake Mead monitoring locations. Lake elevation, Wash (LVW) and CR inflow are displayed as monthly averaged timeseries.	18
Figure 2.3. Spatial variation in biovolume of major phytoplankton groups calculated from 2012-2018. .	21
Figure 2.4. Cluster analysis of chlorophyll <i>a</i> concentrations. a , Optimal number of clusters, including cluster centroids. Each monitoring site is represented by a colored dot. b , Spatial distribution of clusters.	22
Figure 2.5. Phytoplankton community structures for each cluster, showing mean annual total biovolume (left) and relative biovolume of seven major phytoplankton groups (right), for a . cluster 1 (Las Vegas Wash confluence), b . cluster 2 (Inner Las Vegas Bay), and c . cluster 3 (Outer Las Vegas Bay).....	24
Figure 2.6. Overview of machine learning model results for a , chlorophyll <i>a</i> , b , total phytoplankton biovolume, c , diatom biovolume, d , green algae biovolume, and e , cyanobacteria biovolume.	27
Figure S2.1. Lake Mead with all inflows and outflows, basins, water quality sampling stations named according to inter-agency nomenclature, and SNWA’s drinking water intake shown.	41
Figure S2.2. Timeseries of Total Phosphorus (TP) for the different monitoring sites.....	42
Figure S2.3. Timeseries of Total Nitrogen (TN) for the different monitoring sites.	43
Figure S2.4. Chlorophyll- <i>a</i> (ChlA) timeseries for the different monitoring sites, showing highest values occur near the Wash inflow (Wash Confluence).	44
Figure S2.5. Secchi depth timeseries for the different monitoring sites, showing lowest values occur near inflows (Wash Confluence, CR below confluence, and upper Overton).	45
Figure S2.6. Temperature timeseries for the different monitoring sites.	46
Figure S2.7. Conductivity timeseries for the different monitoring sites, showing highest conductivity occurs near the Wash inflow (Wash Confluence).	47

Figure S2.8. pH timeseries for the different monitoring sites.....	48
Figure S2.9. Number of Secchi depth measurements collected during winter, spring, summer, and fall for the Middle Colorado River arm station.....	49
Figure S2.10. Seasonal Mann-Kendall trend test at monitoring site LW0.9 in the Las Vegas Wash for a. total phosphorus, showing a significant negative trend ($p = 1.01 \times 10^{-15}$) between 2003-2023 and b. total nitrogen showing a significant negative trend ($p = 3.98 \times 10^{-3}$) between 2013-2023.....	50
Figure S2.11. Spearman’s rank correlation analysis for water quality parameters of all monitoring stations in Lake Mead (* = $p < 0.05$, ** = $p < 0.01$).....	51
Figure S2.12. Mean annual biovolume of major phytoplankton groups for 9 monitoring stations in Lake Mead.....	52
Figure S2.13. Average biovolume of major phytoplankton groups in Lake Mead in summer (left) and winter (right) for a. Cluster 1, b. Cluster 2, and c. Cluster 3.....	53
Figure S2.14. Biovolume of genera constituting 90% of phytoplankton biovolume between 2012-2018 for a. diatoms, b. green algae, and c. cyanobacteria.....	54
Figure S2.15. Distributions for chlorophyll <i>a</i> , total biovolume, and biovolume of major phytoplankton groups at all monitoring stations.....	54
Figure 3.1. Study locations at Ash Meadows and Shoshone along the Amargosa River in California/Nevada, the Virgin River in Nevada, the Gila River in Arizona, and the Rio Grande in New Mexico.....	65
Figure 3.2. Annual average normalized NDVI during the growing season (Apr 1-Oct 31) for areas experiencing riparian woodland mortality along the Amargosa River in a. Ash Meadows, b. Shoshone, and c. Tecopa, and along the d. Virgin, and e. Muddy Rivers, compared to vegetation along the f. Gila River in New Mexico.....	72
Figure 3.3. Climatic variables in relation to the regional wide die-off event of screwbean mesquite, shown by the red shaded area. a. Average annual normalized NDVI for the growing season (Apr-Oct) in Shoshone (Sho 2 site), CA, showing rapid decrease in NDVI between 2010-2012. b. Monthly	

precipitation for Pahrump, CA, showing a peak in precipitation occurred right before the die-off event in December 2010. **c.** Average drought severity and coverage index for counties experiencing die-off (Clark, Inyo, and Nye counties), where 0 means none of the area is experiencing drought, and 500 means the entire area is in exceptional drought. 74

Figure 3.4. Regression tree showing classification of NDVI trends based on mean annual drought index and mean annual precipitation. 75

Figure 3.5. Monthly depth of water table and monthly precipitation in **a.** Ash Meadows, Amargosa River Basin from 1994-1998, and **b.** along the Virgin River near Littlefield, Arizona from 1990-1995. 77

Figure 3.6. Tamarisk-dominated riparian vegetation along the lower Virgin River showing a gradient in tree mortality when moving away from the river, Google Earth imagery 05/2013, **b.** Summer (Jun 1 – Aug 1) NDVI in 2013 compared to the 30-year average (1991-2020), where red indicated values lower than average, green higher than averages and white no change. **c.** Elevation transect showing die-off is limited to topographic lows, where flood water accumulates. 78

Figure 3.7. Root structure of three screwbean mesquite seedlings, grown on coarse sand with limited capillary rise on three different water table scenarios: 1) surface irrigation (left), 2) a constant water table at 40 cm depth (middle), and 3) a constant water table at 40 cm depth for 4 months, then a slowly receding water table to 60 cm depth (right). 80

Figure 3.8. Conceptual model of the relationship of the upper (near surface) and lower (near groundwater) root system of groundwater dependent vegetation on **a.** low and **b.** high water tables during a normal year, and on **c.** low and **d.** high water tables after a multi-year drought. 82

Figure S3.1. Monthly precipitation for **a.** Southern California (Tecopa, CA), with a winter-storm dominated climate, and **b.** New Mexico (Las Cruces), with a monsoon dominated climate. 94

Figure S3.2. Experimental setup to study the root distribution of three screwbean mesquite seedlings under different groundwater level scenarios. 95

Figure S3.3. Stacked bars of annual average normalized NDVI during the growing season (Apr 1-Oct 30) for all studied sites in regions experiencing woodland mortality in winter storm dominated climate

systems for riparian vegetation along the Amargosa River in **a.** Ash Meadows, **b.** Shoshone, and **c.** Tecopa, and along the **d.** Virgin, and **e.** Muddy Rivers, compared to vegetation sites along the **f.** Gila River in New Mexico..... 98

Figure S3.4. Annual average NDVI during the growing season (Apr 1-Oct 31) for areas experiencing riparian woodland mortality along the Amargosa River in **a.** Ash Meadows, **b.** Shoshone, and **c.** Tecopa, and along the **d.** Virgin, and **e.** Muddy Rivers, compared to vegetation along the **f.** Gila River in New Mexico.. 99

Figure S3.5. Climatic variables for a riparian woodland along the Gila River, AZ. **a.** Average annual normalized NDVI for the growing season (Apr-Oct). **b.** Monthly precipitation showing frequent peaks representing monsoonal precipitation, **c.** Drought severity and coverage index, where 0 means none of the area is experiencing drought, and 500 means the entire area is in exceptional drought, source = US drought monitor..... 100

Figure S3.6. Average annual NDVI during the growing season (Apr-Oct) for riparian woodlands in **a.** Ash Meadows, California, showing die-off between 2015-2017, and **b.** Lake Mohave, Nevada/Arizona, showing no signs of mortality between 2011-2012. 101

Figure S3.7. a. Mortality of riparian trees in the lower Virgin River showing patches of surviving trees near the river. **b.** Elevation transect showing die-off is focused in topographic lows, where flood water accumulates..... 102

Figure S3.8. Root structure of screwbean mesquite from a field excavation, showing lateral surface roots and a taproot splitting off and moving laterally. 103

Figure 4.1. a. Location of the field study site in Nevada, United States, **b.** Drone image showing the distribution of ant circles in both annual vegetation (light green) and sagebrush (dark green); the scale bar represents 40 m. **c.** Ant circle surrounded by sagebrush, including a central nest approximately 0.3m in height. 108

Figure 4.2. Gravimetric soil moisture from 0.1-0.2 m depth for ant circles and natural vegetation gaps in **a.** sagebrush dominated vegetation, and **b.** annual dominated vegetation. Error bars display standard deviation with $n = 3$ for August and October, and $n = 1$ for May. 116

Figure 4.3. Precipitation, air temperature, and daily TDR averages from 5/15/2019 to 7/10/2019. **a.** Daily precipitation from a weather station in Pioche, NV (Western Regional Climate Center, 2023c). **b.** Daily averaged soil temperature at 0.5 m depth inside the ant circle and under vegetation canopy near the circle (left axis) and air temperature (right axis) from a weather station in Pioche, NV (Western Regional Climate Center, 2023c). **c.** Daily averaged volumetric soil moisture at 0.5 m depth inside the ant circle and under vegetation canopy near the circle, with soil moisture significantly different in timeframes A and C ($p < 0.05$), and not significantly different in B (May 29 – June 08) ($p = 0.06$)..... 118

Figure 4.4. Distribution of root area per 1kg of soil from 0.2m depth in a natural vegetation gap and an ant circle..... 119

Figure 4.5. Model performance for simulating soil moisture **a.** inside an ant circle and **b.** on the vegetated circle margin at 0.5 m depth using HYDRUS 2D, from May 15, 2019 to July 10, 2019. 120

Figure 4.6. Simulated soil moisture levels through the growing season, showing faster moisture loss from vegetated areas and natural vegetation gaps compared to the ant circle. **a.** Day 83 (5/22/2019), **b.** Day 132 (7/10/2019), and **c.** day 214 (9/30/2019)..... 122

Figure 4.7. Daily averaged mass movement across system boundaries, showing high **a.** infiltration, **b.** evaporation, **c.** root water uptake (RWU), and **d.** drainage in spring and early summer, and sharp declines throughout the progression of summer..... 123

Figure 4.8. Example of distribution of ant circles linked to drainage features in the landscape (location = 38.69511, -116.0231), where a continuously vegetated area (left) is intersected by a drainage feature (right). Ant circle occurrence is closely related to the drainage feature, and **b.** generally occupies the lower parts of the landscape..... 124

Figure 4.9. a. Abandoned circle near the study site that still contains pebbles that used to make up the ant mound, currently occupied by kangaroo rats evident from multiple entry tunnels around the mound area and barren circle, b. circles revegetated with annuals, c. circles revegetated with shrubs..	126
Figure 4.10. Pair correlation function showing the spatial pattern of active ant circles (a-d) and abandoned circles (e-f), with peaks representing the most frequent distance between circles.	127
Figure 4.11. The effect of an ant circle on soil moisture and root density..	130
Figure S4.1. Average monthly temperature and precipitation at Pioche, NV (Western Regional Climate Center, 2023c).	142
Figure S4.2. Range of ant circle and barren areas of similar dimensions and shape as ant circles in the southwestern and western United States.	143
Figure S4.3. Model domain of a three-dimensional soil slice of 400*100*100 cm in xyz-dimensions with atmospheric boundary as upper boundary and free drainage as lower drainage.	145
Figure S4.4. Meteorological input data used for the HYDRUS model including precipitation, minimum and maximum temperature, wind speed, humidity, and radiation from March 1, 2019, to September 30, 2019, obtained from a weather station in Pioche, Nevada (Western Regional Climate Center, 2023c)...	147
Figure S4.5. Distribution of root water uptake (RWU) in the model domain, fit to match the root distribution of two plants.	149
Figure S4.6. Satellite view of ant circles in western Utah.	149
Figure S4.7. Precipitation and TDR readings from 5/15/2019 to 7/10/2019. a. Daily precipitation from a weather station in Pioche, NV (Western Regional Climate Center, 2023c). b. Soil temperature at 1m depth inside the ant circle and under vegetation on the circle margin, c. Volumetric soil moisture at 1m depth inside the ant circle and under vegetation on the circle margin.	150
Figure S4.8. Velocity vectors (water flow velocity) in the ant circle and natural vegetation gap for a. Day 83 (5/22/2019), b. Day 132 (7/10/2019), and c. day 214 (9/30/2019), showing largely reduced velocity vectors through the progression of summer and the growing season.	151

Figure S4.9. Distribution of ant circles through the western United States, showing the range in circle distribution from Arizona and New Mexico to Montana. 152

Figure S4.10. a. Example of distribution of ant circles linked to drainage features in the landscape, where a continuously vegetated area (left) is intersected by a drainage feature (right). Ant circle occurrence is closely related to the drainage feature, and **b.** generally occupies the lower parts of the landscape. 153

CHAPTER 1 - INTRODUCTION

Climate change is considered as one of the most severe threats to terrestrial and aquatic ecosystems globally (Rosenzweig et al., 2007; Ormerod et al., 2010; Li et al., 2018; Griffith and Gobler, 2020). While severe climatic changes have occurred in the past, for example during glacial-interglacial cycles, present climate change occurs at a much faster rate than most previous changes (Pörtner et al., 2022).

Climate change in the southwestern United States has rapidly intensified drought conditions. Since 2000, droughts have become hotter and drier, with the period of 2000-2022 classified as the driest period in 1,400 years, also referred to as a Megadrought (Cook et al., 2018; Williams et al., 2022; Alizadeh et al., 2023). Drought conditions are predicted to persist throughout the twenty-first century, with recent studies suggesting the region is moving to a drier climate (Overpeck and Udall, 2020; Wahl et al., 2022). The effects of climate change in the southwestern United States are visible everywhere; lakes and reservoirs are near their lowest elevations ever recorded (United States Bureau of Reclamation, 2023), snowpack volumes and river streamflow have drastically decreased (Harpold et al., 2012; Woodhouse et al., 2016; Bass et al., 2023), the intensity of droughts and wildfires has increased (Williams et al., 2019; Overpeck and Udall, 2020), and precipitation events have become more erratic, leading to more frequent flooding (Swain et al., 2018).

The effects of climate change span across many ecosystems found in the southwestern United States. Climate change affects ecosystems through for example temperature and precipitation changes (Malhi et al., 2020). Responses to such changes are often ecosystem dependent. Certain ecosystems are more resilient to environmental change and can return to their original state after disturbance (Li et al., 2018). Other ecosystems might already operate near their tipping point of rapid ecosystem change, such that a small change in environmental conditions can cause a rapid ecosystem shift (Van De Koppel and

Rietkerk, 2004; Rietkerk et al., 2004). It is therefore important to study the effects of climate change on (semi)-arid ecosystems using an ecosystem specific approach.

In this dissertation, I will study three ecosystems that are believed to be among the most sensitive to climate change: lacustrine, riparian, and dryland ecosystems (Rood et al., 2000; Reynolds et al., 2007; Adrian et al., 2009; Woolway et al., 2020; Williams et al., 2022).

Lakes and reservoirs in (semi)-arid regions often serve as important sources for drinking water and as recreational areas (Ding et al., 2014; Hannoun et al., 2021). Climate change can negatively impact water quality in such waterbodies if the phytoplankton community structure shifts to favor proliferation of bloom and toxin forming species (Rosenzweig et al., 2007; Ho et al., 2019). A growing need therefore exists to study and predict water quality and phytoplankton community changes in reservoirs in arid environments. In this chapter, I investigate 17 years of phytoplankton community structure data and chlorophyll *a* concentrations in Lake Mead combined with quantitative water quality data including nutrients, temperature, and water clarity to analyze effects of environmental change on phytoplankton communities. Additionally, I evaluate the use of machine learning for creating reliable models to predict total phytoplankton biovolume and community structures.

Riparian ecosystems typically cover only a small percentage of land surface yet harbor a disproportionately high biodiversity in arid environments (Stevens et al., 1977; Naiman et al., 1993), improve water quality (Naiman and Décamps, 1997), and aid in erosion and flood control (Simon and Collison, 2002; Thomas and Nisbet, 2007). Climate change can result in forest mortality, which is well documented for many non-riparian forests globally (Creeden et al., 2014; Hammond et al., 2022). However, recent observations of riparian woodland dieback and mortality at sites in Nevada and California suggest riparian woodlands might be more vulnerable to climate change than previously believed. In this chapter, I present a conceptual model to explain the occurrence of riparian woodland mortality by analyzing long-term trends in riparian woodland health combined with drought, precipitation, and topographic data.

Dryland ecosystems cover approximately 40% of the Earth's surface (Safriel et al., 2005), and are home to more than 2 billion people (Adeel et al., 2005). Vegetation patterns ranging from stripes to gaps and spots are a common phenomenon in dryland ecosystems. Previous research indicates vegetation patterns emerge prior to the ecosystem reaching its tipping point. Understanding drivers of pattern formation is therefore essential to predict ecosystem change. In this chapter, I study soil moisture as driver for a vegetation pattern created by the Western Harvester ant, *Pogonomyrmex occidentalis*, through field measurements, numerical simulations, and remote sensing. The vegetation pattern may disappear following increases in aridity and ant colony mortality. This can result in loss of plant and animal diversity, making the ecosystem more vulnerable to rapid state change.

Understanding how individual ecosystems respond to altered climatic conditions is essential for understanding future biological and ecological change, assisting management decisions, and aiding conservation efforts.

References

- Adeel, Z., Safriel, U., Niemeijer, D., and White, R., 2005, Ecosystems and human well-being: desertification synthesis: World Resources Institute (WRI).
- Adrian, R. et al., 2009, Lakes as sentinels of climate change: *Limnology and Oceanography*, v. 54, p. 2283–2297, doi:https://doi.org/10.4319/lo.2009.54.6_part_2.2283.
- Alizadeh, M.R., Adamowski, J., Nikoo, M.R., AghaKouchak, A., Dennison, P., and Sadegh, M., 2023, A century of observations reveals increasing likelihood of continental-scale compound dry-hot extremes: *Science Advances*, v. 6, p. eaaz4571, doi:10.1126/sciadv.aaz4571.
- Bass, B., Goldenson, N., Rahimi, S., and Hall, A., 2023, Aridification of Colorado River Basin's Snowpack Regions Has Driven Water Losses Despite Ameliorating Effects of Vegetation: *Water Resources Research*, v. 59, p. e2022WR033454, doi:<https://doi.org/10.1029/2022WR033454>.
- Cook, B.I., Mankin, J.S., and Anchukaitis, K.J., 2018, Climate Change and Drought: From Past to Future: *Current Climate Change Reports*, v. 4, p. 164–179, doi:10.1007/s40641-018-0093-2.
- Creeden, E.P., Hicke, J.A., and Buotte, P.C., 2014, Climate, weather, and recent mountain pine beetle outbreaks in the western United States: *Forest Ecology and Management*, v. 312, p. 239–251, doi:<https://doi.org/10.1016/j.foreco.2013.09.051>.
- Ding, L., Hannoun, I.A., List, E.J., and Tietjen, T., 2014, Development of a phosphorus budget for Lake Mead: *Lake and Reservoir Management*, v. 30, p. 143–156, doi:10.1080/10402381.2014.899656.
- Griffith, A.W., and Gobler, C.J., 2020, Harmful algal blooms: A climate change co-stressor in marine and freshwater ecosystems: *Harmful Algae*, v. 91, p. 101590, doi:<https://doi.org/10.1016/j.hal.2019.03.008>.
- Hammond, W.M., Williams, A.P., Abatzoglou, J.T., Adams, H.D., Klein, T., López, R., Sáenz-Romero, C., Hartmann, H., Breshears, D.D., and Allen, C.D., 2022, Global field observations of tree die-off reveal hotter-drought fingerprint for Earth's forests: *Nature Communications*, v. 13, p. 1761, doi:10.1038/s41467-022-29289-2.
- Hannoun, D., Tietjen, T., and Brooks, K., 2021, The potential effects of climate change and drawdown on a newly constructed drinking water intake: Study case in Las Vegas, NV, USA: *Water Util. J.*, v. 27, p. 1–13.
- Harpold, A., Brooks, P., Rajagopal, S., Heidbuchel, I., Jardine, A., and Stielstra, C., 2012, Changes in snowpack accumulation and ablation in the intermountain west: *Water Resources Research*, v. 48, doi:<https://doi.org/10.1029/2012WR011949>.
- Ho, J.C., Michalak, A.M., and Pahlevan, N., 2019, Widespread global increase in intense lake phytoplankton blooms since the 1980s: *Nature*, v. 574, p. 667–670, doi:10.1038/s41586-019-1648-7.

- Van De Koppel, J., and Rietkerk, M., 2004, Spatial Interactions and Resilience in Arid Ecosystems: *American Naturalist*, v. 163, p. 113–121, doi:10.1086/380571/ASSET/IMAGES/LARGE/FG4.JPEG.
- Li, D., Wu, S., Liu, L., Zhang, Y., and Li, S., 2018, Vulnerability of the global terrestrial ecosystems to climate change: *Global Change Biology*, v. 24, p. 4095–4106, doi:https://doi.org/10.1111/gcb.14327.
- Malhi, Y., Franklin, J., Seddon, N., Solan, M., Turner, M.G., Field, C.B., and Knowlton, N., 2020, Climate change and ecosystems: threats, opportunities and solutions: *Philosophical Transactions of the Royal Society B: Biological Sciences*, v. 375, p. 20190104, doi:10.1098/rstb.2019.0104.
- Naiman, R.J., and Décamps, H., 1997, The Ecology of Interfaces: Riparian Zones: *Annual Review of Ecology and Systematics*, v. 28, p. 621–658, doi:10.1146/annurev.ecolsys.28.1.621.
- Naiman, R.J., Decamps, H., and Pollock, M., 1993, The Role of Riparian Corridors in Maintaining Regional Biodiversity: *Ecological Applications*, v. 3, p. 209–212, doi:10.2307/1941822.
- Ormerod, S.J., Dobson, M., Hildrew, A.G., and Townsend, C.R., 2010, Multiple stressors in freshwater ecosystems: *Freshwater Biology*, v. 55, p. 1–4, doi:https://doi.org/10.1111/j.1365-2427.2009.02395.x.
- Overpeck, J., and Udall, B., 2020, Climate change and the aridification of North America: *Proceedings of the National Academy of Sciences*, v. 117, p. 202006323, doi:10.1073/pnas.2006323117.
- Pörtner, H.-O. et al., 2022, Climate Change 2022: Impacts, Adaptation and Vulnerability Working Group II Contribution to the Sixth Assessment Report of the Intergovernmental Panel on Climate Change:, doi:10.1017/9781009325844.
- Reynolds, J.F. et al., 2007, Global Desertification: Building a Science for Dryland Development: *Science*, v. 316, p. 847–851, doi:10.1126/science.1131634.
- Rietkerk, M., Dekker, S.C., de Ruiter, P.C., and van de Koppel, J., 2004, Self-Organized Patchiness and Catastrophic Shifts in Ecosystems: *Science*, v. 305, p. 1926–1929, doi:10.1126/science.1101867.
- Rood, S.B., Patiño, S., Coombs, K., and Tyree, M.T., 2000, Branch sacrifice: cavitation-associated drought adaptation of riparian cottonwoods: *Trees*, v. 14, p. 248–257, doi:10.1007/s004680050010.
- Rosenzweig, C., Casassa, G., Karoly, D.J., Imeson, A., Liu, C., Menzel, A., Rawlins, S., Root, T.L., Seguin, B., and Tryjanowski, P., 2007, Assessment of observed changes and responses in natural and managed systems, 79-131.
- Safriel, U., Adeel, Z., Niemeijer, D., Puigdefabregas, J., White, R., Lal, R., Winslow, M., Ziedler, J., Prince, S., and Archer, E., 2005, Dryland systems, *in* *Ecosystems and human well-being: current state and trends*, Island Press, p. 623–662.
- Simon, A., and Collison, A.J.C., 2002, Quantifying the mechanical and hydrologic effects of riparian vegetation on streambank stability: *Earth Surface Processes and Landforms*, v. 27, p. 527–546, doi:https://doi.org/10.1002/esp.325.

- Stevens, L.E., Brown, B.T., Simpson, J.M., and Johnson, R.R., 1977, The Importance of Riparian Habitat to Migrating Birds¹, *in* Importance, Preservation and Management of Riparian Habitat: A Symposium, Tucson, Arizona, Department of Agriculture, Forest Service, Rocky Mountain Forest and Range, v. 43, p. 156.
- Swain, D.L., Langenbrunner, B., Neelin, J.D., and Hall, A., 2018, Increasing precipitation volatility in twenty-first-century California: *Nature Climate Change*, v. 8, p. 427–433, doi:10.1038/s41558-018-0140-y.
- Thomas, H., and Nisbet, T., 2007, An Assessment of the Impact of Floodplain Woodland on Flood Flows: *Water and Environment Journal*, v. 21, p. 114–126, doi:10.1111/j.1747-6593.2006.00056.x.
- United States Bureau of Reclamation, 2023, Lake Mead at Hoover Dam, End of Month Elevation: <https://www.usbr.gov/lc/region/g4000/hourly/mead-elv.html>.
- Wahl, E.R., Zorita, E., Diaz, H.F., and Hoell, A., 2022, Southwestern United States drought of the 21st century presages drier conditions into the future: *Communications Earth & Environment*, v. 3, p. 202, doi:10.1038/s43247-022-00532-4.
- Williams, A.P., Abatzoglou, J.T., Gershunov, A., Guzman-Morales, J., Bishop, D.A., Balch, J.K., and Lettenmaier, D.P., 2019, Observed Impacts of Anthropogenic Climate Change on Wildfire in California: *Earth's Future*, v. 7, p. 892–910, doi:https://doi.org/10.1029/2019EF001210.
- Williams, A.P., Cook, B.I., and Smerdon, J.E., 2022a, Rapid intensification of the emerging southwestern North American megadrought in 2020–2021: *Nature Climate Change*, v. 12, p. 232–234, doi:10.1038/s41558-022-01290-z.
- Williams, J., Stella, J.C., Voelker, S.L., Lambert, A.M., Pelletier, L.M., Drake, J.E., Friedman, J.M., Roberts, D.A., and Singer, M.B., 2022b, Local groundwater decline exacerbates response of dryland riparian woodlands to climatic drought: *Global Change Biology*, v. 28, p. 6771–6788, doi:https://doi.org/10.1111/gcb.16376.
- Woodhouse, C.A., Pederson, G.T., Morino, K., McAfee, S.A., and McCabe, G.J., 2016, Increasing influence of air temperature on upper Colorado River streamflow: *Geophysical Research Letters*, v. 43, p. 2174–2181, doi:https://doi.org/10.1002/2015GL067613.
- Woolway, R.I., Kraemer, B.M., Lenters, J.D., Merchant, C.J., O'Reilly, C.M., and Sharma, S., 2020, Global lake responses to climate change: *Nature Reviews Earth & Environment*, v. 1, p. 388–403, doi:10.1038/s43017-020-0067-5.

CHAPTER 2 – LACUSTRINE ECOSYSTEMS

Stable phytoplankton community compositions in Lake Mead (Nevada-Arizona, USA) during two decades of severe drought

Prepared for submission to Ecosystem Science and Ecotechnology by

Charlotte van der Nagel, Deena Hannoun, and Todd Tietjen

2.1 Abstract

Water quality in Lake Mead, a large reservoir on the Colorado River that serves as a drinking water source in the southwestern United States, is generally high with low nutrient and chlorophyll-*a* concentrations. This is despite both the inflow of highly-treated wastewater since the 1960s and rapid water level decline since 2000 due to the combination of the ongoing Megadrought and basin-wide consumptive use. However, environmental change may shift phytoplankton communities. This can negatively impact water quality and the aquatic ecosystem if cyanobacteria abundance increases, potentially increasing bloom and toxin occurrences. Here, 17 years of phytoplankton community structure and chlorophyll *a* concentrations in Lake Mead were combined with quantitative water quality data including nutrients, temperature, and water clarity to analyze effects of environmental change on phytoplankton communities. Cyanobacteria abundance was hypothesized to have increased throughout the reservoir; however, results indicated stable community structures, apart from restricted shallow locations where temperature or phosphorus had increased. This study highlights the current buffering capacity of large, oligotrophic reservoirs to maintain stable phytoplankton communities even in the presence of environmental change, but also highlights potential community shifts once this capacity is passed. Machine learning models were evaluated for predicting changes in phytoplankton community

structures. Models predicted changes in total phytoplankton biovolume and chlorophyll *a* concentrations confidently within input parameter boundaries. However, prediction of peak biovolume contained large prediction uncertainty, stressing the need for including uncertainty analysis when communicating forecast results.

2.2 Introduction

Lake Mead is a large, meso-oligotrophic reservoir on the Colorado River in the southwestern United States. Maintaining high water quality is important as the reservoir functions as a drinking water source, recreational area, and anthropogenic ecological habitat home to the endangered razorback sucker (*Xyrauchen texanus*) (Hickey, 2010; Ding et al., 2014; Hannoun et al., 2021). Phytoplankton blooms can alter water quality by changing nutrient availability, releasing toxins, and depleting dissolved oxygen levels through microbial degradation upon bloom death (Elliott, 2012; Granéli & Turner, 2006; Hansson et al., 2007; Paerl et al., 2001). Large-scale blooms in Lake Mead are rare (Ding et al., 2014) and phytoplankton community structures remain stable inter-annually (Beaver et al., 2018). However, *Microcystis* spp. has been observed in Lake Mead, including a bloom of toxin-producing *M. aeruginosa* in 2015 (Beaver et al., 2018). Environmental changes can shift phytoplankton communities (De Senerpont Domis et al., 2007; Winder and Sommer, 2012), potentially decreasing water quality if proliferation of bloom forming and toxin producing species is favored.

Phytoplankton in Lake Mead may be affected by climate change, drought, and inflow of highly treated wastewater. Lake levels in Lake Mead have decreased rapidly since 2000 due to runoff decline in the Colorado River basin caused by reduced seasonal snowpacks (Heldmyer et al., 2023; Bass et al., 2023) and overallocation of water resources (Wheeler et al., 2022). Drought and climate warming increase water temperatures, prolong stratification, lengthen the growing season, and increase nutrient concentrations as dilution in hypolimnion decreases and mineralization from sediments increases (Zohary and Ostrovsky, 2011; Butcher et al., 2015; Mosley, 2015; Woolway et al., 2020, 2021). These changes

may shift the phytoplankton structure and increase total biomass. Increased water temperatures and nutrient concentrations have been linked to increased abundance of cyanobacteria, including toxin-producing species (Paerl and Huisman, 2008; O'Neil et al., 2012; Paerl and Otten, 2013). Population growth of the neighboring Las Vegas metropolitan area since the 1960s can also shift the phytoplankton composition by increasing nutrient concentrations through discharge of nutrient-rich highly treated wastewater into Lake Mead through the Las Vegas Wash (the Wash) (Holdren and Turner, 2010). Wash flow is predicted to further increase following future population growth (Hannoun and Tietjen, 2023). While daily loading limits have been maintained, increased Wash discharge introduces additional nutrients into Lake Mead and could shift the future phytoplankton structure.

Machine learning can aid in predicting changes in phytoplankton community structures. Machine learning has been used to predict chlorophyll *a* (Yajima and Derot, 2017; Zhang et al., 2021), total phytoplankton biomass (Liu et al., 2023), and individual phytoplankton groups (Rao et al., 2021; Liu et al., 2023) using environmental and water quality parameters such as temperature and nutrients. However, most models are based on one to two years of data, while evaluation of long-term phytoplankton community change requires long-term datasets (Zhi et al., 2021; Woelmer et al., 2022). Additionally, the seasonally and inter-annually varying nature of phytoplankton communities combined with the simplification of models can cause large model uncertainty (Niu et al., 2015), yet uncertainty quantification is absent from most published studies. Here, 17 years of phytoplankton community structures, environmental, and water quality data including water temperature, nutrients and Secchi depth are analyzed to evaluate 1) if drought has impacted water quality and the stability of the phytoplankton community structure in Lake Mead, 2) spatial variability in phytoplankton communities throughout the reservoir, and 3) the performance and uncertainty of machine learning models to predict phytoplankton based on three target variables: chlorophyll *a*, total phytoplankton biovolume and biovolume of major phytoplankton groups. Phytoplankton communities are hypothesized to vary significantly throughout the reservoir and to have shifted locally in response to water quality changes, for example near the nutrient-

rich Wash inflow. Phytoplankton is hypothesized to be best predicted using broad target variables such as chlorophyll *a* as opposed to more specific target variables such as phytoplankton groups.

2.3 Material and methods

2.3.1 Study area

Phytoplankton communities, hydrological, and water quality parameters were studied for Lake Mead, a reservoir impounded by the Hoover Dam on the Colorado River, along the border of Nevada and Arizona (Fig. 2.1). The reservoir currently operates at 32% capacity, at an elevation of 322m, 48 m down from its elevation in 2000 (U.S. Bureau of Reclamation, 2023, accessed July 26, 2023). Lake Mead consists of various interconnected basins and arms (Fig. 2.1). The Colorado River enters through the Colorado River Arm and travels west through Gregg and Temple Basins, towards Virgin Basin. The Virgin and Muddy Rivers enter through the Overton Arm and flow south to Virgin Basin. The Overton and Colorado River arm combine in Virgin Basin and flow west towards Boulder Basin, the most downstream located basin, east of Las Vegas.

The Colorado River flowing out of Grand Canyon constitutes 97% of inflow into Lake Mead (LaBounty and Burns, 2005); this water is limited in ortho-phosphorus and colder than the ambient lake temperature, causing it to enter the reservoir as an inter- or underflow (Holdren and Turner, 2010). 2-3% of inflow comes from the Wash, in Boulder Basin (Holdren and Turner, 2010); this water contains elevated levels of nutrients from treated wastewater effluent and serves as main bioavailable nutrient source for Lake Mead algal communities (Ding et al., 2014). Improved wastewater treatment processes since the early 2000s have significantly reduced phosphorus loading: by 2009, bioavailable phosphorus in the Las Vegas Bay and Boulder Basin were down to 2 µg/L, a reduction of 98% from 1970-1980 (Rosen et al., 2012). The remaining inflow into Lake Mead originates from the combined inflow of the Muddy and Virgin Rivers in the north (Fig. 2.1). Flow in these rivers is in part drainage from agriculture and

rangeland and characterized by slightly higher nutrients than ambient lake water (Holdren and Turner, 2010).

Phytoplankton community structure and quantitative water quality data were obtained from nine sampling sites throughout Lake Mead. Stations were named based on their geographical location regarding river arms and basins (Fig. 2.1; Fig. S2.1 for inter-agency names). The sampling site called Las Vegas Wash Confluence (Wash Confl.) is located at the Wash-Lake Mead confluence. The position of this site changes temporally following lake level decline. Sampling site Inner Las Vegas Bay (Inner Bay) is located 6.7 km from the original Wash inflow, but currently located almost at the same location as the Wash Confluence.

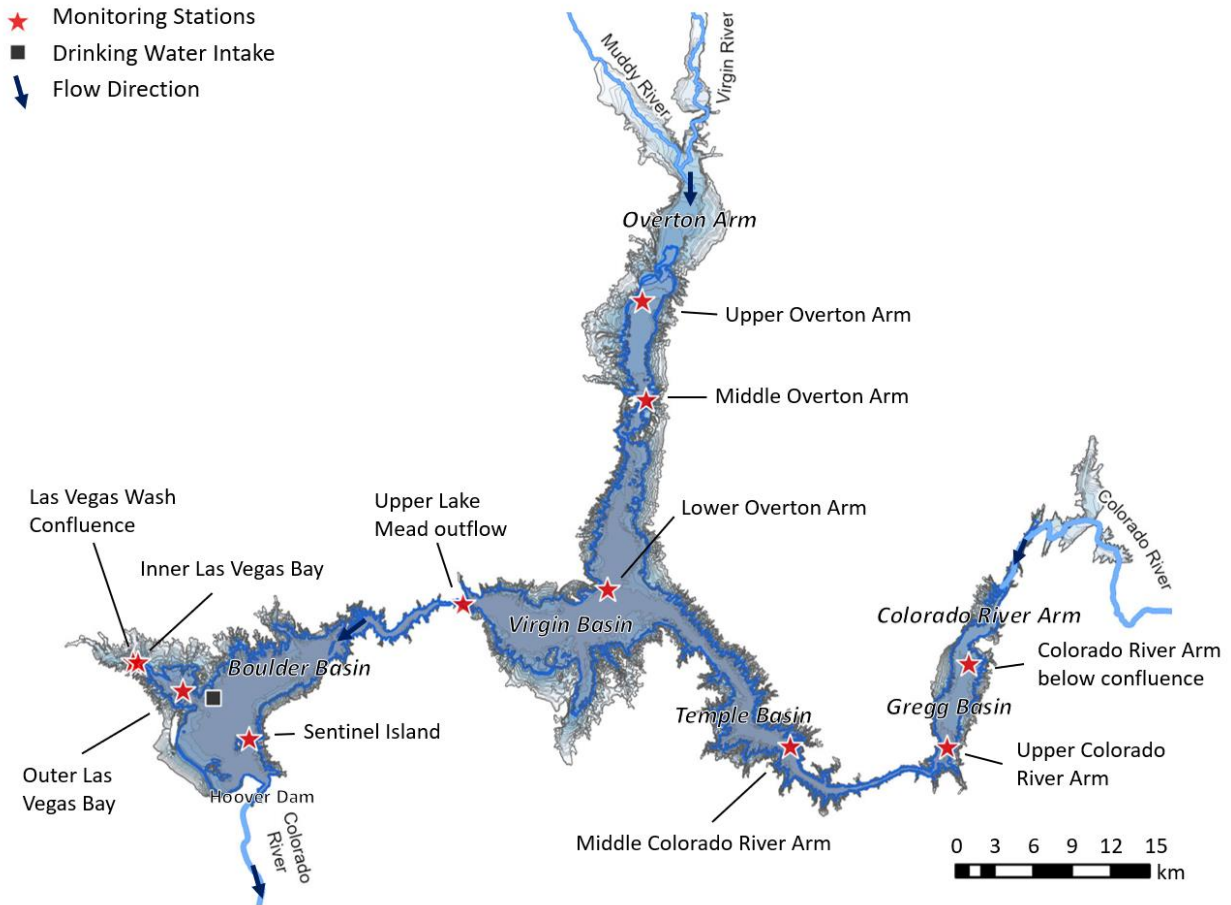


Figure 2.1. Lake Mead, including inflows, outflows, basins, river arms, and sampling stations. June 2023 lake level elevation is marked as dark blue contour line, previous lake elevations are shown as grey contour lines.

2.3.2 Data collection

Water samples were analyzed for total phytoplankton biovolume, community structure, and water quality parameters including temperature, total phosphorus (TP), total nitrogen (TN), Secchi depth, conductivity, and pH. Samples were collected biweekly for Boulder Basin sites and monthly for remaining monitoring stations. Water samples for phytoplankton analysis were collected by the Southern Nevada Water Authority (SNWA). Water quality samples were collected either by SNWA, the United

States Bureau of Reclamation, or the City of Las Vegas. Phytoplankton and water quality data were collected from 2002-2019 for Boulder Basin, and from 2012-2019 for remaining basins.

2.3.2.1 Phytoplankton community structure and chlorophyll *a*

Water samples for phytoplankton and chlorophyll *a* analysis were collected from an integrated sample from 0-6 m depth. Subsamples for biovolume analysis were preserved in a glutaraldehyde solution to final concentration of 0.25-0.5% upon collection and stored on ice. Triplicate permanent slide mounts were prepared by capturing algal cells on a membrane filter and mounting the filter in HPMA resin (Crumpton, 1987). All slides were analyzed for taxonomic identification and biovolume by Dr. Ann St. Amand (Phycotech Inc., St. Joseph, Michigan) using compound microscopes with appropriate magnification. A minimum of 400 natural units and 15 fields at 400x magnification were counted, until the standard error of the mean was below 10%. The average dimensions of phytoplankton cells were used to calculate the biovolume in mm³/L by approximating cell morphology by regular geometric shapes as described in Hillebrand et al. (1999).

Samples for chlorophyll *a* were filtered on a Whatman GF/C filter upon collection and stored on ice. Analysis was performed using a dual beam UV/VIS spectrophotometer according to U.S. EPA method 446.0 (Arar, 1997). Chlorophyll *a* was calculated as µg/L following the trichromatic equations of Jeffrey & Humphrey (1975).

2.3.2.2 Water quality and hydrological data

Water samples for TN and TP were collected as composite samples from 0-6 m using a flexible hose and stored on ice upon collection. Sample analysis was performed by the Clark County Water Reclamation District from 2000-2003, by Montgomery Watson Harza (MWH) Laboratories from 2003-2005, and by the Southern Nevada Water Authority after 2005. TN (mg/L) analysis was performed by pyrolysis and chemiluminescence detection using a total nitrogen analyzer (Shimadzu TNM-1) in a total organic carbon series (Shimadzu TOC-VCSH), according to the ASTM D5176 protocol. TP (mg/L) analysis was performed using the automated ascorbic acid method using a segmented flow analyzer (Seal

Analytical AA3), according to the standard method SM4500-P B for sample preparation and SM4500-P F for analysis. Detection limits for TN were 0.5 mg/L prior to May 2016, and 0.1 mg/L after May 2016. Detection limits for TP were 0.01 mg/L prior to November 2007, and 0.001 mg/L after November 2007. Values below the detection limit were calculated as the detection limit divided by the square root of two.

Profiles of water temperature ($^{\circ}\text{C}$), conductivity ($\mu\text{S}/\text{cm}$), and pH were measured using a multiparameter sonde (various manufacturers over the years) with accuracies of $\pm 0.1^{\circ}\text{C}$, $\pm 0.5\%$, and ± 0.1 for temperature, conductivity, and pH, respectively. Surface layer (0-5m) averages were used for the statistical analyses of this study. Water transparency was measured using Secchi disks (Wetzel and Likens, 2000).

Wash and Colorado River flow rates (m^3/s) were obtained from the United States Geological Survey (USGS) for 2002-2022. The Wash flow monitoring station (09419800) is located below Lake Las Vegas, near the confluence of the Wash into Lake Mead. The Colorado River flow monitoring station (09404200) is located near Peach Springs, Arizona. Daily lake elevation data were obtained from the U.S. Bureau of Reclamation.

2.3.3 Statistical analyses

2.3.3.1 Trend analysis

To test the hypothesis that phytoplankton biovolume and water quality parameters have significantly changed, I analyzed trends using the seasonal Mann-Kendall (MK) test. This test assesses for consistent upward or downward seasonal trends, with the overall trend calculated by summing each seasonal statistic (Hirsch et al., 1982). Magnitude of trends (Theil-Sen slopes) were calculated as the annual rate of change of each water quality parameter at every monitoring station. Trend tests were performed on phytoplankton and water quality data from 2005-2018 to avoid bias from higher nutrient loading into Boulder Basin prior to 2005. Analyses were performed in RStudio (v4.2.2; R Core Team,

2022) using the *kendallSeasonalTrendTest* function of the *EnvStats* package (v2.8.1; Millard, 2013) and a significance level of 0.05.

2.3.3.2 Variance and correlation analysis

To test the hypothesis that water quality varies between monitoring stations, I analyzed significant differences in water quality parameters using one-way analysis of variance (ANOVA). The analysis was carried out in MATLAB using the function *anova1*. Additionally, I evaluated the relationship between hydrodynamical and water quality parameters, using Spearman correlation analysis. This analysis tests correlation without making assumptions about parameter distributions (Spearman, 1961; Hauke and Kossowski, 2011). The analysis was carried out in RStudio using the function *cor* with method *spearman* with significance levels of 0.01 and 0.05.

2.3.3.3 Clustering

To test the hypothesis that phytoplankton varies spatially throughout Lake Mead, I used cluster analysis to evaluate how different monitoring stations can be grouped together. Chlorophyll *a* was used for clustering purposes instead of total biovolume as it provided consistent clustering results when comparing different clustering algorithms, whereas total biovolume caused erratic results when comparing clustering algorithms. Cluster analysis was performed using the k-means algorithm (Lloyd, 1982), using the average chlorophyll *a* concentration between 2005-2018 for each monitoring station. The optimal number of clusters was determined by calculating the Akaike Information Criterion (AIC) for each number of clusters possible (Eq. 2.1),

$$AIC = \sum \text{sumd}^2 + 2 i n \quad (\text{Equation 2.1})$$

where *sumd* is the observation-to-centroid distance, *i* is the number of clusters used, and *n* is the number of stations. The optimal number of clusters was characterized by the lowest AIC. Cluster analysis was

carried out using the *kmeans* function of the Statistics and Machine Learning Toolbox in MATLAB (v2022b; MathWorks, 2022).

2.3.3.4 Machine learning

To test the hypothesis that model performance for predicting phytoplankton varies depending on target variable, I constructed machine learning models for five different target variables. Models were constructed for chlorophyll *a*, total biovolume, and biovolume of diatoms (*Bacillariophyta*), green algae (*Chlorophyta*), and cyanobacteria (*Cyanophyta*), using the random forest (RF) algorithm, using the *Treebagger* function of the Statistics and Machine Learning Toolbox in MATLAB. This algorithm reduces overfitting by averaging outputs from multiple decision trees (Breiman, 2001). Models were constructed using water temperature, TP, Secchi depth, conductivity, and lake elevation as input variables. These variables were chosen because the initial four parameters most importantly influence phytoplankton growth in Lake Mead (Liebig, 1843; Ding et al., 2014), and lake elevation reflects drought conditions. Input and output data for all stations were aggregated to create a lake wide model. This data was normalized and divided into a training, testing, and validation dataset to minimize overfitting (Lever et al., 2016; Chicco, 2017). The training dataset contained 70% of data from 2002-2016; the validation dataset contained 30% of data from 2002-2016. The testing dataset consisted of all data from 2017-2018, to evaluate model prediction capabilities. The validation dataset was used to optimize RF algorithm hyperparameters: 1) number of trees grown, ranging from 1 to 5000, 2) minimum number of leaf node observations, ranging from 1 to 20, and 3) number of predictor variables for each decision split, ranging from 1 to 5. Hyperparameters were optimized by evaluating RF models with combinations of hyperparameter values to minimize model error using the Bayesian optimization function *bayesopt* of the Statistics and Machine Learning Toolbox in MATLAB. Sensitivity analysis was conducted by evaluating how the output variable of each model was affected by changes in input variables, yielding the relative importance of each input variable. This analysis was carried out on the training dataset. The testing dataset was used to evaluate model performance and uncertainty. Uncertainty analysis quantified

variability in model predictions by calculating response quantiles based on the distribution of the predicted outcome. Distributions are obtained by running input data through all trees in the RF. Uncertainty analysis was carried out using the *QuantilePredict* function of the Statistics and Machine Learning Toolbox in MATLAB and a 95% confidence interval (Meinshausen, 2006).

2.4. Results

In this study, I analyzed 17 years of phytoplankton community structures, environmental, and water quality data in Lake Mead. First, I calculated trends and differences in water quality parameters between monitoring stations. Second, I analyzed trends and spatial variability in the phytoplankton community structure throughout the reservoir. Last, I used machine learning to evaluate the performance and uncertainty of models constructed for predicting phytoplankton based on three target variables: chlorophyll *a*, total phytoplankton biovolume, and biovolume of major phytoplankton groups.

2.4.1 Water quality parameters

Hydrodynamical and water quality parameters differed significantly between monitoring stations in Lake Mead (Fig. 2.2, S2.2-8; Table S2.1). Sites near the Wash inflow (Wash Confl. and Inner Bay) showed highest TP and TN, with medians of 41.0 $\mu\text{g/L}$ TP and 3.6 mg/L TN for the Wash Confluence site while nutrient concentrations were low for remaining locations, with medians of 7.1 $\mu\text{g/L}$ TP and 0.73 mg/L TN. Chlorophyll *a* varied significantly throughout Lake Mead, with a median of 1.4 $\mu\text{g/L}$, and standard deviation of 7.2 $\mu\text{g/L}$ (min = 0 $\mu\text{g/L}$, max = 90.3 $\mu\text{g/L}$, n = 2921). Highest chlorophyll *a* occurred at the Wash Confluence, and rapidly decreased moving away from the confluence to Sentinel Island. Chlorophyll *a* was also elevated near the inflow of the Colorado River (CR blw confl.). Surface water temperature varied little throughout the reservoir, with slightly higher temperatures near the Wash inflow. Conductivity was highest at the Wash inflow, and lowest at the Colorado River inflow.

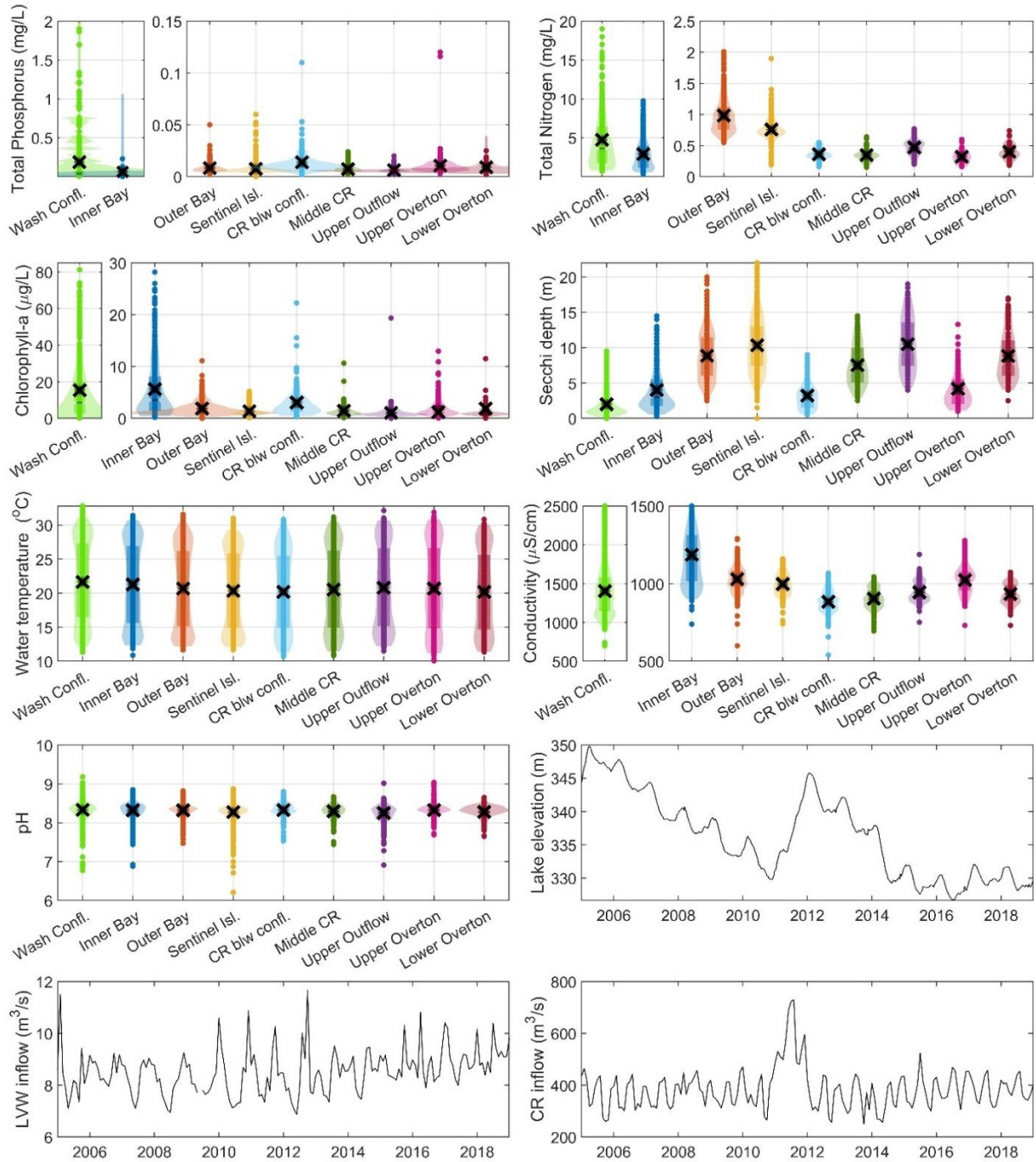


Figure 2.2. Summary of water quality and hydrological parameters at Lake Mead monitoring locations. Each violin plot displays data distribution (shaded area), mean (symbol x), interquartile range between the 25th and 75th data percentiles (box), and individual datapoints (dots or bold line if dots are close together). Lake elevation, Wash (LVW) and CR inflow are displayed as monthly averaged timeseries.

Trends in water quality and hydrological parameters were analyzed using seasonal Mann-Kendall tests (Table 2.1). Chlorophyll *a* significantly increased at all stations except the Upper Outflow and Lower Overton, and Secchi depth significantly decreased at all stations except the Wash Confluence. Conductivity significantly decreased in Lake Mead over the analyzed period, consistent with efforts to reduce salinity in the Colorado River Basin (Rumsey et al., 2021). Sample collection occurred most frequently in summer and fall, and least frequently in winter (Fig. S2.9). TP significantly increased for stations near inflows, including Inner Bay, CR blw. Confl., and Upper Overton. TN significantly increased for stations in the Las Vegas Bay. TP and TN for a monitoring station 1.4 km upstream from the original Wash confluence were also analyzed to compare to trends in the Las Vegas Bay; both TP and TN showed significant negative trends (Fig. S2.10).

Lake Mead elevation significantly decreased since the early 2000s ($p = 8.4 \times 10^{-14}$, seasonal MK test). During this time, Wash inflow volume significantly increased ($p = 1.2 \times 10^{-7}$, seasonal MK test), whereas Colorado River inflow showed no significant trend ($p = 0.90$, seasonal MK test). The only exception is 2012 when a large release of water from Lake Powell was made to address decreasing lake elevations in Lake Mead that threatened drinking water infrastructure.

Correlation analysis between water quality parameters showed moderate to high correlations between most water quality parameters (Fig. S2.11). Quagga mussels, *Dreissena bugensis*, measured as veliger counts, showed no significant correlations with chlorophyll *a* or Secchi depth.

Table 2.1. Trend analysis of water quality parameters for Lake Mead monitoring stations, including chlorophyll *a*, TP, TN, TN:TP, surface water temperature, conductivity, and Secchi depth.

Station	Chl- <i>a</i> (µg/L)	TP (µg/L)	TN (µg/L)	Water Temp (°C)	Conductivity (µS/cm)	Secchi depth (m)	pH
Wash confl.	0.2	0.9	74.5				-0.003
Inner Bay	0.26	1.2		0.1		-0.09	
Outer Bay	0.04				-12.2	-0.10	
Sentinel Isl.	0.01	-0.02	-11.1	0.06	-13.1	-0.06	-0.007
CR blw. confl.	0.07	0.5			-5.0	-0.22	-0.006
Middle CR arm	0.02				-5.4	-0.25	
Upper Outflow		-0.02			-6.9	-0.21	-0.005
Upper Overton	0.05	0.3			-4.9	-0.22	
Lower Overton		-0.05			-7.7	-0.15	

Note: a positive number represents a significant positive trend, and a negative number represents a significant negative trend at a significance level of 0.05. Blank means no significant trend was detected.

2.4.2 Phytoplankton community structures and trends

2.4.2.1 Spatial variability of phytoplankton communities

Total phytoplankton biovolume and community structure differed throughout Lake Mead. Median total phytoplankton biovolume was 0.19 mm³/L, with a standard deviation of 1.7 mm³/L (min = 0.0039 mm³/L, max = 33 mm³/L, n = 1517). Highest total biovolume occurred near the Wash inflow (Wash confl. and Inner Bay) with values an order of magnitude larger than remaining stations (Fig. S2.12). Summer and winter phytoplankton total biovolume differed significantly for all stations (Fig. S2.13). Community structures at each monitoring site were dominated by diatoms (primarily species of genera *Cyclotella*, *Synedra*, and *Anomoeoneis*), green algae (primarily species of genera *Pyramichlamys*, and *Spirogyra*), and cyanobacteria (primarily species of genera *Synechococcus*, *Microcystis* and family Chroococcaceae) (Figs. 2.3, S2.14), with positively skewed distributions (Fig. S2.15). Diatoms, green algae, and cyanobacteria represented on average 77% of total phytoplankton biovolume. The remaining members of the community consisted of dinoflagellates (*Pyrrophyta*), golden algae (*Chrysophyta*), cryptomonads

(*Cryptophyta*), and haptophytes (*Haptophyta*) which collectively represented 23% of the total biovolume. Cyanobacteria constituted a larger percentage of the phytoplankton community at stations further away from inflows (Fig. 2.3).

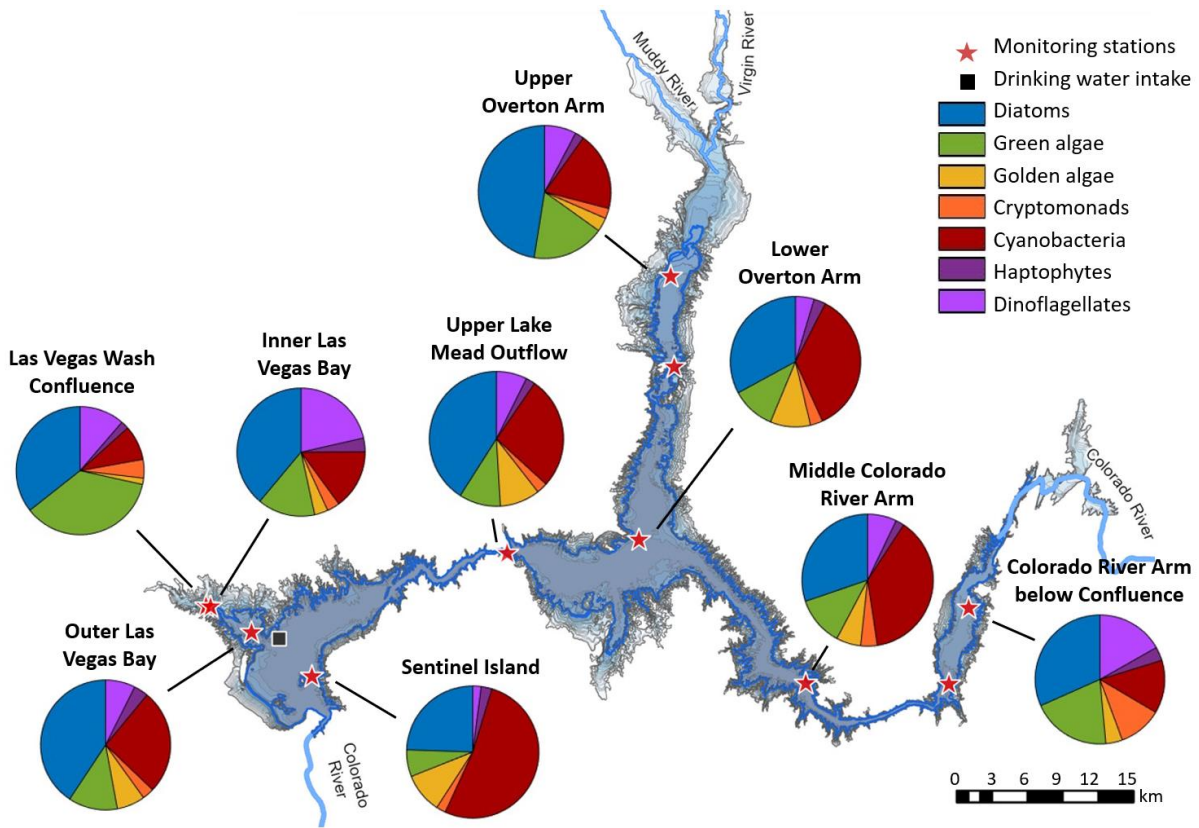


Figure 2.3. Spatial variation in biovolume of major phytoplankton groups calculated from 2012-2018.

2.4.3.2 Cluster analysis

Cluster analysis based on chlorophyll *a* indicated Lake Mead was optimally divided into three clusters, (Fig. 2.4). Cluster 1 contained sampling station Las Vegas Wash Confluence with median

chlorophyll *a* of 8.12 µg/L. Cluster 2 contained sampling station Inner Las Vegas Bay with median chlorophyll *a* of 3.67 µg/L. Cluster 3 contained all other sampling stations with median chlorophyll *a* of 1.25 µg/L. Station Outer Las Vegas Bay was located closest to the centroid of cluster 3 and used for further cluster specific analyses.

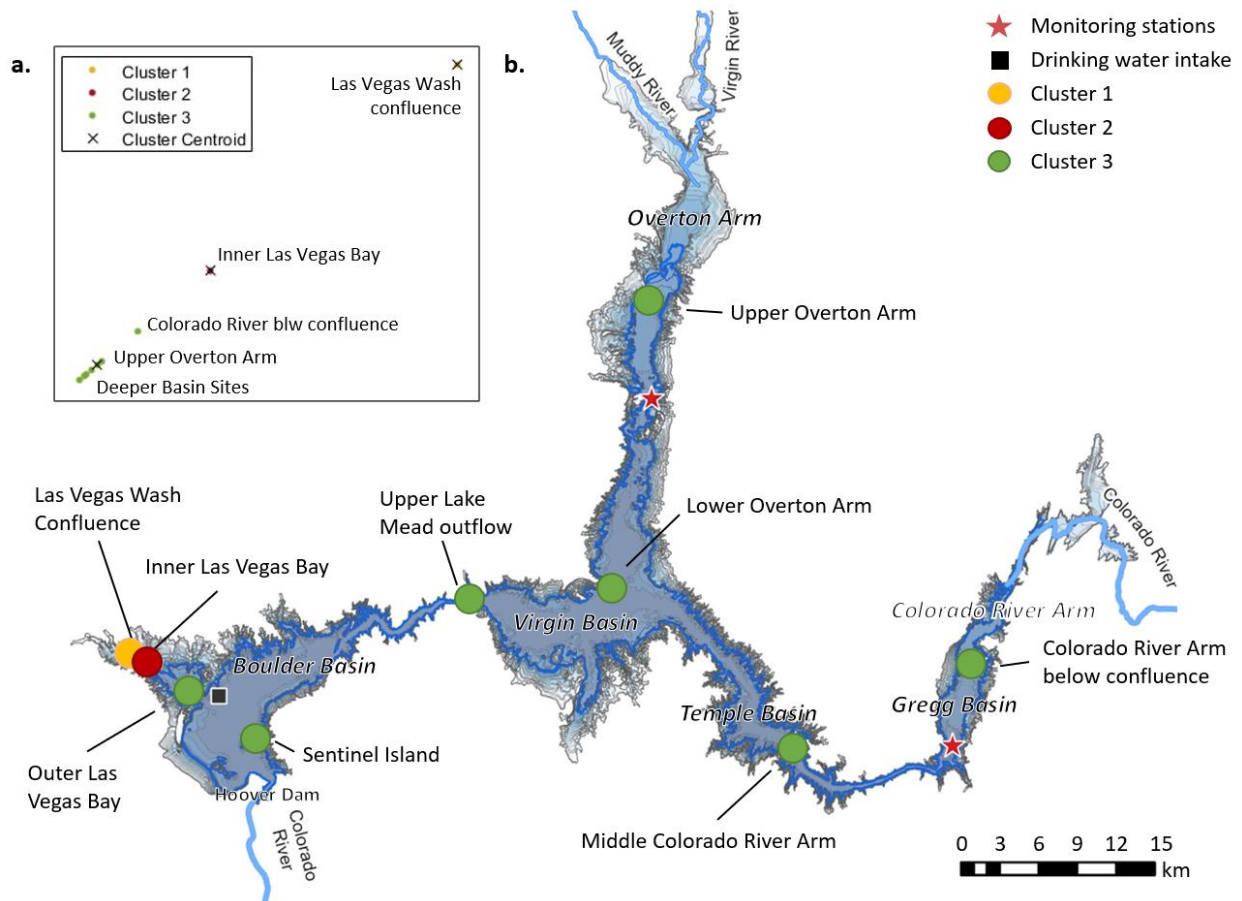


Figure 2.4. Cluster analysis of chlorophyll *a* concentrations. **a**, Optimal number of clusters, including cluster centroids. Each monitoring site is represented by a colored dot. **b**, Spatial distribution of clusters.

2.4.3.3 Phytoplankton community structures and trends

Total phytoplankton biovolume differed significantly between the three clusters identified through cluster analysis. Average annual total biovolumes were 2.2 mm³/L, 0.93 mm³/L, and 0.3 mm³/L for clusters 1, 2, and 3, respectively. Phytoplankton community structures also differed between clusters, with green algae and dinoflagellates constituting a larger portion of the total biovolume in cluster 1, and cyanobacteria constituting a larger portion of cluster 3 (Fig. 2.5). For example, cyanobacteria made up 6.6% of total phytoplankton biovolume in cluster 1, 13.3% in cluster 2, and 23.8% in cluster 3.

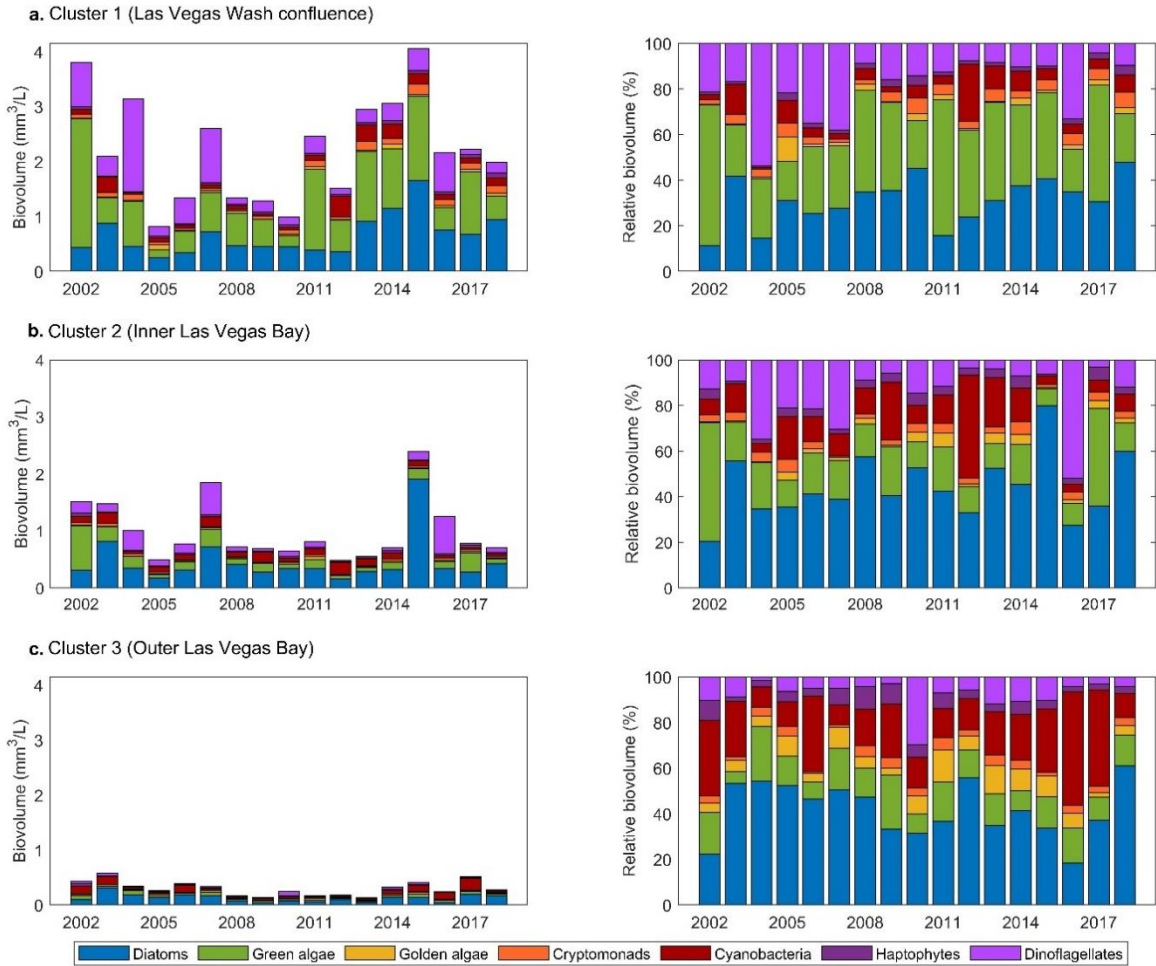


Figure 2.5. Phytoplankton community structures for each cluster, showing mean annual total biovolume (left) and relative biovolume of seven major phytoplankton groups (right), for **a.** cluster 1 (Las Vegas Wash confluence), **b.** cluster 2 (Inner Las Vegas Bay), and **c.** cluster 3 (Outer Las Vegas Bay).

Significant trends in total phytoplankton and group specific biovolume were absent from most monitoring sites, apart from the station closest to the Wash inflow (Wash confl.) where all trends were significantly positive (Table 2.2; Table S2.2). Other significant increasing trends occurred at shallow monitoring sites near river inflows, including Inner Bay, CR blw confl., and Upper Overton with depths of 16, 24, and 20m, respectively, as per June 2021. Significant changes were mostly absent in deeper parts

of the reservoir, including Outer Bay, Sentinel Isl., Upper outflow, and Lower Overton with depths of 66, 105, 93, and 80m, respectively, as per June 2021.

Table 2.2. Trends in total phytoplankton biovolume and cell abundance, and biovolume of Bacillariophyta, Chlorophyta, and Cyanophyta.

Station	Cluster	Diatoms	Green algae	Cyanobacteria	Total biovolume
Wash confl.	1	0.019	6.23×10^{-3}	1.50×10^{-3}	0.053
Inner Bay	2	2.27×10^{-3}			
Outer Bay	3				
Sentinel Isl.	3	-5.67×10^{-4}	-1.58×10^{-4}	-3.54×10^{-4}	-2.02×10^{-3}
CR blw. confl.	3			1.43×10^{-3}	
Middle CR arm	3				
Upper Outflow	3				
Upper Overton	3		2.73×10^{-3}		
Lower Overton	3				

Note: a positive number represents a significant positive trend, and a negative number represents a significant negative trend at a significance level of 0.05. Blank means no significant trend was detected.

2.4.4 Prediction of phytoplankton biovolume and major groups

Machine learning models were constructed to evaluate model performance and predict lake-wide chlorophyll *a*, total phytoplankton biovolume, and biovolume of diatoms, green algae, and cyanobacteria (Fig. 2.6). The RF algorithm was used for model construction due to superior training and testing R-squared values compared to other algorithms, although p-values for all models were found to be below the machine's epsilon (Table S2.3). Hyperparameters were fitted to reduce model error (Table S2.4) for cross-validated models with highest testing R-squared (Table S2.5). Models for chlorophyll *a* and total biovolume performed well for testing and training datasets, with the chlorophyll *a* model performing slightly better than the total biovolume model, with testing R-squared scores of 0.78 and 0.72,

respectively. Performance for group specific biovolume models was lower, with testing R-squared scores between 0.5-0.6. All models were most sensitive to changes in temperature (Fig. 2.6, middle graphs, Table S2.6).

Uncertainty analysis was used to evaluate model prediction uncertainty in models constructed with different target variables (Fig. 2.6). The chlorophyll *a* model was associated with lowest prediction uncertainty. Mean predicted chlorophyll *a* was 2.4 $\mu\text{g/L}$, with mean upper uncertainty of 6 $\mu\text{g/L}$ and lower uncertainty of 0.7 $\mu\text{g/L}$. Models for total and group specific biovolume contained higher uncertainty, with up to 2 orders of magnitude between upper and lower bounds of the 95% confidence intervals (Fig. 2.6b-e). For example, mean predicted total biovolume was 0.24 mm^3/L , with mean upper uncertainty of 1.6 mm^3/L and mean lower uncertainty of 0.041 mm^3/L . Largest uncertainty occurred in models for diatoms, green algae, and cyanobacteria biovolume.

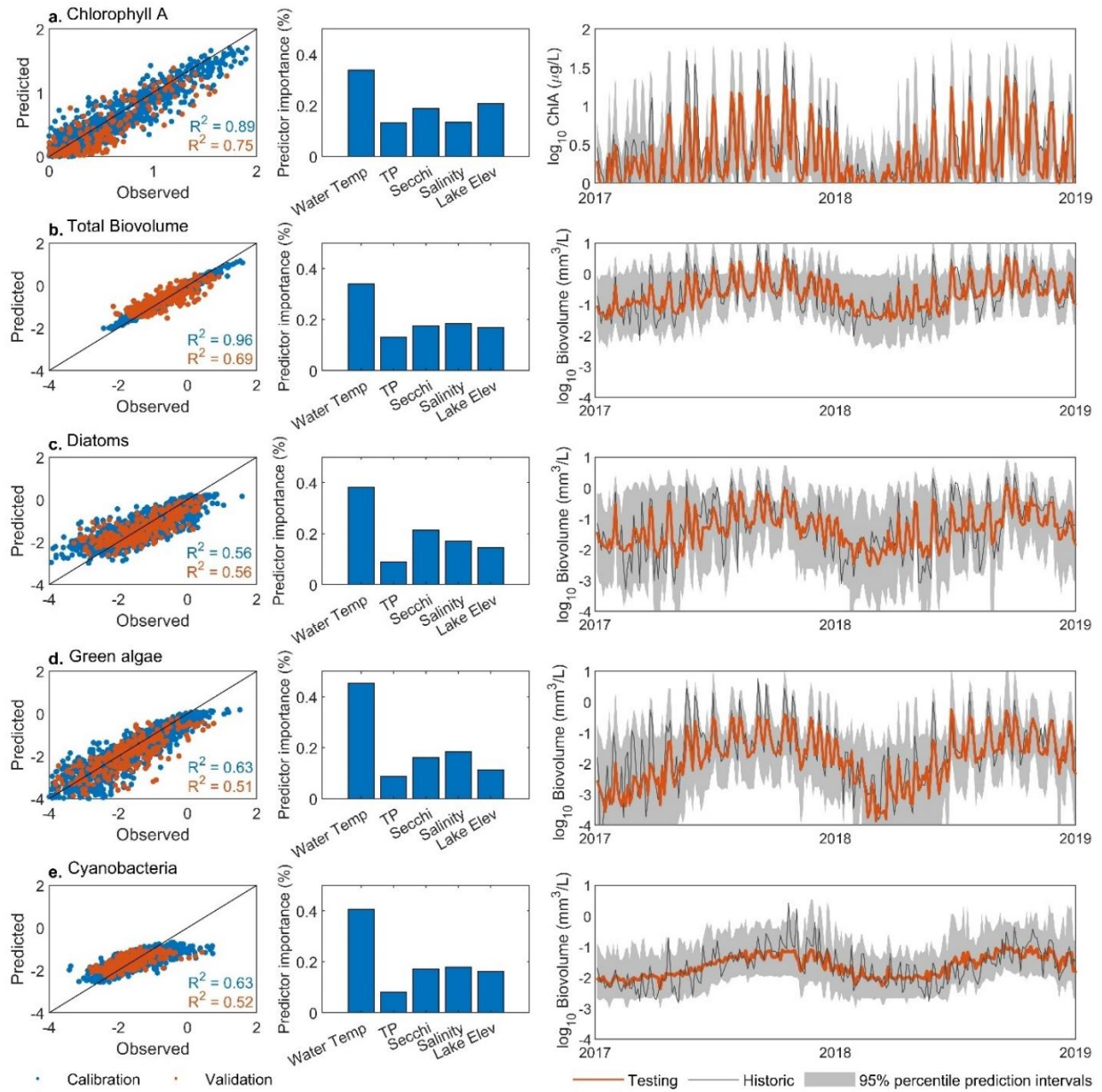


Figure 2.6. Overview of machine learning model results for **a**, chlorophyll *a*, **b**, total phytoplankton biovolume, **c**, diatom biovolume, **d**, green algae biovolume, and **e**, cyanobacteria biovolume. Model performance is shown for training and testing datasets (left). Predictor importance is shown for each input parameter (middle). Timeseries of the testing dataset are shown including the 95% prediction intervals (right) on a logarithmic scale.

2.5. Discussion

2.5.1 Phytoplankton response to environmental stressors

Phytoplankton community structures in Lake Mead remained largely stable despite rapid lake elevation decline and increased Wash inflow. Biovolume of major phytoplankton groups significantly increased only in shallow areas of the reservoir (Table 2.2), where water temperature or nutrient concentrations had significantly increased (Table 2.1). TP significantly increased at monitoring sites near river inflows. Lake level decline can facilitate sediment resuspension and release of sediment phosphorus, as shown for upstream Lake Powell (Wildman Jr. and Hering, 2011). However, nutrient trends could also be influenced by lake elevation decline. For example, as lake levels decline, the Wash confluence moves closer hydrologically to downstream stations. The Wash is currently located 6 km downstream from its original location, close to the Inner Bay station (Fig. 2.1). This decreases dilution rates, causing a positive trend in nutrient concentrations at the Inner Bay station. However, this trend is inconsistent with a monitoring station upstream from the Wash confluence (Fig. S2.10) and a previous study that found decreasing TP trends upstream from the Wash (Hannoun and Tietjen, 2023). Additionally, trends can be affected by seasonal irregularities in sample collection (Fig. S9). For the Middle Colorado River arm station, samples were least frequently collected in winter, when for example deepest Secchi depths occur. The large decline in Secchi depth (-0.25 m/year) at this station could therefore partly be an artifact of inconsistent sampling biased to periods of low water clarity, in addition to slightly increasing chlorophyll *a* (0.02 µg/L/year).

The overall lack of trends in phytoplankton biovolume throughout Lake Mead is attributable to its large volume and inflow of high-quality water. About 97% of water is supplied by cold, hypolimnetic Colorado River water released from Lake Powell (Wright et al., 2009; Hannoun and Tietjen, 2022). As the dominant inflow, a change in Colorado River water quality will largely affect Lake Mead. Climate change can affect water quality of the Colorado River inflow. As lake elevations in Lake Powell drop, warmer epilimnetic water is released into the Colorado River towards Lake Mead (Hannoun and Tietjen, 2022;

Wang et al., 2022; Scholl et al., 2024). Additionally, warmer winters increase the mixing temperature of Lake Powell, releasing slightly warmer water from the hypolimnion at higher surface elevations. Increased Colorado River temperatures may shift the phytoplankton structure to taxa with higher optimal temperatures, such as cyanobacteria (Paerl & Huisman, 2008). However, phytoplankton growth is generally restrained by nutrient limitation (Elliott et al., 2006). Therefore, increases in phytoplankton biovolume due to temperature increases are expected to be limited to nutrient-rich areas such as the Wash inflow, consistent with Brookes and Carey (2011) who suggested nutrient limited systems will not respond to water temperature increases without nutrient increases.

2.5.2 Spatial variability in total phytoplankton biomass and community structure

Spatial variability of total phytoplankton biovolume in Lake Mead was most affected by proximity to nutrient providing inflows to the otherwise meso-oligotrophic reservoir. Highest total biovolume occurred near the Wash, the major bioavailable nutrient source of the reservoir. Effects of nutrient-rich inflow were localized as phytoplankton rapidly take up bioavailable nutrients and concentrations are reduced by dilution (LaBounty and Burns, 2005). Total phytoplankton biovolume declined significantly moving away from the Wash from 2.2 mm³/L at the confluence (cluster 1) to 0.3 mm³/L the Outer Las Vegas Bay (cluster 3), an 86% reduction in approximately 4km. This encompasses the zone of transition, moving from the nutrient-rich riverine inflow to the nutrient-limited lacustrine zone (Thornton et al., 1981). Total biovolume was also elevated near the Muddy, Virgin and Colorado Rivers inflows (Fig. S2.12). The effects were more subtle compared to the Wash inflow, as available nutrients were lower (Fig. 2.2) and the monitoring stations (Upper Overton and CR blw confl.) were located 6-9km from the confluences (Fig. 2.1).

Phytoplankton at the Wash confluence differed from other stations. Based on relative biovolume, cyanobacteria constituted a larger percentage of community structure in stations away from the Wash, contrary to most studies that indicate cyanobacteria are most competitive under enhanced temperature and

eutrophic conditions, as characteristic to the Wash (Duarte et al., 1992; Paerl et al., 2001; Wiedner et al., 2007; Paerl and Otten, 2013). However, other Wash characteristics could have deterred cyanobacteria dominance. First, Wash flow rate combined with wind action can generate turbulent mixing, which favors larger cells such as diatoms and green algae (Barton et al., 2014; Zhou et al., 2015). Second, differences in salinity can affect phytoplankton communities. Various studies have shown certain species of cyanobacteria, such as *Microcystis*, have low tolerance for salinity (Paerl et al., 2001; Robson and Hamilton, 2003; Taş et al., 2006; Haakonsson et al., 2020). Conductivity near the Wash inflow is higher than the ambient Lake Mead conductivity, 2,400 $\mu\text{S}/\text{cm}$ compared to 1,000 $\mu\text{S}/\text{cm}$, respectively, indicating higher salinity (LaBounty and Horn, 1997), which could alter cyanobacteria abundance. Third, while cyanobacteria are known to thrive in eutrophic conditions, certain taxa are adapted to thrive in oligotrophic systems as they can regulate their buoyancy to access deeper, nutrient-rich waters (Walsby, 1994), have a high affinity to access and store phosphorus (Reynolds, 2006), can fix nitrogen (Oliver and Ganf, 2000) and can resist grazing (Vanni and Temte, 1990). Zooplankton grazing and dynamics between phytoplankton taxa can significantly affect the phytoplankton community composition between clusters (Tilman et al., 1982; Bergquist et al., 1985). A previous study identified the zooplankton community in Lake Mead was dominated by *Daphnia* spp. (*Daphnia pulex* complex and *Daphnia galeata mendotae*) with highest biomass occurring near the Wash inflow (Beaver et al., 2018); however, these variables were not evaluated in the current study.

2.5.3 Using machine learning to predict total and phytoplankton group biovolume

Machine learning can aid in predicting phytoplankton structures, yet the applicability of a machine learning model depends on its capability to make accurate predictions. Models for chlorophyll *a* and total phytoplankton biovolume showed best performance metrics (Fig. 2.6), with R-squared values comparable to machine learning models reviewed in Roussio et al. (2020). Models constructed for biovolume of specific phytoplankton groups were based on less data and performed poorer than the total

biovolume model. Model performance was improved by limiting the number of input parameters and correlated parameters to prevent model convolution (Mutshinda et al., 2013; Liu et al., 2023). However, correlation was not fully prevented as all water quality parameters displayed some degree of correlation (Fig. S10), typical for many water quality parameters (e.g., Zhang et al., 2021). As such, it was impossible to completely prevent correlation between input variables.

Uncertainty analysis showed model uncertainty increased when predicting broad target variables such as chlorophyll *a* to more specific target variables such as biovolume of major phytoplankton groups. Large model uncertainty could have been caused by the nature of environmental monitoring programs, making it particularly hard to sample biovolume peaks and troughs. Total phytoplankton biovolume can vary greatly on short timescales, even during non-bloom conditions (Reynolds, 2006; Yajima and Derot, 2017), in response to changes in nutrients, temperature, and storms (Kalin et al., 2001; Yajima and Derot, 2017; Díaz-Torres et al., 2021; Liu et al., 2021). However, water quality monitoring programs tend to collect data on a weekly to monthly basis, with data in Lake Mead collected bi-weekly to monthly. This decreased the chance of sampling phytoplankton peaks and troughs, which are thus underrepresented in the data and increase uncertainty. Group specific biovolume also varied significantly between monitoring stations (e.g., green algae biovolume in cluster 1 compared to cluster 3, Fig. 2.5), which can increase uncertainty when training lake-wide models. Additionally, the models were simplified by only considering a select number of abiotic factors, whereas phytoplankton assemblages are also strongly impacted by biotic factors such as zooplankton grazing and interactions between phytoplankton taxa. In fact, zooplankton grazing has been identified as the most important factor for causing model uncertainty when predicting marine phytoplankton (Rohr et al., 2023), and is expected to also contribute to observed uncertainty in this study. As the models remain simplified representations of real-world conditions and contain highly variable data such as phytoplankton biovolume, uncertainty analysis should be included to show prediction intervals to communicate model uncertainty.

2.5.4 Broader implications

Many lakes and reservoirs in the southwestern United States have experienced rapid volume loss due to prolonged drought conditions since 2000 (Wahl et al., 2022). These waterbodies often serve as drinking water sources, recreational areas, and ecological habitats where water quality can be negatively impacted by changes in phytoplankton biomass and composition. For example, phytoplankton can negatively impact drinking water quality and treatment processes by clogging up filters (Palmer, 1959), increasing the formation of disinfection byproducts (Fang et al., 2010), and increasing overall water treatment costs (Dunlap et al., 2015). Additionally, phytoplankton community shift to increased cyanobacteria dominance can negatively affect aquatic life: cyanobacteria can have an allelopathic effect on the growth of their competitors (Suikkanen et al., 2004), are of low edibility to zooplankton (Porter, 1977), and can produce toxins in quantities toxic to mammals, including humans, during blooms (Carmichael, 2001).

Phytoplankton in large, oligotrophic reservoirs are expected to show a similar lack of temporal trends as Lake Mead, unless they are accompanied by increased nutrient loading. However, changes in future water management can alter water levels which can affect hydrological and water quality parameters, as shown for the Colorado River Basin (Bruckerhoff et al., 2022). Machine learning can be used as a tool for predicting chlorophyll *a* concentrations and total phytoplankton biovolume. As machine learning models are based on a few easily attainable water quality parameters, such as water temperature and nutrients, they are easy to use and can be used to study phytoplankton response to changes in hydrologic and water quality parameters. For example, the effect of temperature change on phytoplankton could be simulated by increasing the temperature input parameter and analyzing changes in model outputs. This study presented a reproducible workflow for model setup and prediction uncertainty analysis.

2.6. Conclusion

Drought, climate change, and eutrophication can affect total phytoplankton biovolume and shift species compositions in lakes and reservoirs. Besides rapid water level decline and inflow of highly-treated wastewater, the phytoplankton community in a large, meso-oligotrophic reservoir has not significantly changed. This finding highlights the buffering capacity of large, oligotrophic reservoirs to maintain stable water quality and phytoplankton communities. However, changes in phytoplankton biovolume and community structure can occur once this buffering capacity is passed. This was most noticeable in shallow areas near river inflows where water temperature or TP had increased, although lake level decline and encroaching river confluences affecting dilution rates needed to be accounted for. Predicting future phytoplankton biomass in areas identified prone to phytoplankton change is important to understand potential water quality changes. Machine learning proved to be a robust tool for predicting chlorophyll *a* concentrations and total phytoplankton biovolume. Regardless of the constructed model, prediction uncertainty was high, owing to the highly erratic nature of phytoplankton, infrequent (bi-weekly to monthly) sampling, and simplification of the model; this study therefore provided a framework to include uncertainty analysis when communicating prediction results.

2.7 References

- Arar, E.J., 1997, In Vitro Determination of Chlorophylls a, b, c1 + c2 and Pheopigments in Marine And Freshwater Algae by Visible Spectrophotometry (Method 446.0): Ohio: National Exposure Research Laboratory, Office of Research and Development, US Environmental Protection Agency Cincinnati.
- Barton, A.D., Ward, B.A., Williams, R.G., and Follows, M.J., 2014, The impact of fine-scale turbulence on phytoplankton community structure: *Limnology and Oceanography: Fluids and Environments*, v. 4, p. 34–49, doi:<https://doi.org/10.1215/21573689-2651533>.
- Bass, B., Goldenson, N., Rahimi, S., and Hall, A., 2023, Aridification of Colorado River Basin's Snowpack Regions Has Driven Water Losses Despite Ameliorating Effects of Vegetation: *Water Resources Research*, v. 59, p. e2022WR033454, doi:<https://doi.org/10.1029/2022WR033454>.
- Beaver, J.R., Kirsch, J.E., Tausz, C.E., Samples, E.E., Renicker, T.R., Scotese, K.C., McMaster, H.A., Blasius-Wert, B.J., Zimba, P. V, and Casamatta, D.A., 2018, Long-term trends in seasonal plankton dynamics in Lake Mead (Nevada-Arizona, USA) and implications for climate change: *Hydrobiologia*, v. 822, p. 85–109, doi:[10.1007/s10750-018-3638-4](https://doi.org/10.1007/s10750-018-3638-4).
- Bergquist, A.M., Carpenter, S.R., and Latino, J.C., 1985, Shifts in phytoplankton size structure and community composition during grazing by contrasting zooplankton assemblages1: *Limnology and Oceanography*, v. 30, p. 1037–1045, doi:<https://doi.org/10.4319/lo.1985.30.5.1037>.
- Breiman, L., 2001, Random Forests: *Machine Learning*, v. 45, p. 5–32, doi:[10.1023/A:1010933404324](https://doi.org/10.1023/A:1010933404324).
- Brookes, J.D., and Carey, C.C., 2011, Resilience to Blooms: *Science*, v. 334, p. 46–47, doi:[10.1126/science.1207349](https://doi.org/10.1126/science.1207349).
- Bruckerhoff, L.A., Wheeler, K., Dibble, K.L., Mihalevich, B.A., Neilson, B.T., Wang, J., Yackulic, C.B., and Schmidt, J.C., 2022, Water Storage Decisions and Consumptive Use May Constrain Ecosystem Management under Severe Sustained Drought: *JAWRA Journal of the American Water Resources Association*, v. 58, p. 654–672, doi:<https://doi.org/10.1111/1752-1688.13020>.
- Butcher, J.B., Nover, D., Johnson, T.E., and Clark, C.M., 2015, Sensitivity of lake thermal and mixing dynamics to climate change: *Climatic Change*, v. 129, p. 295–305, doi:[10.1007/s10584-015-1326-1](https://doi.org/10.1007/s10584-015-1326-1).
- Carmichael, W.W., 2001, Health Effects of Toxin-Producing Cyanobacteria: “The CyanoHABs”: Human and Ecological Risk Assessment: *An International Journal*, v. 7, p. 1393–1407, doi:[10.1080/20018091095087](https://doi.org/10.1080/20018091095087).
- Chicco, D., 2017, Ten quick tips for machine learning in computational biology: *BioData Mining*, v. 10, p. 35, doi:[10.1186/s13040-017-0155-3](https://doi.org/10.1186/s13040-017-0155-3).
- Crumpton, W.G., 1987, A simple and reliable method for making permanent mounts of phytoplankton for light and fluorescence microscopy1: *Limnology and Oceanography*, v. 32, p. 1154–1159, doi:<https://doi.org/10.4319/lo.1987.32.5.1154>.

- Díaz-Torres, O., de Anda, J., Lugo-Melchor, O.Y., Pacheco, A., Orozco-Nunnally, D.A., Shear, H., Senés-Guerrero, C., and Gradilla-Hernández, M.S., 2021, Rapid Changes in the Phytoplankton Community of a Subtropical, Shallow, Hypereutrophic Lake During the Rainy Season: *Frontiers in Microbiology*, v. 12, <https://www.frontiersin.org/articles/10.3389/fmicb.2021.617151>.
- Ding, L., Hannoun, I.A., List, E.J., and Tietjen, T., 2014, Development of a phosphorus budget for Lake Mead: *Lake and Reservoir Management*, v. 30, p. 143–156, doi:10.1080/10402381.2014.899656.
- Duarte, C.M., Agustí, S., and Canfield Jr., D.E., 1992, Patterns in phytoplankton community structure in Florida lakes: *Limnology and Oceanography*, v. 37, p. 155–161, doi:<https://doi.org/10.4319/lo.1992.37.1.0155>.
- Dunlap, C.R., Sklenar, K.S., and Blake, L.J., 2015, A Costly Endeavor: Addressing Algae Problems in a Water Supply: *Journal AWWA*, v. 107, p. E255–E262, doi:<https://doi.org/10.5942/jawwa.2015.107.0055>.
- Elliott, J.A., 2012, Is the future blue-green? A review of the current model predictions of how climate change could affect pelagic freshwater cyanobacteria: *Water Research*, v. 46, p. 1364–1371, doi:<https://doi.org/10.1016/j.watres.2011.12.018>.
- Elliott, J.A., Jones, I.D., and Thackeray, S.J., 2006, Testing the Sensitivity of Phytoplankton Communities to Changes in Water Temperature and Nutrient Load, in a Temperate Lake: *Hydrobiologia*, v. 559, p. 401–411, doi:10.1007/s10750-005-1233-y.
- Fang, J., Ma, J., Yang, X., and Shang, C., 2010, Formation of carbonaceous and nitrogenous disinfection by-products from the chlorination of *Microcystis aeruginosa*: *Water Research*, v. 44, p. 1934–1940, doi:<https://doi.org/10.1016/j.watres.2009.11.046>.
- Granéli, E., and Turner, J.T., 2006, *Ecology of harmful algae*: Springer, v. 189.
- Haakonsson, S., Rodríguez, M.A., Carballo, C., Pérez, M. del C., Arocena, R., and Bonilla, S., 2020, Predicting cyanobacterial biovolume from water temperature and conductivity using a Bayesian compound Poisson-Gamma model: *Water Research*, v. 176, p. 115710, doi:<https://doi.org/10.1016/j.watres.2020.115710>.
- Hannoun, D., and Tietjen, T., 2022, A three-part coupled statistical and physical model to monitor water quality parameters governing disinfection byproduct risk at an urban drinking water intake: *Frontiers in Water*, v. 4, <https://www.frontiersin.org/articles/10.3389/frwa.2022.983257>.
- Hannoun, D., and Tietjen, T., 2023, Lake management under severe drought: Lake Mead, Nevada/Arizona: *JAWRA Journal of the American Water Resources Association*, v. 59, p. 416–428, doi:<https://doi.org/10.1111/1752-1688.13090>.
- Hannoun, D., Tietjen, T., and Brooks, K., 2021, The potential effects of climate change and drawdown on a newly constructed drinking water intake: Study case in Las Vegas, NV, USA: *Water Util. J.*, v. 27, p. 1–13.
- Hansson, L.-A., Gustafsson, S., Rengefors, K., and Bomark, L., 2007, Cyanobacterial chemical warfare affects zooplankton community composition: *Freshwater Biology*, v. 52, p. 1290–1301, doi:<https://doi.org/10.1111/j.1365-2427.2007.01765.x>.

- Hauke, J., and Kossowski, T., 2011, Comparison of values of Pearson's and Spearman's correlation coefficients on the same sets of data: *Quaestiones geographicae*, v. 30, p. 87–93.
- Heldmyer, A.J., Bjarke, N.R., and Livneh, B., 2023, A 21st-Century perspective on snow drought in the Upper Colorado River Basin: *JAWRA Journal of the American Water Resources Association*, v. 59, p. 396–415, doi:<https://doi.org/10.1111/1752-1688.13095>.
- Hickey, V., 2010, The Quagga Mussel Crisis at Lake Mead National Recreation Area, Nevada (U.S.A.): *Conservation Biology*, v. 24, p. 931–937, doi:<https://doi.org/10.1111/j.1523-1739.2010.01490.x>.
- Hillebrand, H., Dürselen, C., Kirschtel, D., Pollinger, U., and Zohary, T., 1999, Biovolume calculation for pelagic and benthic microalgae: *Journal of phycology*, v. 35, p. 403–424.
- Hirsch, R.M., Slack, J.R., and Smith, R.A., 1982, Techniques of trend analysis for monthly water quality data: *Water Resources Research*, v. 18, p. 107–121, doi:<https://doi.org/10.1029/WR018i001p00107>.
- Holdren, G.C., and Turner, K., 2010, Characteristics of Lake Mead, Arizona–Nevada: *Lake and Reservoir Management*, v. 26, p. 230–239, doi:[10.1080/07438141.2010.540699](https://doi.org/10.1080/07438141.2010.540699).
- Jeffrey, S.W., and Humphrey, G.F., 1975, New spectrophotometric equations for determining chlorophylls a, b, c1 and c2 in higher plants, algae and natural phytoplankton: *Biochemie und Physiologie der Pflanzen*, v. 167, p. 191–194, doi:[https://doi.org/10.1016/S0015-3796\(17\)30778-3](https://doi.org/10.1016/S0015-3796(17)30778-3).
- Kalin, M., Cao, Y., Smith, M., and Olaveson, M.M., 2001, Development of the phytoplankton community in a pit-lake in relation to water quality changes: *Water Research*, v. 35, p. 3215–3225, doi:[https://doi.org/10.1016/S0043-1354\(01\)00016-1](https://doi.org/10.1016/S0043-1354(01)00016-1).
- LaBounty, J., and Burns, N., 2005, Characterization of Boulder Basin, Lake Mead, Nevada-Arizona, USA – Based on Analysis of 34 Limnological Parameters: *Lake and Reservoir Management*, v. 21, p. 277–307, doi:[10.1080/07438140509354435](https://doi.org/10.1080/07438140509354435).
- LaBounty, J.F., and Horn, M.J., 1997, The Influence of Drainage From the Las Vegas Valley on the Limnology of Boulder Basin, Lake Mead, Arizona-Nevada: *Lake and Reservoir Management*, v. 13, p. 95–108, doi:[10.1080/07438149709354301](https://doi.org/10.1080/07438149709354301).
- Lever, J., Krzywinski, M., and Altman, N., 2016, Model selection and overfitting: *Nature Methods*, v. 13, p. 703–704, doi:[10.1038/nmeth.3968](https://doi.org/10.1038/nmeth.3968).
- Liebig, J., 1843, *Chemistry in its application to agriculture and physiology*.
- Liu, M., Huang, Y., Hu, J., He, J., and Xiao, X., 2023, Algal community structure prediction by machine learning: *Environmental Science and Ecotechnology*, v. 14, p. 100233, doi:<https://doi.org/10.1016/j.ese.2022.100233>.
- Liu, Q., Tian, Y., Liu, Y., Yu, M., Hou, Z., He, K., Xu, H., Cui, B., and Jiang, Y., 2021, Relationship between dissolved organic matter and phytoplankton community dynamics in a human-impacted subtropical river: *Journal of Cleaner Production*, v. 289, p. 125144, doi:<https://doi.org/10.1016/j.jclepro.2020.125144>.

- Lloyd, S., 1982, Least squares quantization in PCM: IEEE Transactions on Information Theory, v. 28, p. 129–137, doi:10.1109/TIT.1982.1056489.
- MathWorks, 2022, MATLAB version: 9.13.0 (R2022b): The MathWorks Inc., Natick, Massachusetts, United States, <https://www.mathworks.com>.
- Meinshausen, N., 2006, Quantile Regression Forests: Journal of Machine Learning Research, v. 7, p. 983–999.
- Millard, S.P., 2013, EnvStats: An R Package for Environmental Statistics: New York, Springer, <https://www.springer.com> (accessed January 2024).
- Mosley, L.M., 2015, Drought impacts on the water quality of freshwater systems; review and integration: Earth-Science Reviews, v. 140, p. 203–214, doi:<https://doi.org/10.1016/j.earscirev.2014.11.010>.
- Mutshinda, C.M., Finkel, Z. V, and Irwin, A.J., 2013, Which environmental factors control phytoplankton populations? A Bayesian variable selection approach: Ecological Modelling, v. 269, p. 1–8, doi:<https://doi.org/10.1016/j.ecolmodel.2013.07.025>.
- Niu, L., Van Gelder, P., Guan, Y., and Vrijling, J.K., 2015, Uncertainty analysis and modelling of phytoplankton dynamics in coastal waters: Journal of Environment Protection and Sustainable Development, v. 1, p. 193–202.
- Oliver, R.L., and Ganf, G.G., 2000, Freshwater blooms, *in* The ecology of cyanobacteria: their diversity in time and space, Springer, p. 149–194.
- O’Neil, J.M., Davis, T.W., Burford, M.A., and Gobler, C.J., 2012, The rise of harmful cyanobacteria blooms: The potential roles of eutrophication and climate change: Harmful Algae, v. 14, p. 313–334, doi:<https://doi.org/10.1016/j.hal.2011.10.027>.
- Paerl, H.W., Fulton, R.S., Moisander, P.H., and Dyble, J., 2001, Harmful Freshwater Algal Blooms, With an Emphasis on Cyanobacteria: TheScientificWorldJOURNAL, v. 1, p. 139109, doi:10.1100/tsw.2001.16.
- Paerl, H.W., and Huisman, J., 2008, Blooms Like It Hot: Science, v. 320, p. 57–58, doi:10.1126/science.1155398.
- Paerl, H., and Otten, T., 2013, Harmful Cyanobacterial Blooms: Causes, Consequences, and Controls: Microbial ecology, v. 65, doi:10.1007/s00248-012-0159-y.
- Palmer, C.M., 1959, Algae in water supplies: an illustrated manual on the identification, significance, and control of algae in water supplies: US Department of Health, Education and Welfare, Public Health Service, v. 2.
- Porter, K.G., 1977, The plant-animal interface in freshwater ecosystems: microscopic grazers feed differentially on planktonic algae and can influence their community structure and succession in ways that are analogous to the effects of herbivores on terrestrial plant communities: American scientist, v. 65, p. 159–170.

- R Core Team, 2022, R: A Language and Environment for Statistical Computing:, <https://www.R-project.org/> (accessed January 2024).
- Rao, K., Zhang, X., Wang, M., Liu, J., Guo, W., Huang, G., and Xu, J., 2021, The relative importance of environmental factors in predicting phytoplankton shifting and cyanobacteria abundance in regulated shallow lakes: *Environmental Pollution*, v. 286, p. 117555, doi:<https://doi.org/10.1016/j.envpol.2021.117555>.
- Reynolds, C.S., 2006, *The ecology of phytoplankton*: Cambridge University Press.
- Robson, B.J., and Hamilton, D.P., 2003, Summer flow event induces a cyanobacterial bloom in a seasonal Western Australian estuary: *Marine and Freshwater Research*, v. 54, p. 139–151, <https://doi.org/10.1071/MF02090>.
- Rohr, T., Richardson, A.J., Lenton, A., Chamberlain, M.A., and Shadwick, E.H., 2023, Zooplankton grazing is the largest source of uncertainty for marine carbon cycling in CMIP6 models: *Communications Earth & Environment*, v. 4, p. 212, doi:10.1038/s43247-023-00871-w.
- Rosen, M.R., Turner, K., Goodbred, S.L., Miller, J.M., and Survey, U.S.G., 2012, A synthesis of aquatic science for management of Lakes Mead and Mohave:, doi:10.3133/cir1381.
- Rouso, B.Z., Bertone, E., Stewart, R., and Hamilton, D.P., 2020, A systematic literature review of forecasting and predictive models for cyanobacteria blooms in freshwater lakes: *Water Research*, v. 182, p. 115959, doi:<https://doi.org/10.1016/j.watres.2020.115959>.
- Rumsey, C.A., Miller, O., Hirsch, R.M., Marston, T.M., and Susong, D.D., 2021, Substantial Declines in Salinity Observed Across the Upper Colorado River Basin During the 20th Century, 1929–2019: *Water Resources Research*, v. 57, p. e2020WR028581, doi:<https://doi.org/10.1029/2020WR028581>.
- Scholl, E.A., Hanus, K.R., Gardner, T.W., and Kennedy, T.A., 2024, Multiple stressors mediate the effects of warming on leaf decomposition in a large regulated river: *Ecosphere*, v. 15, p. e4804, doi:<https://doi.org/10.1002/ecs2.4804>.
- De Senerpont Domis, L.N., Mooij, W.M., and Huisman, J., 2007, Climate-induced shifts in an experimental phytoplankton community: a mechanistic approach, *in* Gulati, R.D., Lammens, E., De Pauw, N., and Van Donk, E. eds., *Shallow Lakes in a Changing World*, Dordrecht, Springer Netherlands, p. 403–413.
- Spearman, C., 1961, *The Proof and Measurement of Association Between Two Things.*: East Norwalk, CT, US, Appleton-Century-Crofts, 45–58 p., doi:10.1037/11491-005.
- Suikkanen, S., Fistarol, G.O., and Granéli, E., 2004, Allelopathic effects of the Baltic cyanobacteria *Nodularia spumdigena*, *Aphanizomenon flos-aquae* and *Anabaena lemmermannii* on algal monocultures: *Journal of Experimental Marine Biology and Ecology*, v. 308, p. 85–101, doi:<https://doi.org/10.1016/j.jembe.2004.02.012>.
- Taş, S., Okuş, E., and Aslan-Yılmaz, A., 2006, The blooms of a cyanobacterium, *Microcystis cf. aeruginosa* in a severely polluted estuary, the Golden Horn, Turkey: *Estuarine, Coastal and Shelf Science*, v. 68, p. 593–599, doi:<https://doi.org/10.1016/j.ecss.2006.02.025>.

- Thornton, K.W., Kennedy, R.H., Carroll, J.H., Walker, W.W., Gunkel, R.C., and Ashby, S., 1981, Reservoir sedimentation and water quality—an heuristic model, *in* Proceedings of the symposium on surface water impoundments, American Society of Civil Engineers, Minneapolis, p. 654–661.
- Tilman, D., Kilham, S.S., and Kilham, P., 1982, Phytoplankton community ecology: the role of limiting nutrients: *Annual review of Ecology and Systematics*, v. 13, p. 349–372.
- United States Bureau of Reclamation, 2023, Lake Mead at Hoover Dam, End of Month Elevation: <https://www.usbr.gov/lc/region/g4000/hourly/mead-elv.html>.
- Vanni, M.J., and Temte, J., 1990, Seasonal patterns of grazing and nutrient limitation of phytoplankton in a eutrophic lake: *Limnology and Oceanography*, v. 35, p. 697–709, doi:<https://doi.org/10.4319/lo.1990.35.3.0697>.
- Wahl, E.R., Zorita, E., Diaz, H.F., and Hoell, A., 2022, Southwestern United States drought of the 21st century presages drier conditions into the future: *Communications Earth & Environment*, v. 3, p. 202, doi:[10.1038/s43247-022-00532-4](https://doi.org/10.1038/s43247-022-00532-4).
- Walsby, A.E., 1994, Gas vesicles: *Microbiological Reviews*, v. 58, p. 94–144, doi:[10.1128/mr.58.1.94-144.1994](https://doi.org/10.1128/mr.58.1.94-144.1994).
- Wang, J., Udall, B., Kuhn, E., Wheeler, K., and Schmidt, J.C., 2022, Evaluating the Accuracy of Reclamation’s 24-Month Study Lake Powell Projections:
- Wetzel, R.G., and Likens, G., 2000, *Limnological analyses*: Springer Science & Business Media.
- Wheeler, K.G., Udall, B., Wang, J., Kuhn, E., Salehabadi, H., and Schmidt, J.C., 2022, What will it take to stabilize the Colorado River? *Science*, v. 377, p. 373–375, doi:[10.1126/science.abo4452](https://doi.org/10.1126/science.abo4452).
- Wiedner, C., Rücker, J., Bruggemann, R., and Nixdorf, B., 2007, Climate change affects timing and size of populations of an invasive cyanobacterium in temperate regions: *Oecologia*, v. 152, p. 473–484, doi:[10.1007/s00442-007-0683-5](https://doi.org/10.1007/s00442-007-0683-5).
- Wildman Jr., R.A., and Hering, J.G., 2011, Potential for release of sediment phosphorus to Lake Powell (Utah and Arizona) due to sediment resuspension during low water level: *Lake and Reservoir Management*, v. 27, p. 365–375, doi:[10.1080/07438141.2011.632705](https://doi.org/10.1080/07438141.2011.632705).
- Winder, M., and Sommer, U., 2012, Phytoplankton response to a changing climate: *Hydrobiologia*, v. 698, p. 5–16, doi:[10.1007/s10750-012-1149-2](https://doi.org/10.1007/s10750-012-1149-2).
- Woelmer, W.M., Thomas, R.Q., Lofton, M.E., McClure, R.P., Wander, H.L., and Carey, C.C., 2022, Near-term phytoplankton forecasts reveal the effects of model time step and forecast horizon on predictability: *Ecological Applications*, v. 32, p. e2642, doi:<https://doi.org/10.1002/eap.2642>.
- Woolway, R.I. et al., 2021, Phenological shifts in lake stratification under climate change: *Nature Communications*, v. 12, p. 2318, doi:[10.1038/s41467-021-22657-4](https://doi.org/10.1038/s41467-021-22657-4).
- Woolway, R.I., Kraemer, B.M., Lenters, J.D., Merchant, C.J., O’Reilly, C.M., and Sharma, S., 2020, Global lake responses to climate change: *Nature Reviews Earth & Environment*, v. 1, p. 388–403, doi:[10.1038/s43017-020-0067-5](https://doi.org/10.1038/s43017-020-0067-5).

- Wright, S.A., Anderson, C.R., and Voichick, N., 2009, A simplified water temperature model for the Colorado River below Glen Canyon Dam: *River Research and Applications*, v. 25, p. 675–686, doi:<https://doi.org/10.1002/rra.1179>.
- Yajima, H., and Derot, J., 2017, Application of the Random Forest model for chlorophyll-a forecasts in fresh and brackish water bodies in Japan, using multivariate long-term databases: *Journal of Hydroinformatics*, v. 20, p. 206–220, doi:[10.2166/hydro.2017.010](https://doi.org/10.2166/hydro.2017.010).
- Zhang, J., Zhi, M., and Zhang, Y., 2021, Combined Generalized Additive model and Random Forest to evaluate the influence of environmental factors on phytoplankton biomass in a large eutrophic lake: *Ecological Indicators*, v. 130, p. 108082, doi:<https://doi.org/10.1016/j.ecolind.2021.108082>.
- Zhi, W., Feng, D., Tsai, W.-P., Sterle, G., Harpold, A., Shen, C., and Li, L., 2021, From Hydrometeorology to River Water Quality: Can a Deep Learning Model Predict Dissolved Oxygen at the Continental Scale? *Environmental Science & Technology*, v. 55, p. 2357–2368, doi:[10.1021/acs.est.0c06783](https://doi.org/10.1021/acs.est.0c06783).
- Zhou, J., Qin, B., Casenave, C., Han, X., Yang, G., Wu, T., Wu, P., and Ma, J., 2015, Effects of wind wave turbulence on the phytoplankton community composition in large, shallow Lake Taihu: *Environmental Science and Pollution Research*, v. 22, p. 12737–12746, doi:[10.1007/s11356-015-4535-2](https://doi.org/10.1007/s11356-015-4535-2).
- Zohary, T., and Ostrovsky, I., 2011, Ecological impacts of excessive water level fluctuations in stratified freshwater lakes: *Inland Waters*, v. 1, p. 47–59, doi:[10.5268/IW-1.1.406](https://doi.org/10.5268/IW-1.1.406).

2.8 Supplementary materials

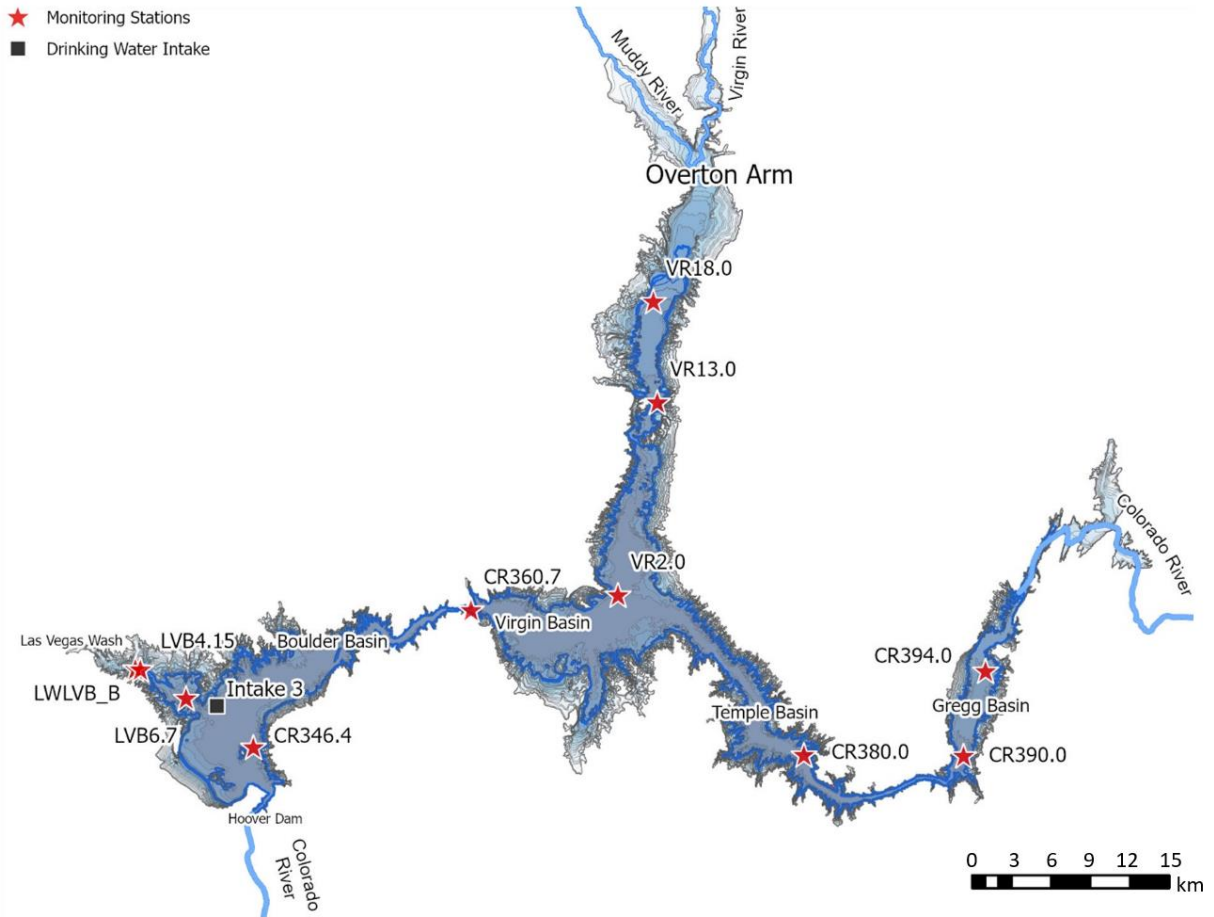


Figure S2.1. Lake Mead with all inflows and outflows, basins, water quality sampling stations named according to inter-agency nomenclature, and SNWA’s drinking water intake shown. The lake elevation of June 2023 is marked with the dark blue contour line, previous lake elevations are shown as grey contour lines.

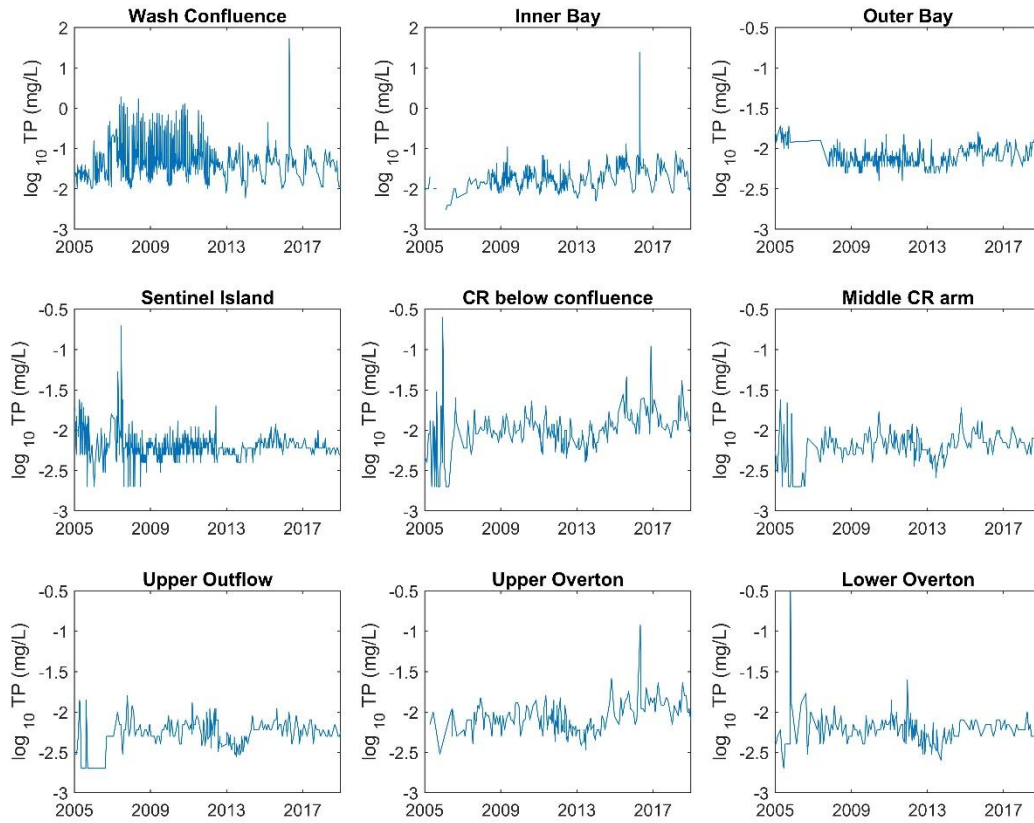


Figure S2.2. Timeseries of Total Phosphorus (TP) for the different monitoring sites. Note: different y-scale for the first two stations.

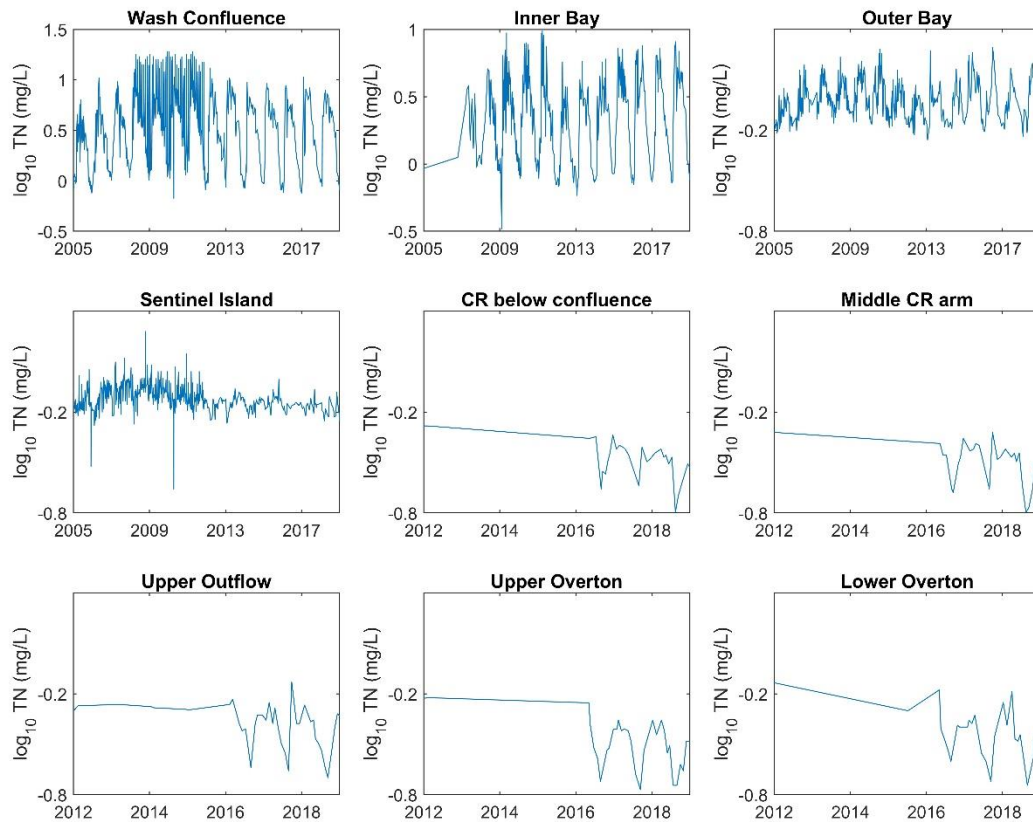


Figure S2.3. Timeseries of Total Nitrogen (TN) for the different monitoring sites. Note: different y-scale for the first two stations. TN at the last five stations was below the detection limit for most observations before 2016, after which the detection limit was lowered from 0.5 mg/L to 0.1 mg/L.

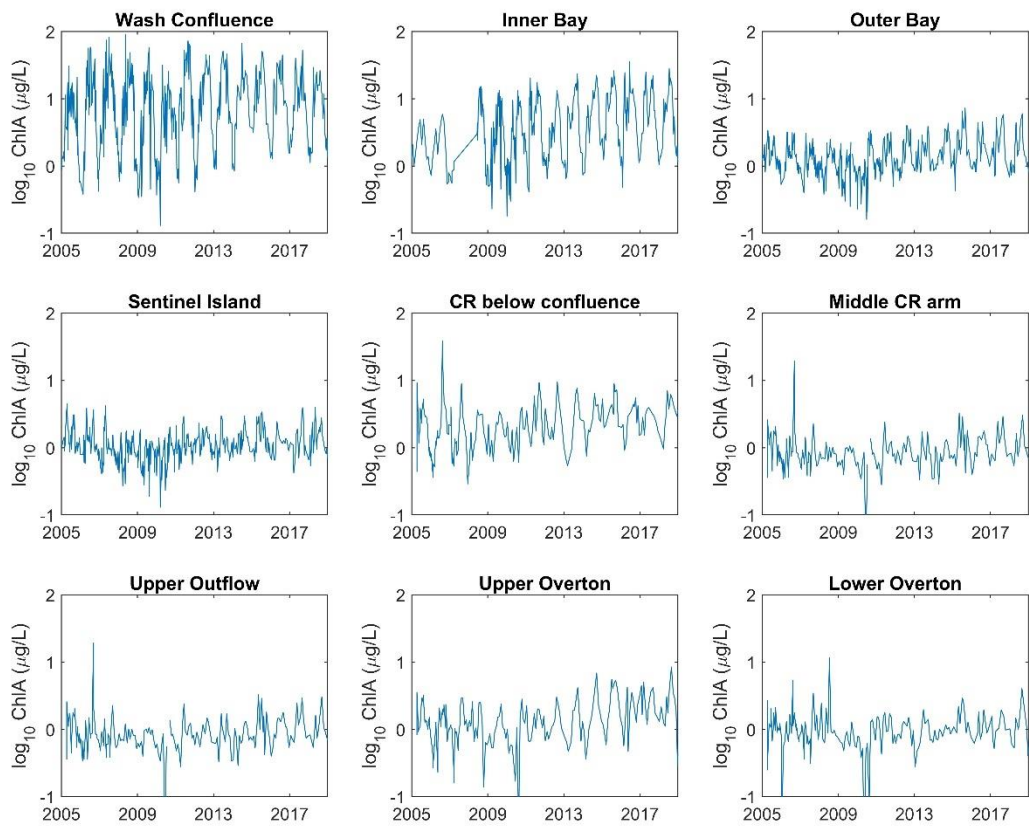


Figure S2.4. Chlorophyll-*a* (ChlA) timeseries for the different monitoring sites, showing highest values occur near the Wash inflow (Wash Confluence).

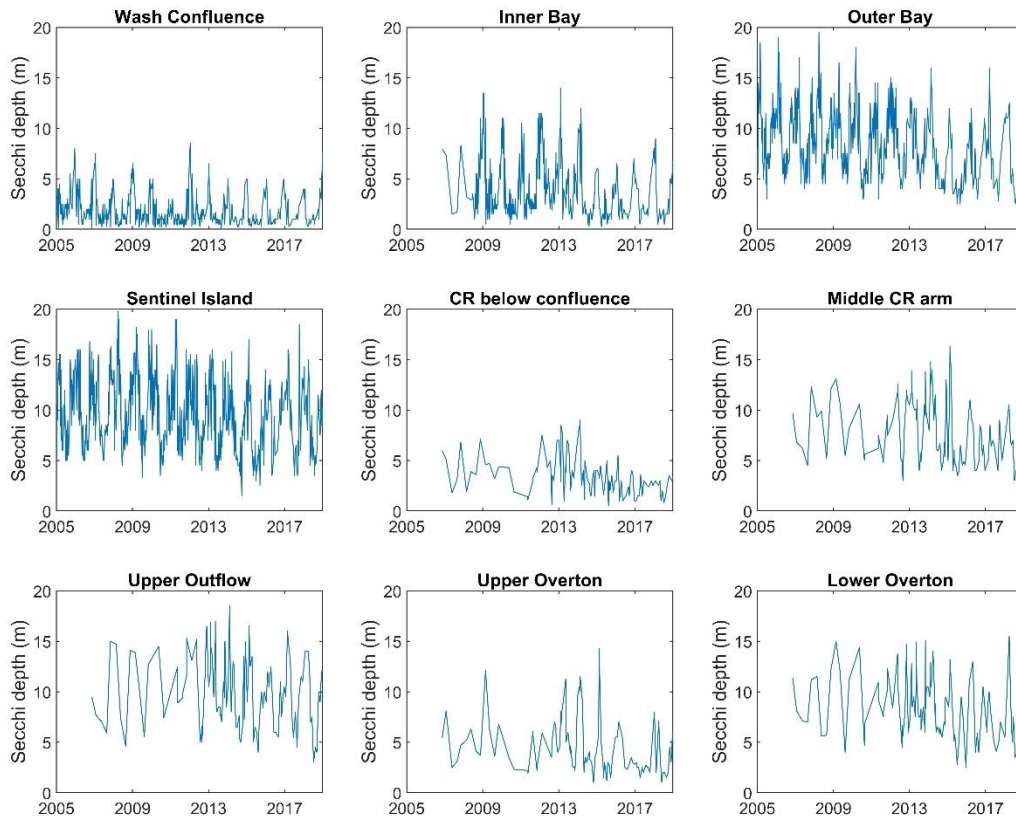


Figure S2.5. Secchi depth timeseries for the different monitoring sites, showing lowest values occur near inflows (Wash Confluence, CR below confluence, and upper Overton).

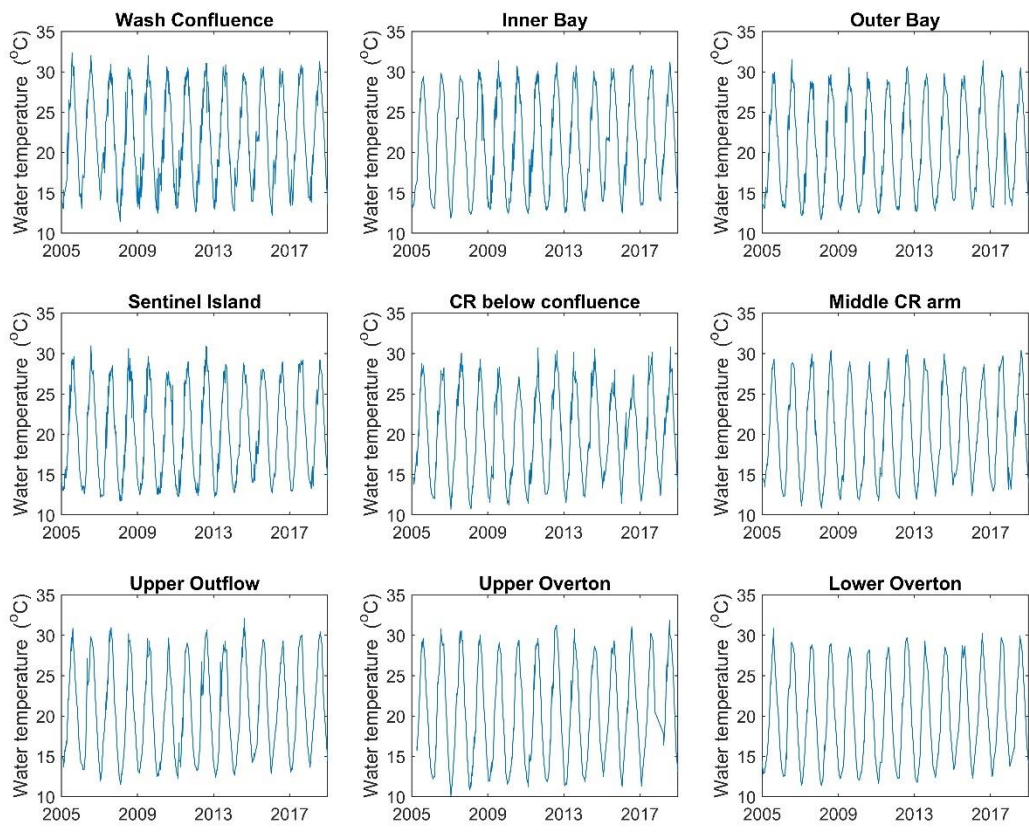


Figure S2.6. Temperature timeseries for the different monitoring sites.

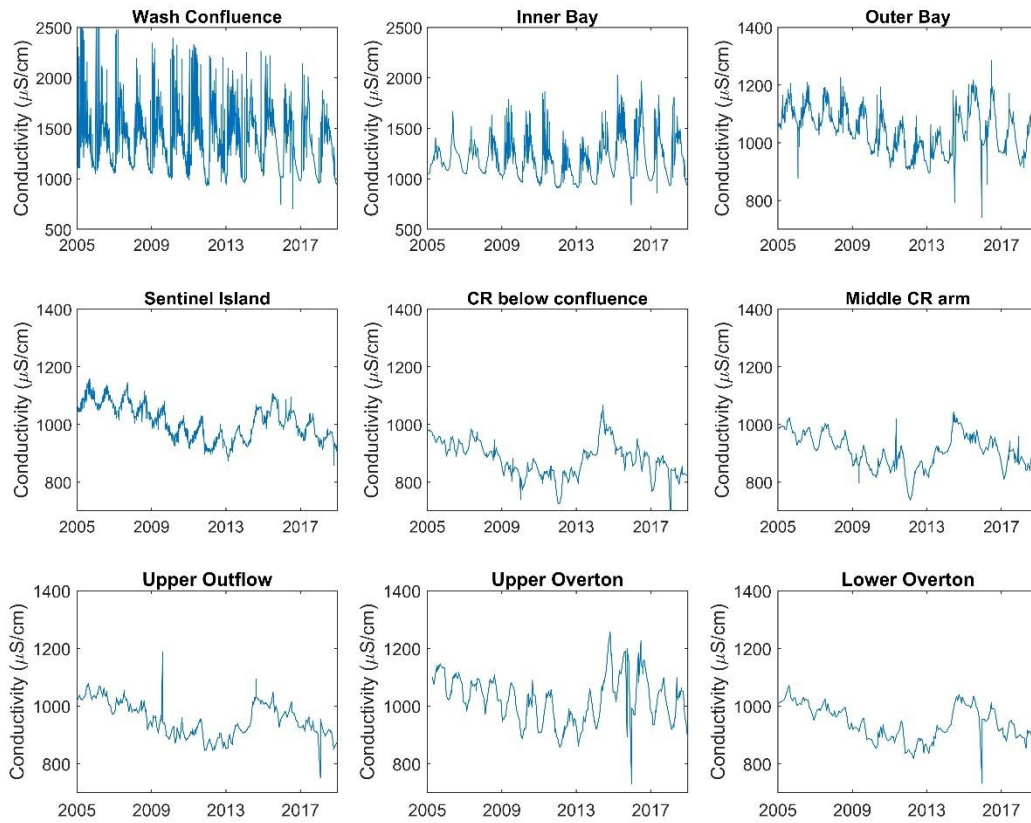


Figure S2.7. Conductivity timeseries for the different monitoring sites, showing highest conductivity occurs near the Wash inflow (Wash Confluence).

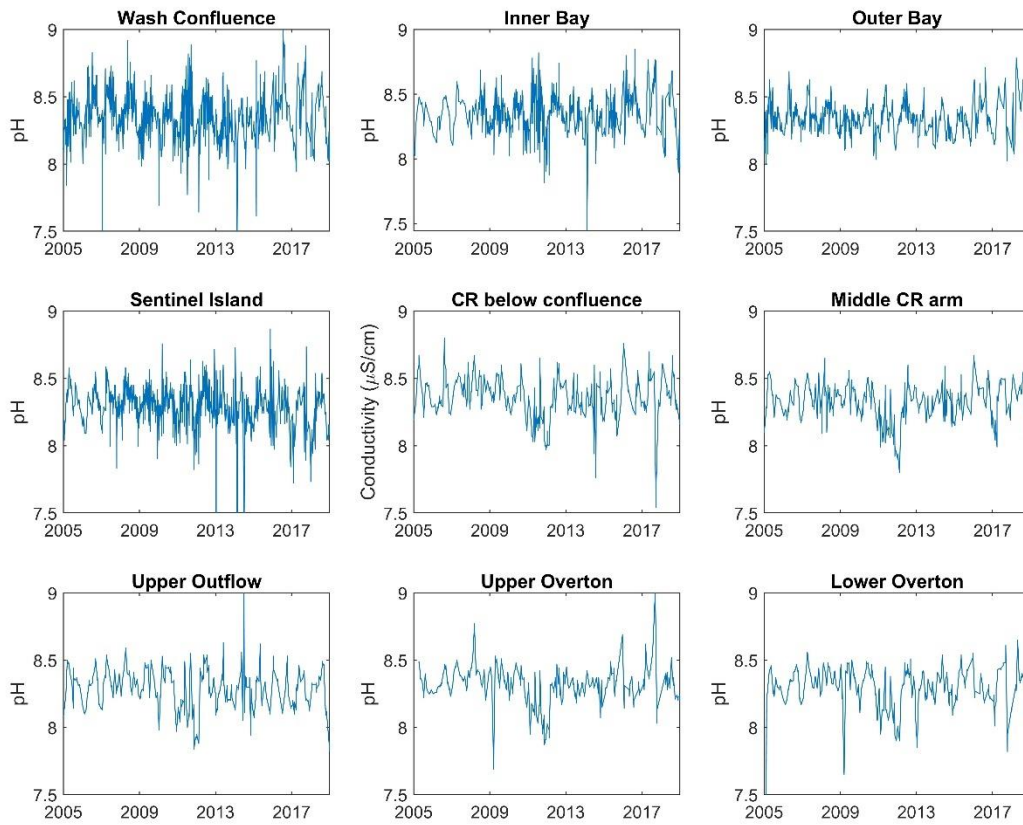


Figure S2.8. pH timeseries for the different monitoring sites.

Table S2.1. Analysis of variance (ANOVA) for environmental and water quality parameters, showing the mean and standard deviation of all stations combined, along with the degrees of freedom (between groups, within groups) and the significance level.

Parameter	Unit	Mean	Standard Deviation	F	P
TP	mg/L	0.043	0.17	57.15 (5, 1589)	4.96×10^{-102}
TN	mg/L	2.43	3.22	76.05 (7, 468)	9.10×10^{-80}
Chlorophyll- <i>a</i>	µg/L	3.07	7.19	133.35 (7, 1828)	2.26×10^{-176}
Secchi Depth	m	7.67	4.33	77.42 (7,495)	2.67×10^{-82}
Water Temp	°C	20.63	5.64	77.42 (7, 2430)	0.0011
Conductivity	µS/cm	1063.30	232.63	662.57 (7, 3816)	0
pH	-	8.36	0.14	662.57 (7, 3123)	8.16×10^{-23}

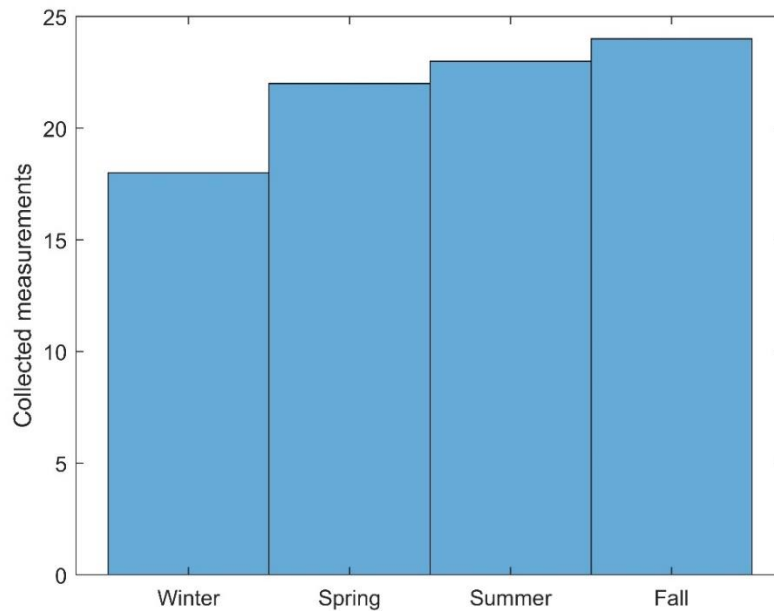


Figure S2.9. Number of Secchi depth measurements collected during winter, spring, summer, and fall for the Middle Colorado River arm station.

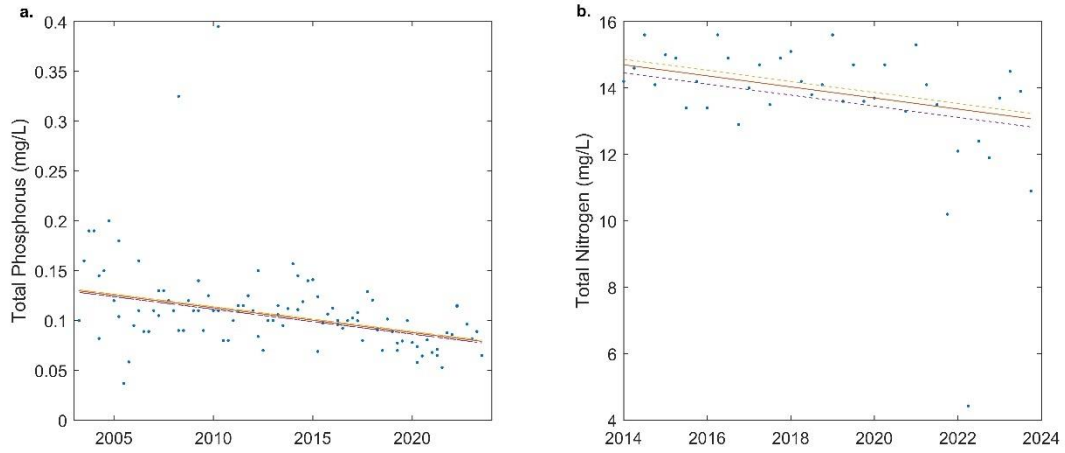


Figure S2.10. Seasonal Mann-Kendall trend test at monitoring site LW0.9 in the Las Vegas Wash for **a.** total phosphorus, showing a significant negative trend ($p = 1.01 \times 10^{-15}$) between 2003-2023 and **b.** total nitrogen showing a significant negative trend ($p = 3.98 \times 10^{-3}$) between 2013-2023.

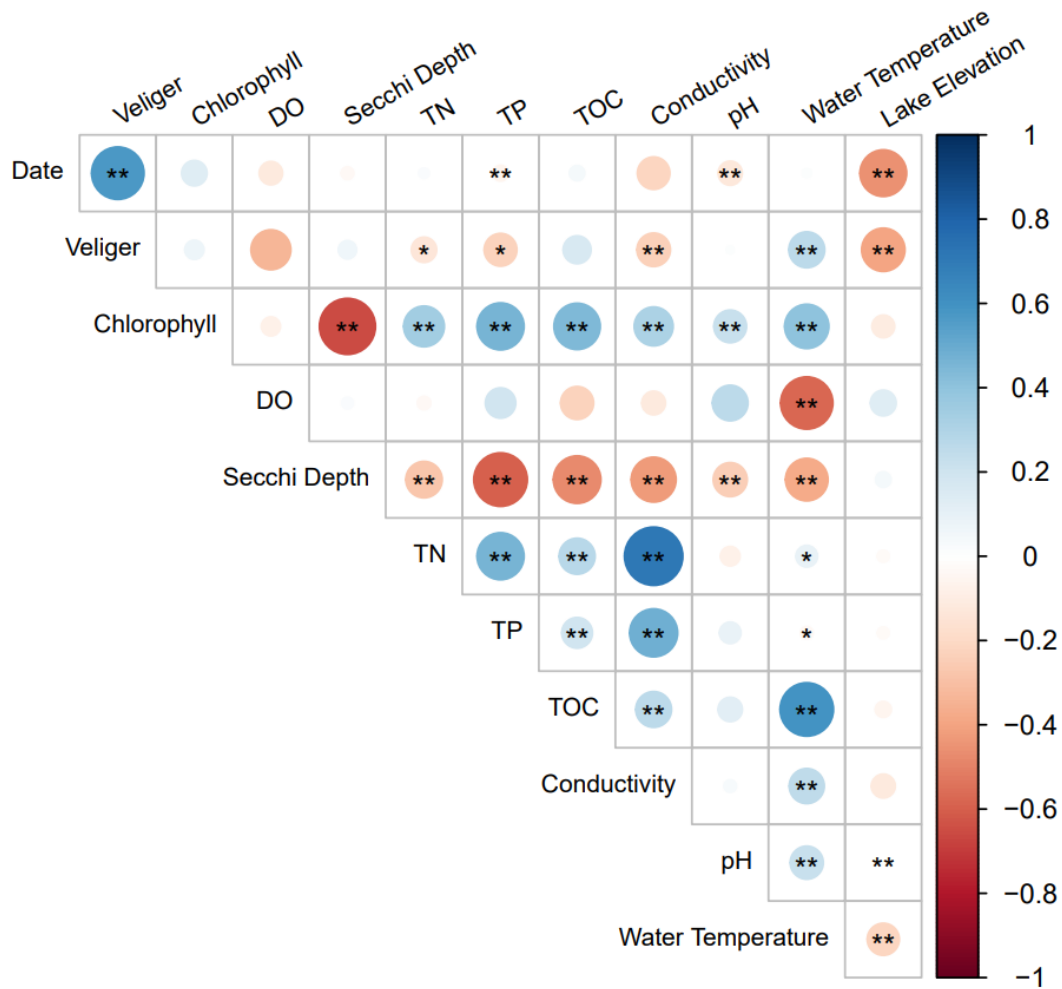


Figure S2.11. Spearman’s rank correlation analysis for water quality parameters of all monitoring stations in Lake Mead (* = $p < 0.05$, ** = $p < 0.01$). Larger circles indicate greater correlation with blue (positive values) indicating a positive correlation and red (negative values) indicating a negative correlation.

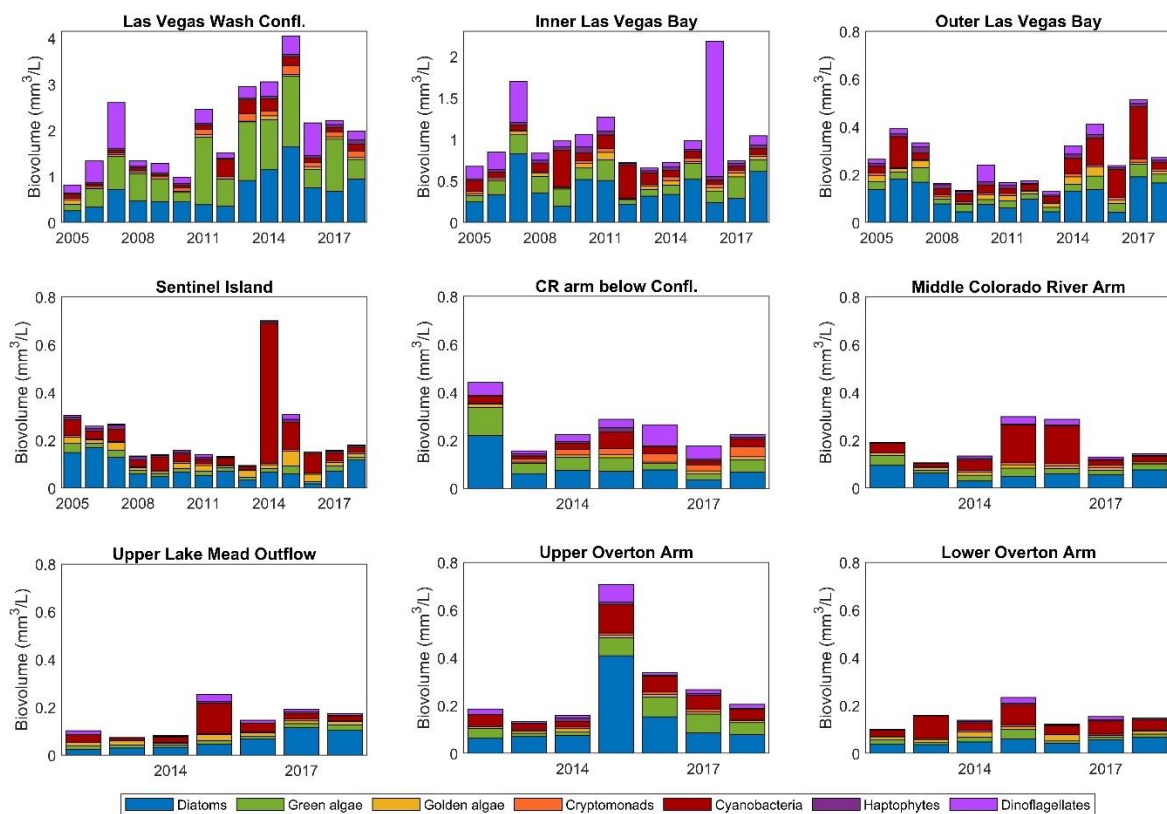


Figure S2.12. Mean annual biovolume of major phytoplankton groups for 9 monitoring stations in Lake Mead. Y-scale adjusted for Las Vegas Wash confl. and Inner Las Vegas Bay. Mean annual biovolume: Las Vegas Wash confl. = $2.2 \times 10^6 \mu\text{m}^3/\text{mL}$, Inner Las Vegas Bay = $9.3 \times 10^5 \mu\text{m}^3/\text{mL}$, Outer Las Vegas Bay = $3.0 \times 10^5 \mu\text{m}^3/\text{mL}$, Sentinel Island = $2.2 \times 10^5 \mu\text{m}^3/\text{mL}$, Colorado River Arm below confl. = $2.5 \times 10^5 \mu\text{m}^3/\text{mL}$, Middle Colorado River Arm = $1.8 \times 10^5 \mu\text{m}^3/\text{mL}$, Upper Lake Mead Outflow = $1.5 \times 10^5 \mu\text{m}^3/\text{mL}$, Upper Overton Arm = $2.9 \times 10^5 \mu\text{m}^3/\text{mL}$, Lower Overton Arm = $1.5 \times 10^5 \mu\text{m}^3/\text{mL}$.

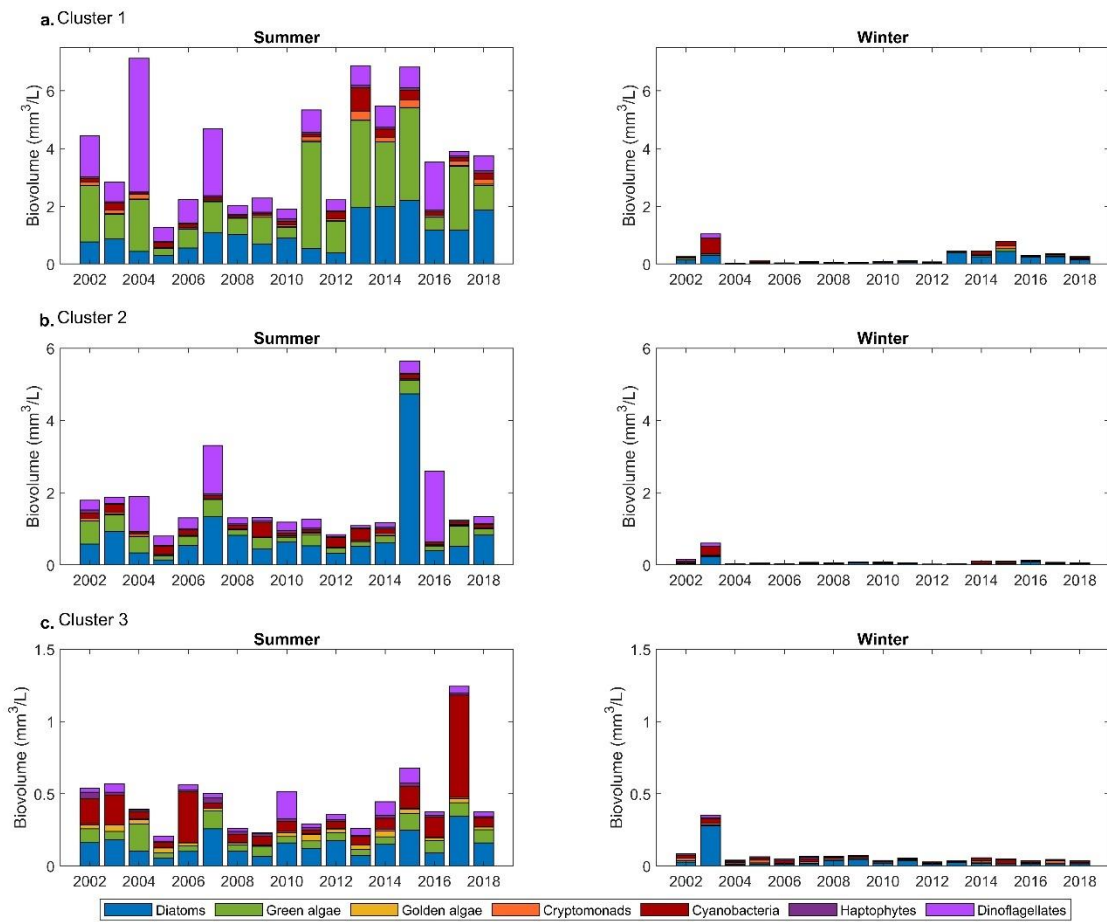


Figure S2.13. Average biovolume of major phytoplankton groups in Lake Mead in summer (left) and winter (right) for **a.** Cluster 1, **b.** Cluster 2, and **c.** Cluster 3.

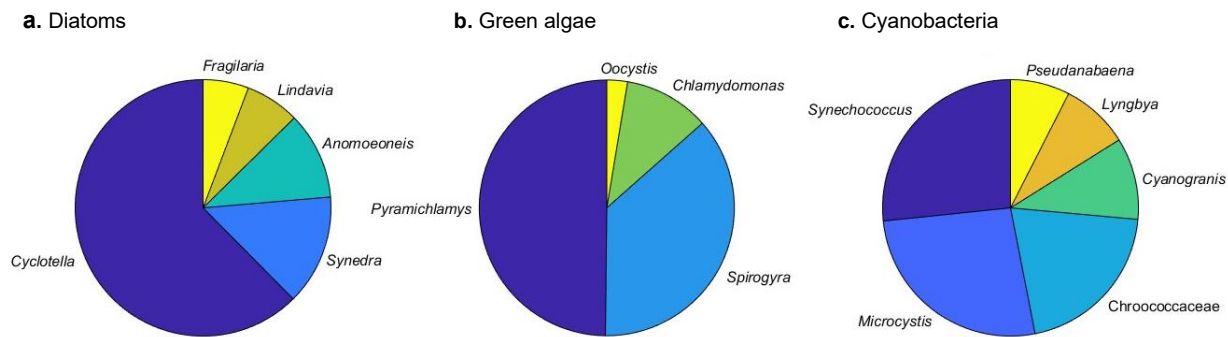


Figure S2.14. Biovolume of genera constituting 90% of phytoplankton biovolume between 2012-2018 for **a.** diatoms, **b.** green algae, and **c.** cyanobacteria.

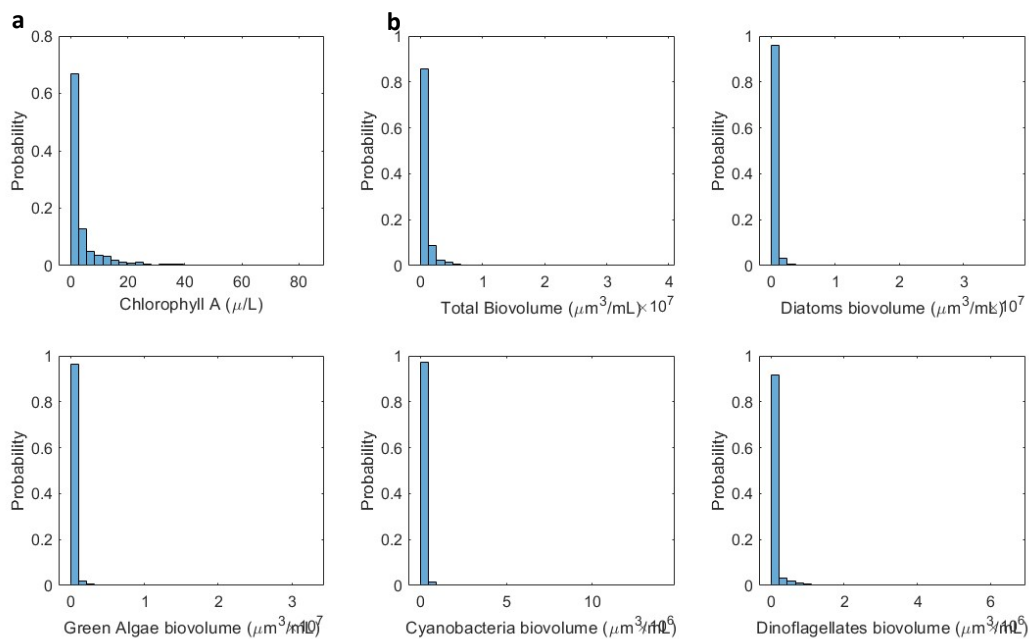


Figure S2.15. Distributions for chlorophyll *a*, total biovolume, and biovolume of major phytoplankton groups at all monitoring stations.

Table S2.2. Trends of biovolume of phytoplankton groups at various locations in Lake Mead using significance level of 0.05. Values mark biovolume (mm^3/L) change per year.

Station	Cluster	Diatoms	Green algae	Cyano-bacteria	Golden algae	Crypto-monads	Hapto-phytes	Dino-flagellates
Wash confl.	1	0.019	6.23×10^{-3}	1.50×10^{-3}		3.26×10^{-3}	3.28×10^{-4}	
Inner Bay	2	2.27×10^{-3}				4.96×10^{-4}	-3.12×10^{-4}	-4.85×10^{-4}
Outer Bay	3					1.88×10^{-4}	-4.48×10^{-4}	
Sentinel Isl.	3	-5.67×10^{-4}	-1.58×10^{-4}	-3.54×10^{-4}		9.89×10^{-5}	-2.98×10^{-4}	
CR blw. confl.	3			1.43×10^{-3}				
Middle CR arm	3					4.58×10^{-4}		
Upper Outflow	3						2.06×10^{-4}	
Upper Overton	3		2.73×10^{-3}					
Lower Overton	3						2.38×10^{-4}	

Note: a positive number represents a significant positive trend, a negative number represents a significant negative trend at a significance level of 0.05. Blank means no significant trend was detected.

Table S2.3. Comparison of regression model performances to predict cyanobacteria biovolume.

Regression model	MATLAB function	Training R-squared	Training RMSE	Testing R-squared	Testing RMSE	Model p-value
Linear regression	fitlm	0.44	0.45	0.44	0.46	2.1×10^{-95}
Gaussian Process Regression Model	fitrgp	0.53	0.42	0.52	0.42	2.7×10^{-127}
Generalized Linear Model	fitglm	0.53	0.42	0.44	0.46	2.1×10^{-95}
Generative Additive Model (GAM)	fitrgam	0.71	0.32	0.39	0.48	1.9×10^{-90}
Regression Tree	fitrtree	0.85	0.23	0.19	0.55	7.6×10^{-74}
Regression Tree Ensembles	fitrensemble	0.99	0.051	0.15	0.56	1.8×10^{-64}
Ensemble of Bagged decision trees	Treebagger	0.77	0.29	0.50	0.43	9.6×10^{-122}

Table S2.4. Hyperparameters for each constructed model after optimization.

RF model	MinLeafSize ¹	NumPredictorstoSample ²	NumTrees ³
Chlorophyll- <i>a</i>	6	4	4598
Total Biovolume	1	1	983
Diatoms	14	4	1117
Green algae	7	1	4408
Cyanobacteria	20	2	3969

¹ Minimum number of leaf node observations

² Number of predictor variables for each decision split

³ Number of trees grown

Table S2.5. Model performance for all subsets of models trained with randomly selected input data and hyperparameters optimized. Models in bold indicate models used for further analysis.

Model	Number	Training R-squared	Testing R-squared
Chlorophyll <i>a</i>	1	0.83	0.72
	2	0.89	0.75
	3	0.90	0.72
	4	0.97	0.72
	5	0.93	0.71
	6	0.95	0.72
	7	0.97	0.72
	8	0.97	0.71
	9	0.93	0.73
	10	0.97	0.71
Total biovolume	1	0.97	0.67
	2	0.96	0.66
	3	0.90	0.66
	4	0.87	0.68
	5	0.97	0.68
	6	0.97	0.66
	7	0.96	0.66
	8	0.97	0.68

	9	0.97	0.68
	10	0.96	0.69
Diatoms	1	0.82	0.40
	2	0.79	0.42
	3	0.56	0.56
	4	0.76	0.48
	5	0.92	0.44
	6	0.66	0.49
	7	0.92	0.42
	8	0.91	0.38
	9	0.92	0.39
	10	0.74	0.45
Green algae	1	0.80	0.44
	2	0.74	0.43
	3	0.75	0.44
	4	0.59	0.48
	5	0.74	0.38
	6	0.84	0.46
	7	0.61	0.46
	8	0.63	0.51
	9	0.58	0.47
	10	0.80	0.44
Cyanobacteria	1	0.94	0.43
	2	0.86	0.41
	3	0.84	0.45
	4	0.91	0.45
	5	0.63	0.52
	6	0.72	0.50
	7	0.94	0.49
	8	0.77	0.46
	9	0.90	0.46
	10	0.82	0.41

Table S2.6. Predictor importance for each model constructed for cross-validation.

Model	Number	Temperature	TP	Secchi	Conductivity	Lake Elevation
Chlorophyll <i>a</i>	1	0.3315	0.1329	0.1925	0.1367	0.2065
	2	0.3422	0.1241	0.1889	0.1242	0.2205
	3	0.2878	0.1559	0.1787	0.1603	0.2173
	4	0.3369	0.1453	0.1818	0.1378	0.1982
	5	0.3527	0.1267	0.2307	0.097	0.1930
	6	0.3234	0.1466	0.1980	0.1358	0.1962
	7	0.2879	0.1714	0.1846	0.1575	0.1986
	8	0.3337	0.1495	0.1934	0.1444	0.1790
	9	0.3609	0.1281	0.2064	0.1086	0.1960
	10	0.2841	0.1774	0.1904	0.1573	0.1907
Total biovolume	1	0.3337	0.1179	0.1771	0.1910	0.1804
	2	0.3953	0.0967	0.1864	0.1802	0.1414
	3	0.4198	0.0933	0.1650	0.1551	0.1668
	4	0.4420	0.0645	0.1922	0.1503	0.1509
	5	0.3303	0.1193	0.1844	0.1868	0.1793
	6	0.3922	0.0873	0.1867	0.1712	0.1626
	7	0.3358	0.1236	0.1880	0.1763	0.1762
	8	0.3158	0.1423	0.1739	0.1929	0.1752
	9	0.3889	0.1070	0.1881	0.1608	0.1552
	10	0.3401	0.1312	0.1761	0.1839	0.1688
Diatoms	1	0.2772	0.1202	0.2096	0.2199	0.1731
	2	0.2835	0.1212	0.2284	0.2139	0.1531
	3	0.3824	0.0888	0.2137	0.1706	0.1445
	4	0.2866	0.0763	0.2492	0.2340	0.1539
	5	0.2117	0.1613	0.2534	0.2178	0.1558
	6	0.3020	0.1038	0.2201	0.2246	0.1494
	7	0.2327	0.1320	0.2331	0.2154	0.1868
	8	0.2638	0.1398	0.2097	0.2013	0.1854
	9	0.2446	0.1602	0.2149	0.1829	0.1974
	10	0.3164	0.1007	0.2336	0.1996	0.1496
Green algae	1	0.4646	0.1305	0.1410	0.1536	0.1103
	2	0.5091	0.0860	0.1188	0.1671	0.1190
	3	0.6711	0.0066	0.1247	0.1113	0.0864
	4	0.5520	0.0493	0.1812	0.1435	0.0741
	5	0.6100	0.0465	0.1500	0.1194	0.0741
	6	0.4661	0.1229	0.0962	0.1620	0.1528
	7	0.5843	0.0388	0.1540	0.1668	0.0561

	8	0.4533	0.0886	0.1611	0.1839	0.1131
	9	0.5683	0.0519	0.1545	0.1697	0.0555
	10	0.5041	0.1036	0.1503	0.1433	0.0987
Cyanobacteria	1	0.3910	0.1030	0.1647	0.1507	0.1906
	2	0.4567	0.0675	0.1292	0.1539	0.1927
	3	0.4175	0.0671	0.1657	0.1596	0.1900
	4	0.4177	0.0818	0.1491	0.1565	0.1948
	5	0.4058	0.0815	0.1710	0.1794	0.1623
	6	0.4392	0.0757	0.1473	0.1574	0.1804
	7	0.3658	0.1165	0.1582	0.1734	0.1861
	8	0.4085	0.0768	0.1473	0.1663	0.2010
	9	0.4377	0.0814	0.1398	0.1610	0.1801
	10	0.4692	0.0685	0.1270	0.1443	0.1911

CHAPTER 3 – RIPARIAN ECOSYSTEMS

Drought-induced flood sensitivity as driver for riparian woodland mortality

3.1 Abstract

Severe drought conditions have occurred throughout the southwestern United States since the start of the Megadrought in 2000. During this period, land managers noticed extensive dieback and mortality of riparian vegetation at sites in Nevada and California, raising the possibility of a link to climate change. Regional synchronicity combined with topographic patterns of woodland mortality indicates phreatophytes might be vulnerable to drought intensification through a previously unknown mechanism. Here, I propose a conceptual model where multi-year drought followed by flooding can be an important driver for riparian woodland mortality. I suggest intense drought affects the ability of riparian vegetation to endure seasonal groundwater fluctuations by reducing shallow root activity. Shallow roots are essential for water uptake during high water tables. However, when a prolonged drought is followed by a wet period, surface roots are unable to sprout rootlets and root hairs quick enough to meet water demands, leading to stress and eventual death. Here, I analyze long-term trends in riparian woodland health at sites in five watersheds in the southwestern United States combined with drought, precipitation, and topographic data. My results indicate riparian woodland mortality may occur globally in regions experiencing intensified drought conditions. This would result in loss of important ecological functions as riparian ecosystems function as biodiversity hotspots, improve water quality, and aid in erosion and flood control.

3.2 Introduction

Intense drought since 2000 has resulted in global forest mortality extending from the tropics to the Arctic (Allen et al., 2010; Hammond et al., 2022). Drought triggers water and heat stress, leading to tissue damage, impaired plant functions, and if sustained over prolonged periods, ultimately death (Teskey et al., 2015; Martinez-Vilalta et al., 2019; Hammond et al., 2019). Recently, public agencies in the southwestern United States reported regional wide dieback and mortality of riparian woodlands (Stephens, 2022), here defined as vegetated areas along waterbodies, dominated by screwbean mesquite, *Prosopis pubescens*, and tamarisk, *Tamarix ramosissima*. The cause of the die-off remains unknown and cannot readily be explained through drought stress alone. Riparian woodlands are believed to be buffered from drought as many trees are phreatophytes that contain taproots to access groundwater (Hultine et al., 2020). During drought, their roots grow deeper to follow the declining water table. Gradual groundwater decline therefore poses little stress to these plants (Scott et al., 1999; Williams et al., 2022).

During wet periods, water table rise may induce hypoxia in the root system, which can lead to tree mortality (Visser et al., 2003; Anderegg et al., 2013). Located in floodplains, riparian trees are exposed to flooding and seasonal groundwater fluctuations. Groundwater is generally hypoxic and unable to support oxygen dependent roots (Shimp et al., 1993). Roots therefore do not grow into groundwater but stay near the capillary fringe (Fan et al., 2017). Groundwater rise during the wet season submerges the lower part of the root structure (Canham et al., 2012). Roots submerged in groundwater are physiologically inactive due to oxygen stress and do not take up water (Dawson and Pate, 1996; Williams and Cooper, 2005). During wet periods, surface roots take up infiltrating water from precipitation and flooding (Canham et al., 2012; Fan et al., 2017). This gives rise to a dimorphic root system where root water uptake comes from surface roots during high water tables and from deeper roots during low water tables.

This unique root system thus protects phreatophytes against plant stress from seasonal groundwater fluctuations. I hypothesize that intense drought weakens this ability to deal with groundwater

fluctuations, leading to the observed mortality. Intense drought can damage shallow roots due to prolonged exposure to dry and hot soil, similarly to how roots of non-riparian trees are damaged by drought (e.g., Cuneo et al., 2016). Shallow root damage will not manifest in shoot stress during drought, as water uptake comes primarily from the deep root system near the water table. Instead, stress occurs when a multi-year drought is followed by a wet period. When water tables are high, damaged surface roots cannot take up water. At this time, both the lower and upper parts of the root system are inactive, causing major water stress, and in some conditions, unrecoverable damage and tree mortality.

To test this hypothesis, I studied the timing, regionality, climatic and topographic control of riparian woodland mortality in the southwestern United States. Based on the proposed hypothesis, riparian plant health is expected to remain stable during drought, with major declines in plant health occurring when a multi-year drought is followed by a wet period. Die-off is expected to occur simultaneously within a region but to be controlled by climatological differences between regions. Within a watershed, topography is expected to control die-off where low laying areas are more susceptible to flooding and die-off.

3.3 Methods

I studied drought-flooding stress as potential driver for riparian woodland mortality at eight study sites in California, Nevada, Arizona, and New Mexico through analysis of remotely sensed vegetation index and climatological data, combined with topographic and root structure data.

3.3.1 Study location

Riparian woodland mortality was studied at sites in Ash Meadows and Shoshone in California, along the Muddy River and the lower Virgin River in Nevada, along the Gila River in Arizona, and along the Rio Grande in New Mexico (Fig. 3.1). While all locations experience hot summer and mild winters,

precipitation regimes differ. California and Nevada experience most precipitation in winter, whereas most precipitation in Arizona and New Mexico occurs during the summer monsoon (Fig. S3.1). Riparian woodlands in Ash Meadows and Shoshone are dominated by screwbean mesquite, *Prosopis pubescens*, honey mesquite, *Prosopis glandulosa*, and leather-leaf ash, *Fraxinus velutina*. Riparian woodlands along the Muddy and Virgin Rivers are primarily dominated by tamarisk, *Tamarix ramosissima*. Riparian woodlands along the Gila River and the Rio Grande contained screwbean mesquite (GBIF.org, 2022, accessed 10/14/2022).

Ash Meadows and Shoshone are part of the Amargosa River Basin, which originates north of Beatty, NV and flows approximately 240 km south and west before terminating in Badwater Basin, Death Valley, CA (Belcher et al., 2019). The river flows perennially only at parts fed by springs; most of the reaches are characterized by subsurface flow (Zdon, 2014) and soil profiles typically range from (fine) sandy loam to silty clay loam (Soil Survey Staff, 2024). The average annual precipitation in this area is 130 mm for 1981-2010 (103 mm for 2000-2021) (Western Regional Climate Center, 2023b). The Virgin River originates north of Zion Canyon, UT, and flows approximately 270 km southwest before terminating in Lake Mead, NV. The Virgin River is partly snow-fed from mountains in Utah, and experiences large fluctuations in streamflow seasonally. Soil profiles in the lower Virgin River typically range from fine sand to silty clay loam (Soil Survey Staff, 2024). The Muddy River is a spring-fed system connected to an extensive groundwater system. The river is approximately 50 km long and terminates in Lake Mead, NV. Soil profiles typically range from fine sandy loam to silty clay (Soil Survey Staff, 2024). Average annual precipitation for the Virgin and Muddy Rivers is 128 mm for 1981-2010 (108 mm for 2000-2021) for Overton, NV (Western Regional Climate Center, 2023a). The Gila River is a 1,044 km long tributary of the Colorado River, originating in western New Mexico. The average annual precipitation in Gila Bend, AZ, near the Gila River study location is 179 mm for 1981-2010 (Western Regional Climate Center, 2024). The Rio Grande is a major North American river, 3,051 km long,

originating in southern Colorado. The average annual precipitation at Las Cruces, NM, near the southern Rio Grande study location is 230 mm (Hendrickx and Walker, 2017).

Study locations were selected based on riparian woodland size, presence of woodland mortality, and dominant tree species, which was validated through fieldwork for sites in California and Nevada (Ash Meadows, Shoshone, Tecopa, Virgin River, Muddy River). Sites in Arizona and New Mexico (Gila River, Rio Grande) were selected using online herbarium data of screwbean mesquite (GBIF.org, 2022, accessed 10/14/2022). At each study location, individual sites were selected for remote sensing analysis ensuring full tree coverage on 30 x 30 m plots (Table S3.1).

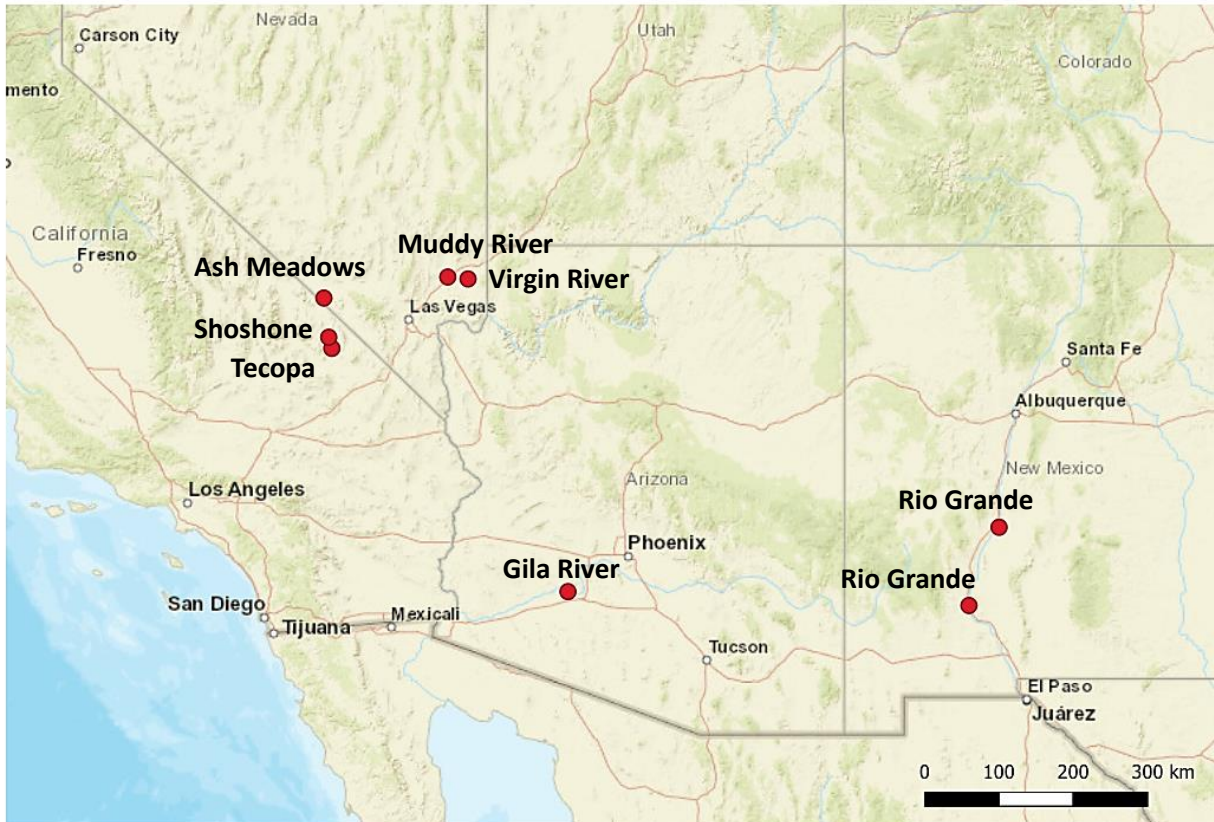


Figure 3.1. Study locations at Ash Meadows and Shoshone along the Amargosa River in California/Nevada, the Virgin River in Nevada, the Gila River in Arizona, and the Rio Grande in New Mexico.

3.3.2 Remote sensing

To test the hypothesis that woodland mortality occurred simultaneously throughout the southwestern United States, I analyzed trends in Normalized Difference Vegetation Index (NDVI) at 48 study sites between 1993-2023. Results of this analysis will identify long-term trends in NDVI and determine the timing of woodland mortality. NDVI is calculated from the ratio between near-infrared (NIR) and red reflection from vegetation and surfaces (Running, 1990; Myneni et al., 1995) (Eq. 3.1),

$$NDVI = \frac{NIR-Red}{NIR+Red} \quad (\text{Equation 3.1})$$

with NDVI values ranging from -1 to 1, where negative values indicate water, values near zero indicate bare soil, and values close to 1 represent healthy, green vegetation (Jones and Vaughan, 2010). NDVI is correlated to plant greenness and used as an indicator of plant productivity and vegetation health (Meneses-Tovar, 2011). Remotely sensed NDVI provides consistent, temporally, and extensive spatially covering records. It has been widely used to evaluate and map tree mortality (Spruce et al., 2019), and as an early indicator of forest mortality (Byer and Jin, 2017; Rogers et al., 2018; Liu et al., 2019). More specific to riparian vegetation, remote sensing has been used to study relationships between NDVI and changes in groundwater level (Aguilar et al., 2012), groundwater flow discharge (Petus et al., 2012), and surface water flooding (Fu and Burgher, 2015).

In this study, Landsat NDVI was used due to its high spatial resolution (30m), allowing for superior trend detection compared to moderate and coarse scale imagery (Ju and Masek, 2016). NDVI data for each study site was downloaded using the web application Climate Engine, that uses the cloud-computing platform of Google Earth Engine to download and visualize remote sensing data (Huntington et al., 2017). Mean NDVI was calculated for each year during the northern growing season (April 1 – October 31) using a data acquisition interval of eight days. NDVI values of different sites were normalized (Eq. 3.2) to allow for direct comparison between sites,

$$Z = \frac{x - \mu}{\sigma} \quad (\text{Equation 3.2})$$

where Z is the normalized value, x the NDVI value (annual average for Apr 1 to Oct 31), μ mean NDVI value between 1993-2023, and σ the standard deviation. Positive values indicate years of above average NDVI, whereas negative values indicate years of below average NDVI.

3.3.3 Statistical analyses

3.3.3.1 Trend analysis

To test the hypothesis that riparian woodland NDVI has decreased over the last decades, I calculated trends using the seasonal Mann-Kendall test. Trend tests were carried out using a significance level of 95% using the *kendallSeasonalTrendTest* function of the EnvStats package (v2.8.1; Millard, 2013).

3.3.3.2 Regression tree analysis

To test the hypothesis that woodland mortality occurs when a multi-year drought is followed by a wet period, I analyzed the relationship between NDVI, drought index, and annual precipitation using regression tree analysis. The results of this analysis will show how drought and precipitation impact NDVI and identify threshold values of input variables. Regression trees explain variation in the output variable by splitting up input variables to minimize the sum of squares in each group of the split (De'ath and Fabricius, 2000). Examples of this methodology can be found in (Valiya Veettil and Mishra, 2020; Beigaitė et al., 2022; Veettil and Mishra, 2023), as well as responses of riparian vegetation NDVI to climate (Fu and Burgher, 2015). Regression tree analysis was carried out in Rstudio using the *ctree* function of the partykit package (Hothorn and Zeileis, 2015; v1.2-20).

Model input data consisted of drought index and precipitation, and output data was defined as NDVI trend. NDVI trends were calculated as percentage NDVI increase or decrease between the prior year and year of interest. Data for model construction was split into a training, testing, and hyperparameter optimization dataset using a 50%, 20%, 30% split, respectively, to minimize overfitting

(Lever et al., 2016; Chicco, 2017). Hyperparameter optimization was carried out to determine the minimum significance level required for splits and maximum tree depth, using the *train* function of the *caret* package (Kuhn, 2008; v6.0-94). Correlation between NDVI, drought, precipitation, and the effect of time lag on correlations was calculated using Spearman correlation analysis (Spearman, 1961). Analysis was carried out using significance levels of 0.01 and 0.05 in RStudio (v4.2.2; R Core Team, 2022) using the function *cor*.

Sources for precipitation data were a weather station in Pahrump, NV (Western Regional Climate Center, 2023b) for the Amargosa River Basin sites (Ash Meadows, Shoshone, and Tecopa), a weather station in Overton, NV (Western Regional Climate Center, 2023a) for the Muddy and Virgin Rivers sites, and a weather station in Las Cruces, NM (Automated Surface Observing System (ASOS), 2023) for Arizona and New Mexico sites. Drought data was obtained from the U.S. Drought Monitor (USDM) (<https://droughtmonitor.unl.edu/DmData/DataTables.aspx>, accessed 12/20/2023). Drought data used was calculated by the USDM as the Drought Severity and Coverage Index (DSCI) to convert categorical drought severity data to single aggregated values by calculating weighted averages of the percent areas under drought (Akyuz, 2017) (Eq. 3.3),

$$DSCI = 1(D0) + 2(D1) + 3(D2) + 4(D3) + 5(D4) \quad (\text{Equation 3.3})$$

where D0 represents abnormally dry conditions, D1 moderate drought, D2 severe drought, D3 Extreme drought, and D4 Exceptional drought. Drought conditions are defined through input of various hydrological inputs and field observations, such as precipitation, streamflow, temperature and evaporative demand, reservoir levels, and soil moisture.

3.3.4 Topography and groundwater depth

To test the hypothesis that topography controls woodland mortality, I analyzed the relationship of topography to NDVI trends using Digital Elevation Model (DEM) data and past water table fluctuations along the lower Virgin River in Nevada, which is dominated by tamarisk. The results of this analysis will show if die-off is limited to areas susceptible to flooding. High-resolution (1m) DEM data were downloaded from the United States Geological Survey (USGS). DEMs were converted to elevation profiles of river cross sections using QGIS. Elevation profiles were assessed against summer NDVI (Jun 1 to Aug 1) in 2013 in comparison to the 30-year average (1991-2020).

Past groundwater levels were obtained from shallow wells in Ash Meadows (well number 362519116201301 for 1994-1998) and along the Virgin River (well numbers 365349113552201, 365345113552301, 365352113551401, 365349113551701 for 1990-1995) from the USGS. Water table data was compared to monthly precipitation for Las Vegas, Nevada (Station ID GHCND:USW00023169) from the National Oceanic and Atmospheric Administration. While no current shallow well information was available, seasonal groundwater fluctuations and the relationship between water table and precipitation are not expected to have changed.

3.3.5 Root distribution analysis

To test the hypothesis that the root system is divided in an upper and lower root system with the lower root system responsible for root water uptake during low water tables, I analyzed the root distribution of screwbean mesquite, *Prosopis pubescens*, through a tree excavation and a greenhouse experiment. The results of this experiment will show how the plants respond to decreasing water tables and how the roots are positioned with regard to the water table. A mature tree was excavated along the lower Virgin River to verify the presence of a dimorphic root system on May 3, 2023. Three screwbean mesquite seedlings were grown for eight months to study the positioning of the root system for three different scenarios: 1) surface irrigation, 2) a constant water table, and 3) a constant water table for five

months, followed by a receding water table for three months. Seedlings were grown in soil tubes constructed of transparent pvc-pipe of 1 m length and 15 cm diameter. Soil tubes were filled with coarse sand as soil material. Seedlings were grown indoors at room temperature underneath a 1000W full spectrum LED grow light (Giixer) connected to a timer to provide 12 hours of light per day. Constant groundwater levels were ensured through a Marriott bottle/siphon system as illustrated in Jarrell & Virginia (1990) (Fig. S3.2). Water for the experiment was collected from a deep well in North Las Vegas. Seedlings were planted on July 25, 2023 and harvested on March 21, 2024. All seedlings were provided with surface irrigation during the first 6 weeks after planting, to allow for establishment of the root system. To guarantee minimal damage to the root system during harvest, soil columns were cut open and sediment was carefully washed off roots.

3.4 Results

In this study, I constructed a conceptual model to explain observations related to riparian woodland mortality in the southwestern United States. First, I used remotely sensed NDVI data to study the regionality and timing of the mortality. Second, I used regression tree analysis to evaluate the link between woodland mortality, drought index, and precipitation. Third, I investigated the link between mortality and die-off on a local, i.e., floodplain, scale using digital elevation data. Last, I conducted a greenhouse experiment to study the positioning of the root system of screwbean mesquite seedlings in regard to groundwater.

3.4.1 Regionality and timing of riparian vegetation mortality

Vegetation mortality affected screwbean mesquite and tamarisk growing in different watersheds, ranging from snow-fed system of the Virgin River to the spring fed systems of the Amargosa and Muddy River Basins (Fig. 3.2a-e). In all locations, riparian vegetation occupied similar ecohydrological environments with shallow groundwater.

Riparian vegetation at the Nevada and California sites experienced overall significantly decreasing trends in growing season NDVI between 1993-2023 ($p < 0.05$, MK-trend test, Table S3.1). Between 2010-2012, most stands experienced simultaneous die-off, resulting in a sharp decrease in NDVI, to below-average values (Fig. 3.2a-e, S3.3). Tree mortality at different sites occurred in a similar fashion: an initial rapid decrease in tree health in 2011, leading to below average values in 2012 that persisted and showed no rebounds the years after. Absolute declines in NDVI were larger for tamarisk (Fig. S3.4d-f) compared to screwbean mesquite (Fig. S3.4a-c).

Riparian vegetation at the Arizona and New Mexico sites did not experience significant decreasing trends in NDVI between 1993-2023 ($p > 0.05$, MK-trend test, Table S3.1). While riparian vegetation at the Arizona and New Mexico sites showed inter-annual variations in NDVI, they did not experience regional wide die-off between 2010-2012 (Fig. 3.2f; S3.3).

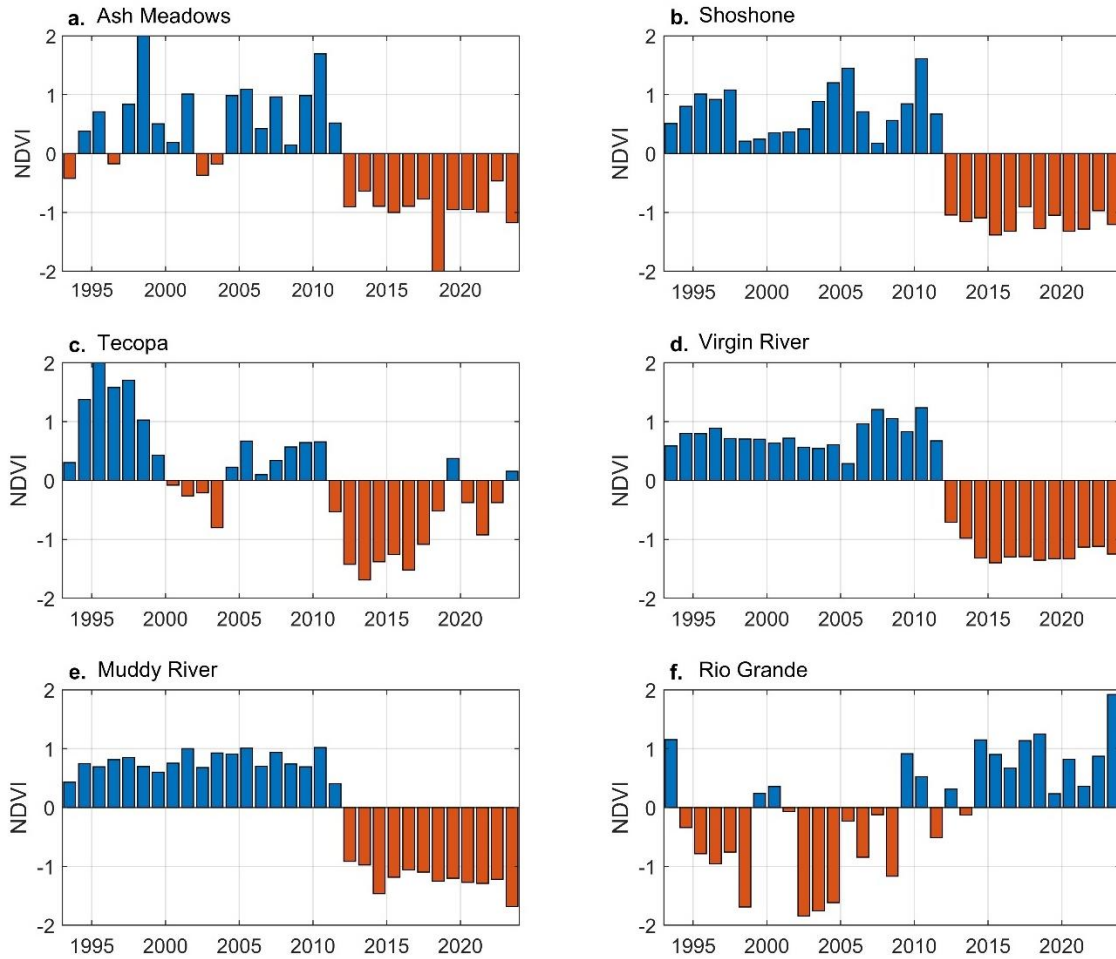


Figure 3.2. Annual average normalized NDVI during the growing season (Apr 1-Oct 31) for areas experiencing riparian woodland mortality along the Amargosa River in **a.** Ash Meadows, **b.** Shoshone, and **c.** Tecopa, and along the **d.** Virgin, and **e.** Muddy Rivers, compared to vegetation along the **f.** Gila River in New Mexico. Sites in Nevada and Arizona (a-e) show rapid decrease in NDVI values between 2010-2012, which was absent from the Rio Grande. Sites a-c were dominated with screwbean mesquite, sites d-e with tamarisk.

3.4.2 Climatic control

Regional wide NDVI declines in riparian vegetation health were observed at the end of drought-flood cycles. Multi-year drought occurred between 2002-2005, 2007-2010, and 2012-2016 (Fig. 3.3c).

The three wettest water years since 2000 occurred in 2005, 2011, and 2016/17, all being significantly

wetter than average water year precipitation ($p < 0.01$ for Amargosa and Virgin rivers, one-sided t-test) (Fig. 3.3b). Rapid NDVI declines were identified between 2005-2007 and 2010-2012 (Fig. 3.3a). NDVI declines occurred directly after a drought-wet cycle. Rapid, unrecoverable declines in riparian vegetation health were absent from riparian woodlands at Arizona and New Mexico sites, where annual precipitation was higher and more constant, and drought cycles were more truncated (Fig. S3.5).

The majority of observed riparian woodland mortality at sites in Nevada and California occurred during the 2010-2012 die-off event (Fig. 3.2). The earlier event of 2005-2007 resulted in a sharp decrease in NDVI for Shoshone (Fig. 3.3a) but did not result in observable die-off; NDVI levels recovered to during the next two years. As most riparian woodlands die-off and dieback occurred between 2010-2012, subsequent die-off occurred only at a smaller scale, slowly increasing the total area of mortality. Die-off after the 2010-2012 event was observed in Ash Meadows, where certain stands died after 2015 (Fig. S3.6a).

Riparian woodland stands at Lake Mohave along the Colorado River, 130 km south from the Virgin River stand showed no mortality event between 2010-2012 (Fig. S3.6b). Here, water level was regulated by water released from the Hoover dam upstream and no water level increase was observed in 2010-2011 compared to other years (U.S. Geological Survey, 2023).



Figure 3.3. Climatic variables in relation to the regional wide die-off event of screwbean mesquite, shown by the red shaded area. **a.** Average annual normalized NDVI for the growing season (Apr-Oct) in Shoshone (Sho 2 site), CA, showing rapid decrease in NDVI between 2010-2012. **b.** Monthly precipitation for Pahrump, CA, showing a peak in precipitation occurred right before the die-off event in December 2010. **c.** Average drought severity and coverage index for counties experiencing die-off (Clark, Inyo, and Nye counties), where 0 means none of the area is experiencing drought, and 500 means the entire area is in exceptional drought.

Regression tree analysis was used to identify threshold values for drought index and annual precipitation that could drive NDVI declines for sites in California and Nevada combined (Fig. 3.4). Through hyperparameter optimization, a minimum significance level of 0.9 and maximum tree depth of

three was identified. Precipitation was the first splitting node, indicating it is the most important variable for predicting NDVI trends (Fig. 3.4). Negative NDVI trends were observed when annual precipitation was larger than 115.8 mm and drought index was higher than 311.1, indicating severe drought conditions (nodes 10 and 11) combined with above average rainfall. Negative NDVI trends were also observed for precipitation below 115.8 mm with drought index between 205.7 - 226.7 (node 5). The 23 observations in this node were further identified as years precipitation between 83.5 – 110.0 mm (Table S3.2).

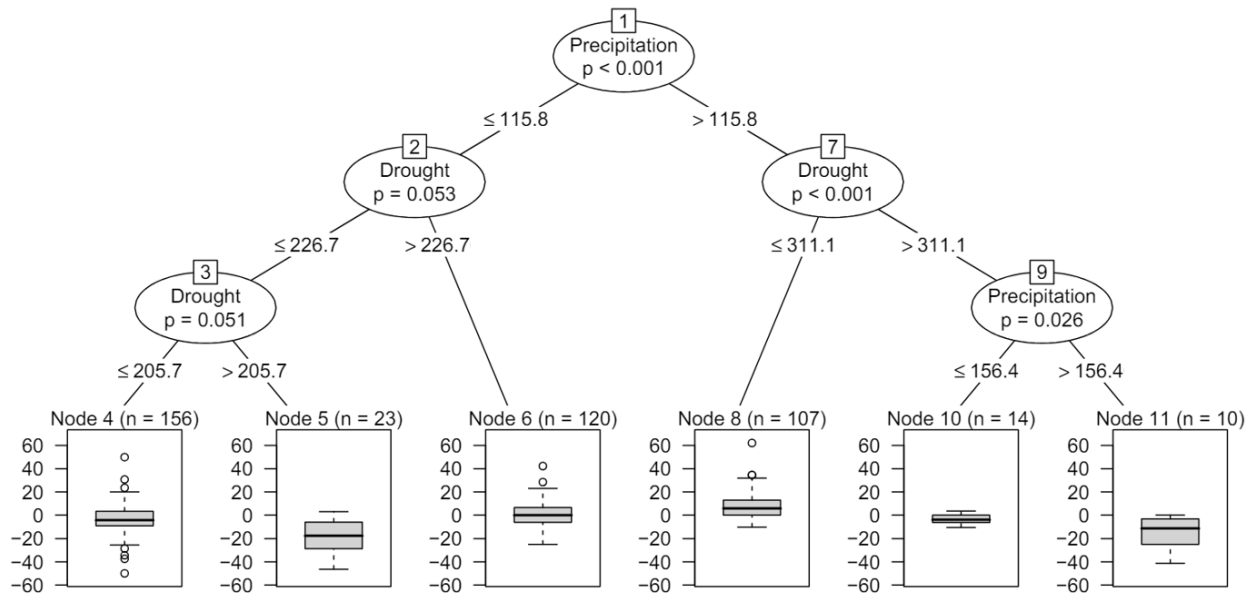


Figure 3.4. Regression tree showing classification of NDVI trends based on mean annual drought index and mean annual precipitation. Precipitation was identified as the most important predictor determining trends in NDVI, with negative trends (Nodes 10 and 11) occurring when precipitation was above 115 mm combined with severe drought (drought index > 311).

3.4.3 Groundwater fluctuations and topographic control on woodland mortality

Historical well data along the Amargosa and Virgin Rivers was analyzed to understand groundwater dynamics at research sites in California and Nevada. Data showed seasonal and inter-annually fluctuating water tables (Fig. 3.5). Highest water tables occurred at the beginning of the growing season, between March and April. Lowest water tables occurred at the end of the growing season, between August and September. Water tables fluctuated up to 0.6m and 1.6m seasonally along the Virgin and Amargosa Rivers, respectively. Interannual variations in water table driven by drought and flood cycles were superimposed on the seasonal fluctuations. 1992 was one of the wettest years in southern Nevada (Las Vegas) with annual precipitation of 251 mm compared to the average of 106 mm (National Weather Service, 2024). Water tables along the Virgin River peaked the following year, in 1993, with water table maxima 0.8m higher compared to the maxima in 1992 (Fig. 3.5b). As such, at this location during non-drought conditions, doubling precipitation raised the water table by 0.8 m the following year.

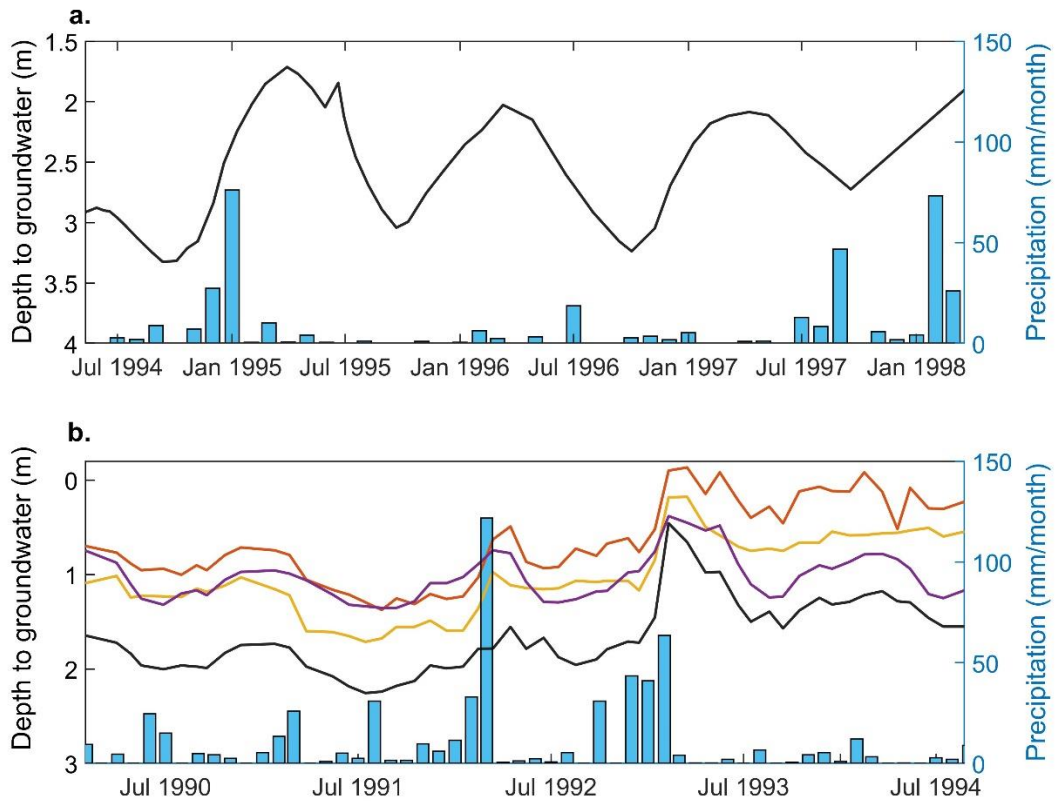


Figure 3.5. Monthly depth of water table and monthly precipitation in **a.** Ash Meadows, Amargosa River Basin from 1994-1998, and **b.** along the Virgin River near Littlefield, Arizona from 1990-1995, showing inter-annual variations in maximum and minimum depth to water table, as well as seasonal fluctuations where highest groundwater levels occur in spring at the beginning of the growing season and lowest levels occur at the end of the growing season.

Tamarisk-dominated riparian vegetation on low-laying areas along the Lower Virgin River showed large NDVI decreases during the 2010-2012 die-off event. At the same time, riparian vegetation at the outer (higher elevation) edge of the floodplain showed no signs of vegetation stress (Fig. 3.6; S3.7).

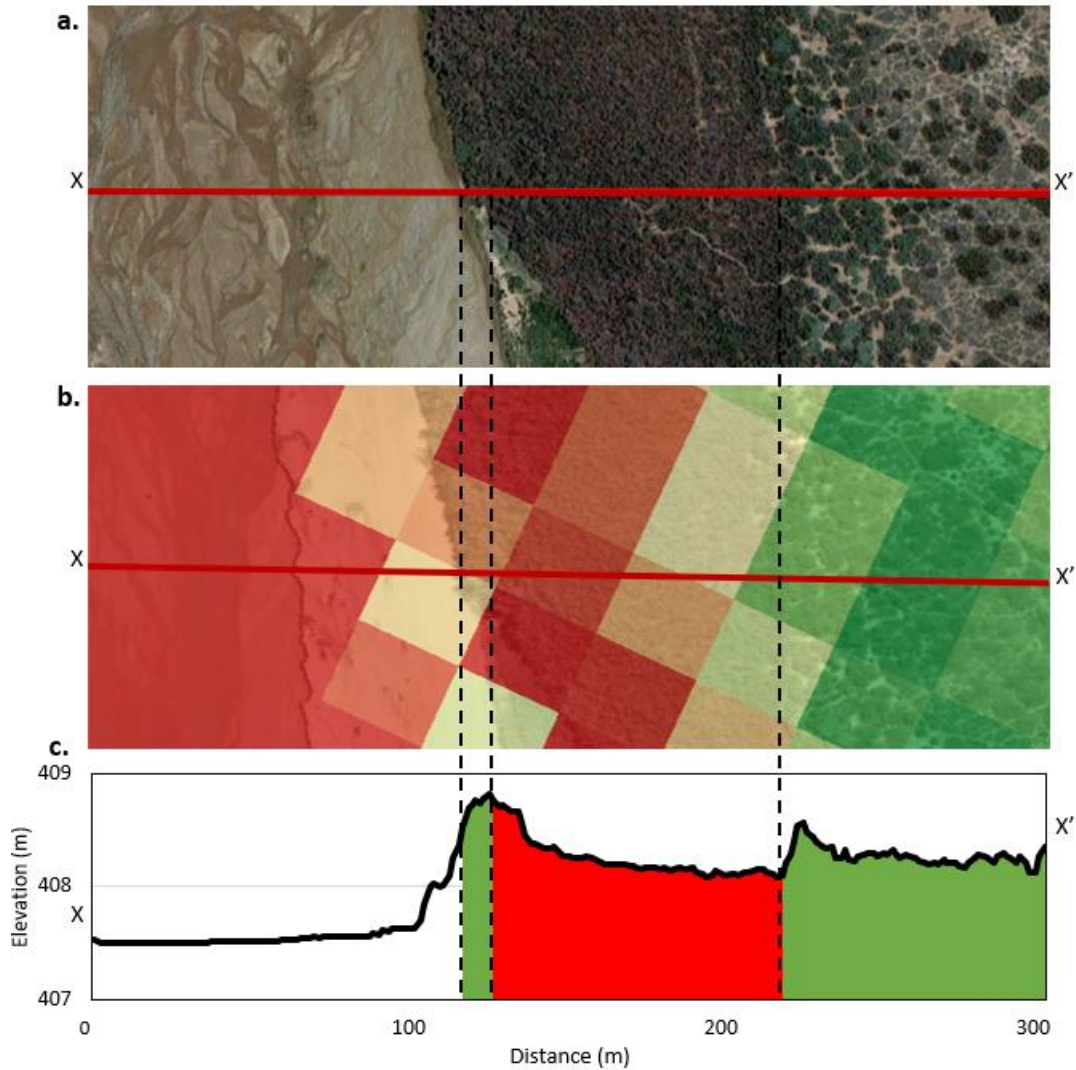


Figure 3.6. Tamarisk-dominated riparian vegetation along the lower Virgin River showing a gradient in tree mortality when moving away from the river, Google Earth imagery 05/2013, **b.** Summer (Jun 1 – Aug 1) NDVI in 2013 compared to the 30-year average (1991-2020), where red indicated values lower than average, green higher than averages and white no change. **c.** Elevation transect showing die-off is limited to topographic lows, where flood water accumulates. Green represents areas where vegetation is not stressed, red represents stressed vegetation.

3.4.4 Root distribution analysis

The root structure of screwbean mesquite was consistent with previous literature indicating the presence of a dimorphic root system of shallow lateral roots and deeper taproots accessing groundwater (Fig. S3.8). A greenhouse experiment with seedlings on varying groundwater levels showed dependence of the root structure on water tables (Fig. 3.7). The deepest root profile was observed at the seedling that only received surface irrigation. Most root biomass existed in the upper (20 cm) soil layer, with a single root extending to the bottom of the soil column at 70 cm depth. The shallowest root profile was observed at the seedling grown on a constant water table. The root profile displayed a larger lateral spread with roots ending at or slightly above (in the capillary fringe) the water table. The largest root profile was observed at the seedling grown on a constant water table for half of the experiment, and a slowly receding water table during the last half. Most root biomass was present in the first 40 cm of the soil, with several roots extending down towards the receding water table.

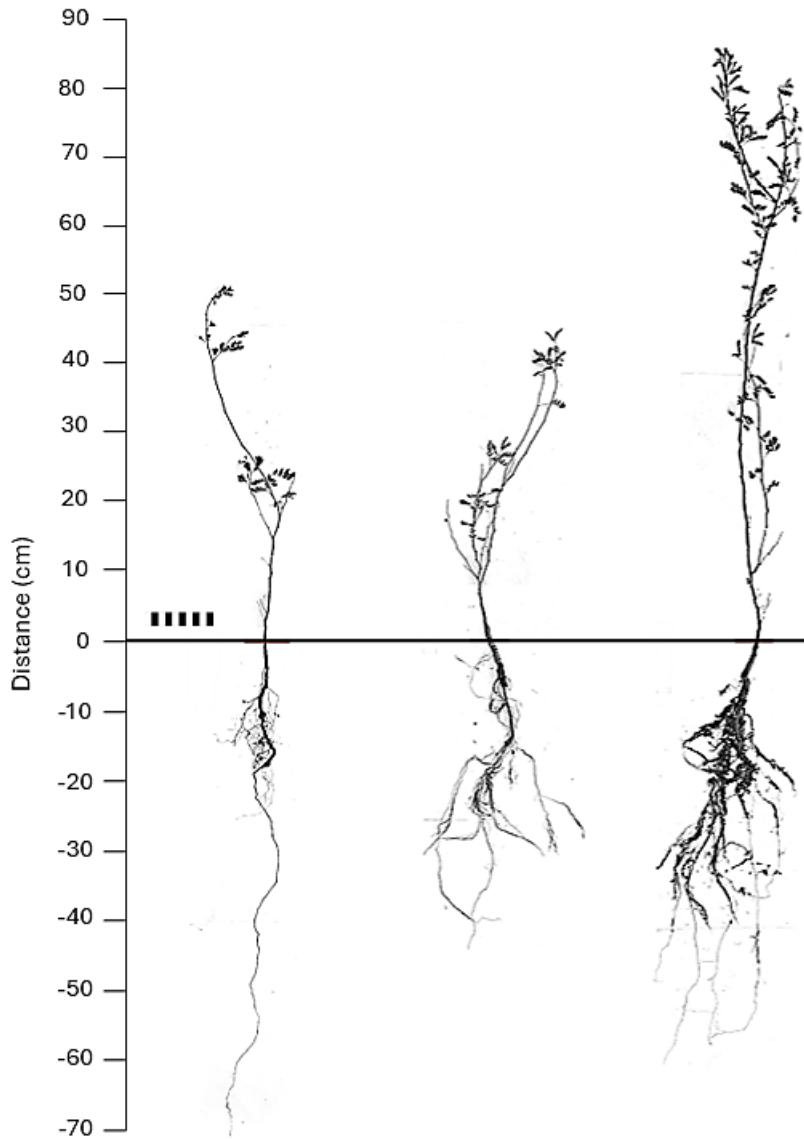


Figure 3.7. Root structure of three screwbean mesquite seedlings, grown on coarse sand with limited capillary rise on three different water table scenarios: 1) surface irrigation (left), 2) a constant water table at 40 cm depth (middle), and 3) a constant water table at 40 cm depth for 4 months, then a slowly receding water table to 60 cm depth (right). Scale bar represents 10 cm.

3.5 Discussion

Timing, regionality, and topographic control of vegetation mortality suggest riparian woodlands in the southwestern United States are not spared from the effects of intensified drought. Unlike non-riparian vegetation which suffer large areal mortality during a drought, riparian woodlands manifest mortality after the drought ends, during the wet pulse that follows. Based on my analyses, I suggest a conceptual model where exposure to intensified drought impacts the ability of riparian trees to survive flooding.

3.5.1 Conceptual model

Root water uptake in the riparian environment is dominated by deep or surface roots depending on groundwater level. Water uptake originates from deep roots near groundwater when water tables are low (Fig. 3.8a). Oppositely, water uptake originates from surface roots when water tables are high (Fig. 3.8b). During this time, the lower root system is submerged in hypoxic groundwater and is inactive due to oxygen stress. The positioning of the root system in regard to the water table, and therefore oxygen concentrations, was confirmed for screwbean mesquite seedlings (Fig. 3.7). The root system was partitioned in surface roots and deeper roots extending to the water table. Intensified drought can decrease surface root activity through heat and water stress, similar to how surface roots of non-riparian trees are damaged (Teskey et al., 2015; Martinez-Vilalta et al., 2019; Hammond et al., 2019). Plant health remains stable during drought, as water uptake is satisfied by deep roots near the water table (Fig. 3.8c). However, high water tables after drought cause both upper and lower root system to be inactive, resulting in die-off when sustained long enough (Fig. 3.8d).

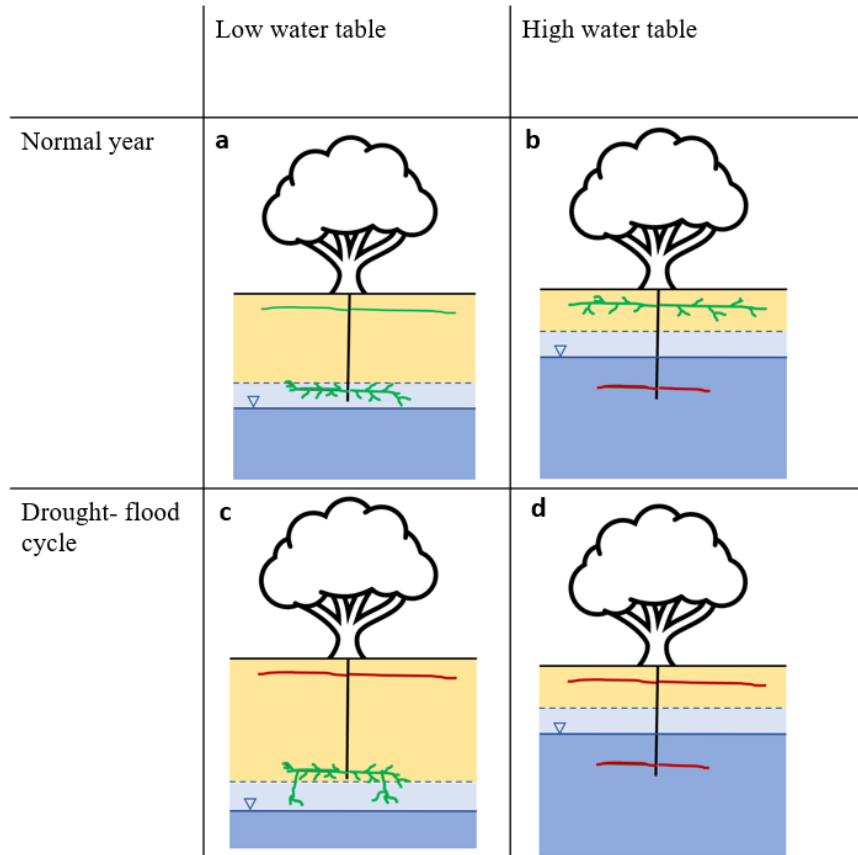


Figure 3.8. Conceptual model of the relationship of the upper (near surface) and lower (near groundwater) root system of groundwater dependent vegetation on **a.** low and **b.** high water tables during a normal year, and on **c.** low and **d.** high water tables after a multi-year drought. Hypothesized root activity is shown as green roots indicating active roots, and red roots indicating physiological inactive roots.

Drought and heat stress can reduce or cease surface root water uptake. While the exact cause remains unknown, drought could decrease surface root water uptake through significantly reducing root hairs (Williams and Cooper, 2005), or affect the functioning of woody roots through for example suberin formation. Suberin is a hydrophobic biopolymer that has been associated with drought response to reduce water loss through roots. However, it also stops water from entering root cells during wet conditions, delaying reactivation which is critical for plant survival during high water tables (Enstone et al., 2002;

Bernards, 2002). Heavily suberized roots were observed in the upper root structure of tamarisk along the Lower Virgin River, from which it took 4-5 weeks for new white roots to be grown (D.A. Devitt, personal communication, May 15, 2024).

The proposed conceptual model is supported by previous studies who confirmed inactivity of shallow roots during dry conditions. Williams and Cooper (2005) studied two stands of cottonwoods, *Populus deltoides*, which are phreatophytes. One stand was located along an unregulated river with frequent floods, the other stand along a regulated river without floods. They noticed upper root dieback in the regulated river stand, in response to dry upper soils, which prevented the trees from responding to temporary increases in soil moisture from an artificial flood. Likewise, Donovan and Ehleringer (1994) found no response of shrubs to summer rains, indicating shallow root dormancy. Reduced shallow root activity during low water tables will not cause major stress in riparian vegetation as deep roots are responsible for water uptake. Instead, stress occurs when water tables are high.

After multi-year drought, damaged shallow roots cannot quickly grow rootlets and root hairs needed for root water uptake. When a wet year follows a drought cycle, water tables can quickly rise to maximum levels higher than observed during preceding years. For example, doubling of precipitation along the Virgin River during non-drought conditions raised the water table up to 0.8 m (Fig. 3.5), although a smaller water table rise is predicted after a drought cycle due to reduced soil moisture. During high water tables, the plant will be unable to meet its water demands, causing stress, and, if sustained, eventual death (Fig. 3.8d). The proposed drought-flood mechanism can explain observations related to riparian woodland mortality, such as timing, regionality, and topographic control.

3.5.2 Timing die-off after a dry-wet cycle

Pronounced NDVI reductions occurred simultaneously at sites in Nevada and California during a wet period that followed severe multi-year drought (Fig. 3.2-4). Most die-off occurred between 2010-

2012, following the 2007-2010 drought and the wet water year of 2011. However, not all drought-flood cycles resulted in die-off as riparian vegetation could recover from damages caused by the event. For example, NDVI rapidly decreased between 2005-2007, but quickly recovered to levels observed before the NDVI decline in the years after (Fig. 3.3). The 2005-2007 drought might not have damaged the surface root structure to such an extent that vegetation could not recover.

3.5.3 Regionality of riparian woodland mortality

Riparian woodland mortality occurred at sites in winter precipitation dominated regions but was absent from sites in monsoon dominated regions (Fig. 3.2; S3.1). Surface root damage occurs in summer when the soil is dry and hot. As such, surface root damage is more likely to occur in winter storm dominated systems where summer are hot and dry than in monsoon dominated systems where summers are wet. If the surface root system is not damaged, a wet period following a multi-year drought will not cause die-off. While die-off is a naturally occurring phenomenon in any forest and woodland, riparian vegetation at sites in Arizona and New Mexico did not experience a regional die-off event in 2010-2012. This is supported by a field study by Cowan et al. (2023) who observed no die-off in screwbean mesquite along the Rio Grande.

3.5.4 Topographic and human control on woodland mortality

Riparian woodland mortality was locally affected by topography. On a local scale, all trees are impacted similarly by drought, yet not all trees are impacted similarly by flooding and groundwater rise. Low-laying areas next to rivers experience most flooding and groundwater rise, whereas vegetation on higher elevation can be spared from most negative effects of groundwater rise (Fig. 3.6). Likewise, Cowan et al. (2023) observed trees experiencing dieback were located closer to perennial surface water

compared to trees that did not experience dieback. Additionally, plant density and soil hydraulic properties could influence water table dynamics but were not tested here.

Riparian woodland mortality can also be affected by human controls. This can prevent mortality in areas where die-off would otherwise be expected to occur. For example, riparian vegetation at Lake Mohave, a reservoir on the Colorado River along the border of Nevada and Arizona, did not show stress during any of the identified die-off events between 2000-2022 (Fig.S3.5b). Apart from runoff from surrounding mountains, water levels in Lake Mohave are controlled by water released from upstream Lake Mead. Water levels are therefore more stable than for example the Virgin and Muddy Rivers, which are undammed. The lack of rapid water rise in Lake Mohave ensured the drought-flood sequence did not occur, sparing riparian vegetation from die-off.

3.5.5 Implications and broader impacts

My findings suggest riparian woodland mortality can be caused through a drought-flood sequence. Climate change is predicted to increase the frequency of extreme hydrological event occurrences. For example, droughts are predicted to become more intense and longer lasting (Williams et al., 2019; Overpeck and Udall, 2020), and precipitation events to become more erratic, leading to increased frequency of flooding (Swain et al., 2018). This increases the chance a drought-flood sequence occurs that will cause regional wide riparian woodland mortality. Changes in extreme hydrological events are not limited to the United States. For example, the Amazon region has experienced increasing droughts and floods (Marengo and Espinoza, 2016), as well as Australia (Moore, 2012).

Large-scale tree mortality can also be caused by biological factors such as pathogens and insect outbreaks. For example, outbreaks of species of bark beetles have been shown to cause widespread mortality in pine forests (Dobbertin et al., 2007; Creeden et al., 2014). Likewise, tamarisk die-off along the Virgin River has been attributed to the tamarisk beetle, *Diorhabda* spp, which arrived at the lower

Virgin River in 2009 (Liebert et al., 2016), and defoliation of tamarisk coincided with NDVI declines. Additionally, screwbean mesquite die-off has been attributed to the fungus, *Neoscytalidium dimidiatum* (Cowan et al., 2023). However, observations of die-off cannot be explained by biological origin solely. For example, not all vegetation in an area is affected, as shown by the topographic control on die-off (Fig. 3.6). It is possible the insect or canker was only successful on previously weakened vegetation, as indicated by rapid declines in growing season NDVI. Climate change can increase the distribution of pathogens and invasive species (Dukes et al., 2009). While biological factors are expected to be a secondary cause to riparian woodland mortality, they can increase the likelihood a weakened tree dies instead of recovers after a drought-flood cycle.

Increased riparian woodland mortality might be a global phenomenon in arid environments experiencing intensified drought conditions. Woodland mortality can negatively impact riparian ecosystems as they function as biodiversity hotspots, harboring a disproportionately high biodiversity for their limited size (Stevens et al., 1977; Naiman et al., 1993). Additionally, riparian woodlands improve water quality through filtering of sediments and potential pollutants (Naiman and Décamps, 1997), reduce flooding and erosion by promoting infiltration (Simon and Collison, 2002; Thomas and Nisbet, 2007), and act as long-term carbon sinks (Cierjacks et al., 2010). Going forward, additional changes in this small yet important ecosystem should therefore not be overlooked.

3.6 Conclusion

Riparian woodland mortality in the southwestern United States suggests this ecosystem is more susceptible to climate change than previously believed. Here, I introduced a mechanism explaining the timing, regional, and local occurrences of mortality through a sequence of extreme hydrological events: intense drought and flooding. Drought affects the ability of riparian vegetation to handle large seasonal variations in groundwater depth, through reducing shallow root activity. Shallow roots are essential for root water uptake during high water tables; reduced shallow root activity therefore leads to stress and

mortality if sustained over many years. Tree mortality is expected to occur more frequently in riparian ecosystems worldwide following increases in drought duration and intensity, and precipitation extremes. Loss of dominant tree species will negatively impact riparian ecosystems as riparian woodlands harbor a large biodiversity, improve water quality, and aid in erosion and flood control.

3.7 References

- Aguilar, C., Zinnert, J.C., Polo, M.J., and Young, D.R., 2012, NDVI as an indicator for changes in water availability to woody vegetation: *Ecological Indicators*, v. 23, p. 290–300, doi:<https://doi.org/10.1016/j.ecolind.2012.04.008>.
- Akyuz, F.A., 2017, Drought Severity and Coverage Index: United States Drought Monitor, <https://droughtmonitor.unl.edu/About/AbouttheData/DSCI.aspx>.
- Allen, C.D. et al., 2010, A global overview of drought and heat-induced tree mortality reveals emerging climate change risks for forests: *Forest Ecology and Management*, v. 259, p. 660–684, doi:<https://doi.org/10.1016/j.foreco.2009.09.001>.
- Anderegg, W.R.L., Kane, J.M., and Anderegg, L.D.L., 2013, Consequences of widespread tree mortality triggered by drought and temperature stress: *Nature Climate Change*, v. 3, p. 30–36, doi:[10.1038/nclimate1635](https://doi.org/10.1038/nclimate1635).
- Automated Surface Observing System (ASOS), 2023, Station Las Cruces International, New Mexico:, https://mesonet.agron.iastate.edu/request/download.phtml?network=NM_ASOS (accessed December 2023).
- Beigaitė, R., Tang, H., Bryn, A., Skarpaas, O., Stordal, F., Bjerke, J.W., and Žliobaitė, I., 2022, Identifying climate thresholds for dominant natural vegetation types at the global scale using machine learning: Average climate versus extremes: *Global Change Biology*, v. 28, p. 3557–3579, doi:<https://doi.org/10.1111/gcb.16110>.
- Belcher, W.R., Sweetkind, D.S., Hopkins, C.B., Poff, M.E., and Survey, U.S.G., 2019, Hydrogeology of Lower Amargosa Valley and groundwater discharge to the Amargosa Wild and Scenic River, Inyo and San Bernardino Counties, California, and adjacent areas in Nye and Clark Counties, Nevada:, doi:[10.3133/sir20185151](https://doi.org/10.3133/sir20185151).
- Bernards, M.A., 2002, Demystifying suberin: *Canadian Journal of Botany*, v. 80, p. 227–240, doi:[10.1139/b02-017](https://doi.org/10.1139/b02-017).
- Byer, S., and Jin, Y., 2017, Detecting Drought-Induced Tree Mortality in Sierra Nevada Forests with Time Series of Satellite Data: *Remote Sensing*, v. 9, doi:[10.3390/rs9090929](https://doi.org/10.3390/rs9090929).
- Canham, C., Froend, R., Stock, W., and Davies, M., 2012, Dynamics of phreatophyte root growth relative to a seasonally fluctuating water table in a Mediterranean-type environment: *Oecologia*, v. 170, doi:[10.1007/s00442-012-2381-1](https://doi.org/10.1007/s00442-012-2381-1).
- Chicco, D., 2017, Ten quick tips for machine learning in computational biology: *BioData Mining*, v. 10, p. 35, doi:[10.1186/s13040-017-0155-3](https://doi.org/10.1186/s13040-017-0155-3).
- Cierjacks, A., Kleinschmit, B., Babinsky, M., Kleinschroth, F., Markert, A., Menzel, M., Ziechmann, U., Schiller, T., Graf, M., and Lang, F., 2010, Carbon stocks of soil and vegetation on Danubian

- floodplains: *Journal of Plant Nutrition and Soil Science*, v. 173, p. 644–653, doi:<https://doi.org/10.1002/jpln.200900209>.
- Cowan, J., Grady, K., and Updike, C., 2023, Screwbean Mesquite Health Monitoring: EcoCulture.
- Creeden, E.P., Hicke, J.A., and Buotte, P.C., 2014, Climate, weather, and recent mountain pine beetle outbreaks in the western United States: *Forest Ecology and Management*, v. 312, p. 239–251, doi:<https://doi.org/10.1016/j.foreco.2013.09.051>.
- Cuneo, I.F., Knipfer, T., Brodersen, C.R., and McElrone, A.J., 2016, Mechanical Failure of Fine Root Cortical Cells Initiates Plant Hydraulic Decline during Drought : *Plant Physiology*, v. 172, p. 1669–1678, doi:10.1104/pp.16.00923.
- Dawson, T.E., and Pate, J.S., 1996, Seasonal Water Uptake and Movement in Root Systems of Australian Phreatophytic Plants of Dimorphic Root Morphology: A Stable Isotope Investigation: *Oecologia*, v. 107, p. 13–20, <http://www.jstor.org/stable/4221302>.
- De'ath, G., and Fabricius, K.E., 2000, Classification and Regression Trees: a Powerful yet Simple Technique for Ecological Data Analysis: *Ecology*, v. 81, p. 3178–3192, doi:[https://doi.org/10.1890/0012-9658\(2000\)081\[3178:CARTAP\]2.0.CO;2](https://doi.org/10.1890/0012-9658(2000)081[3178:CARTAP]2.0.CO;2).
- Dobbertin, M., Wermelinger, B., Bigler, C., Bürgi, M., Carron, M., Forster, B., Gimmi, U., and Rigling, A., 2007, Linking Increasing Drought Stress to Scots Pine Mortality and Bark Beetle Infestations: *The Scientific World Journal*, v. 7, p. 369535, doi:10.1100/tsw.2007.58.
- Donovan, L.A., and Ehleringer, J.R., 1994, Water Stress and Use of Summer Precipitation in a Great Basin Shrub Community: *Functional Ecology*, v. 8, p. 289–297, doi:10.2307/2389821.
- Dukes, J.S. et al., 2009, Responses of insect pests, pathogens, and invasive plant species to climate change in the forests of northeastern North America: What can we predict?: *Canadian Journal of Forest Research*, v. 39, p. 231–248, doi:10.1139/X08-171.
- Enstone, D.E., Peterson, C.A., and Ma, F., 2002, Root Endodermis and Exodermis: Structure, Function, and Responses to the Environment: *Journal of Plant Growth Regulation*, v. 21, p. 335–351, doi:10.1007/s00344-003-0002-2.
- Fan, Y., Miguez-Macho, G., Jobbágy, E.G., Jackson, R.B., and Otero-Casal, C., 2017, Hydrologic regulation of plant rooting depth: *Proceedings of the National Academy of Sciences*, v. 114, p. 10572–10577, doi:10.1073/pnas.1712381114.
- Fu, B., and Burgher, I., 2015, Riparian vegetation NDVI dynamics and its relationship with climate, surface water and groundwater: *Journal of Arid Environments*, v. 113, p. 59–68, doi:<https://doi.org/10.1016/j.jaridenv.2014.09.010>.
- GBIF.org, 2022, GBIF Occurrence Download for *Prosopis pubescens*, doi:<https://doi.org/10.15468/dl.6qdhjw>.
- Hammond, W.M., Williams, A.P., Abatzoglou, J.T., Adams, H.D., Klein, T., López, R., Sáenz-Romero, C., Hartmann, H., Breshears, D.D., and Allen, C.D., 2022, Global field observations of tree die-off

- reveal hotter-drought fingerprint for Earth's forests: *Nature Communications*, v. 13, p. 1761, doi:10.1038/s41467-022-29289-2.
- Hammond, W.M., Yu, K., Wilson, L.A., Will, R.E., Anderegg, W.R.L., and Adams, H.D., 2019, Dead or dying? Quantifying the point of no return from hydraulic failure in drought-induced tree mortality: *New Phytologist*, v. 223, p. 1834–1843, doi:https://doi.org/10.1111/nph.15922.
- Hendrickx, J.M.H., and Walker, G.R., 2017, Recharge from precipitation, *in* Recharge of phreatic aquifers in (semi-) arid areas, Routledge, p. 19–111.
- Hothorn, T., and Zeileis, A., 2015, partykit: A modular toolkit for recursive partytioning in R: *The Journal of Machine Learning Research*, v. 16, p. 3905–3909.
- Hultine, K.R., Froend, R., Blasini, D., Bush, S.E., Karlinski, M., and Koepke, D.F., 2020, Hydraulic traits that buffer deep-rooted plants from changes in hydrology and climate: *Hydrological Processes*, v. 34, p. 209–222, doi:https://doi.org/10.1002/hyp.13587.
- Huntington, J.L., Hegewisch, K.C., Daudert, B., Morton, C.G., Abatzoglou, J.T., McEvoy, D.J., and Erickson, T., 2017, Climate Engine: Cloud Computing and Visualization of Climate and Remote Sensing Data for Advanced Natural Resource Monitoring and Process Understanding: *Bulletin of the American Meteorological Society*, v. 98, p. 2397–2410, doi:https://doi.org/10.1175/BAMS-D-15-00324.1.
- Jarrell, W.M., and Virginia, R.A., 1990, Response of mesquite to nitrate and salinity in a simulated phreatic environment: Water use, dry matter and mineral nutrient accumulation: *Plant and Soil*, v. 125, p. 185–196, doi:10.1007/BF00010656.
- Jones, H.G., and Vaughan, R.A., 2010, Remote sensing of vegetation: principles, techniques, and applications: Oxford University Press, USA.
- Ju, J., and Masek, J.G., 2016, The vegetation greenness trend in Canada and US Alaska from 1984–2012 Landsat data: *Remote Sensing of Environment*, v. 176, p. 1–16, doi:https://doi.org/10.1016/j.rse.2016.01.001.
- Kuhn, M., 2008, Building predictive models in R using the caret package: *Journal of statistical software*, v. 28, p. 1–26.
- Lever, J., Krzywinski, M., and Altman, N., 2016, Model selection and overfitting: *Nature Methods*, v. 13, p. 703–704, doi:10.1038/nmeth.3968.
- Liebert, R., Huntington, J., Morton, C., Sueki, S., and Acharya, K., 2016, Reduced evapotranspiration from leaf beetle induced tamarisk defoliation in the Lower Virgin River using satellite-based energy balance: *Ecohydrology*, v. 9, p. 179–193, doi:https://doi.org/10.1002/eco.1623.
- Liu, Y., Kumar, M., Katul, G.G., and Porporato, A., 2019, Reduced resilience as an early warning signal of forest mortality: *Nature Climate Change*, v. 9, p. 880–885, doi:10.1038/s41558-019-0583-9.
- Marengo, J.A., and Espinoza, J.C., 2016, Extreme seasonal droughts and floods in Amazonia: causes, trends and impacts: *International Journal of Climatology*, v. 36, p. 1033–1050, doi:https://doi.org/10.1002/joc.4420.

- Martinez-Vilalta, J., Anderegg, W.R.L., Sapes, G., and Sala, A., 2019, Greater focus on water pools may improve our ability to understand and anticipate drought-induced mortality in plants: *New Phytologist*, v. 223, p. 22–32, doi:<https://doi.org/10.1111/nph.15644>.
- Meneses-Tovar, C.L., 2011, NDVI as indicator of degradation: *Unasylva*, v. 62, p. 39–46.
- Millard, S.P., 2013, *EnvStats: An R Package for Environmental Statistics*: New York, Springer, <https://www.springer.com> (accessed January 2024).
- Moore, G.M., 2012, Flooding following Drought: a Swift and Subtle Killer of Stressed Trees, *in* 13th National Street Tree Symposium, Burnley College, University of Melbourne, p. 81–94.
- Myneni, R.B., Hall, F.G., Sellers, P.J., and Marshak, A.L., 1995, The interpretation of spectral vegetation indexes: *IEEE Transactions on Geoscience and Remote Sensing*, v. 33, p. 481–486, doi:10.1109/TGRS.1995.8746029.
- Naiman, R.J., and Décamps, H., 1997, The Ecology of Interfaces: Riparian Zones: *Annual Review of Ecology and Systematics*, v. 28, p. 621–658, doi:10.1146/annurev.ecolsys.28.1.621.
- Naiman, R.J., Decamps, H., and Pollock, M., 1993, The Role of Riparian Corridors in Maintaining Regional Biodiversity: *Ecological Applications*, v. 3, p. 209–212, doi:10.2307/1941822.
- National Weather Service, 2024, *Las Vegas Climate Book*, <https://www.weather.gov/media/vef/Wettest%20and%20Driest%20Months%20Seasons%20and%200Years.pdf> (accessed February 2024).
- Overpeck, J., and Udall, B., 2020, Climate change and the aridification of North America: *Proceedings of the National Academy of Sciences*, v. 117, p. 202006323, doi:10.1073/pnas.2006323117.
- Petus, C., Lewis, M., and White, D., 2012, Using MODIS Normalized Difference Vegetation Index to monitor seasonal and inter-annual dynamics of wetland vegetation in the Great Artesian Basin: A baseline for assessment of future changes in a unique ecosystem: *ISPRS - International Archives of the Photogrammetry, Remote Sensing and Spatial Information Sciences*, v. XXXIX-B8, p. 187–192, doi:10.5194/isprsarchives-XXXIX-B8-187-2012.
- R Core Team, 2022, *R: A Language and Environment for Statistical Computing*, <https://www.R-project.org/> (accessed January 2024).
- Rogers, B.M., Solvik, K., Hogg, E.H., Ju, J., Masek, J.G., Michaelian, M., Berner, L.T., and Goetz, S.J., 2018, Detecting early warning signals of tree mortality in boreal North America using multiscale satellite data: *Global Change Biology*, v. 24, p. 2284–2304, doi:<https://doi.org/10.1111/gcb.14107>.
- Running, S.W., 1990, Estimating Terrestrial Primary Productivity by Combining Remote Sensing and Ecosystem Simulation, *in* Hobbs, R.J. and Mooney, H.A. eds., *Remote Sensing of Biosphere Functioning*, New York, NY, Springer New York, p. 65–86, doi:10.1007/978-1-4612-3302-2_4.
- Scott, M.L., Shafroth, P.B., and Auble, G.T., 1999, Responses of Riparian Cottonwoods to Alluvial Water Table Declines: *Environmental Management*, v. 23, p. 347–358, doi:10.1007/s002679900191.

- Shimp, J.F., Tracy, J.C., Davis, L.C., Lee, E., Huang, W., Erickson, L.E., and Schnoor, J.L., 1993, Beneficial effects of plants in the remediation of soil and groundwater contaminated with organic materials: *Critical reviews in environmental science and technology*, v. 23, p. 41–77.
- Simon, A., and Collison, A.J.C., 2002, Quantifying the mechanical and hydrologic effects of riparian vegetation on streambank stability: *Earth Surface Processes and Landforms*, v. 27, p. 527–546, doi:<https://doi.org/10.1002/esp.325>.
- Soil Survey Staff, 2024, Web Soil Survey: Natural Resources Conservation Service, United States Department of Agriculture. Available online at <https://websoilsurvey.nrcs.usda.gov/> (accessed 05/13/2024).
- Spearman, C., 1961, *The Proof and Measurement of Association Between Two Things.*: East Norwalk, CT, US, Appleton-Century-Crofts, 45–58 p., doi:10.1037/11491-005.
- Spruce, Hicke, Hargrove, W., Grulke, N., and Meddens, A., 2019, Use of MODIS NDVI Products to Map Tree Mortality Levels in Forests Affected by Mountain Pine Beetle Outbreaks: *Forests*, v. 10, p. 811, doi:10.3390/f10090811.
- Stephens, R., 2022, Mesquite tree deaths remain a mystery: *Pahrump Valley Times*, <https://pvtimes.com/news/mesquite-tree-deaths-remain-a-mystery-107810/> (accessed September 2023).
- Stevens, L.E., Brown, B.T., Simpson, J.M., and Johnson, R.R., 1977, The Importance of Riparian Habitat to Migrating Birds¹, *in* Importance, Preservation and Management of Riparian Habitat: A Symposium, Tucson, Arizona, July 9, 1977, Department of Agriculture, Forest Service, Rocky Mountain Forest and Range ..., v. 43, p. 156.
- Swain, D.L., Langenbrunner, B., Neelin, J.D., and Hall, A., 2018, Increasing precipitation volatility in twenty-first-century California: *Nature Climate Change*, v. 8, p. 427–433, doi:10.1038/s41558-018-0140-y.
- Teskey, R., Wertin, T., Bauweraerts, I., Ameye, M., McGuire, M.A., and Steppe, K., 2015, Responses of tree species to heat waves and extreme heat events: *Plant, Cell & Environment*, v. 38, p. 1699–1712, doi:<https://doi.org/10.1111/pce.12417>.
- Thomas, H., and Nisbet, T., 2007, An Assessment of the Impact of Floodplain Woodland on Flood Flows: *Water and Environment Journal*, v. 21, p. 114–126, doi:10.1111/j.1747-6593.2006.00056.x.
- U.S. Geological Survey, 2023, Water Data for the Nation for Lake Mohave at Davis Dam, Az-Nv - 09422500:, <https://waterdata.usgs.gov/monitoring-location/09422500/#parameterCode=00065&showMedian=true&startDT=2004-10-01&endDT=2014-01-01> (accessed October 2023).
- Valiya Veetil, A., and Mishra, A. k., 2020, Multiscale hydrological drought analysis: Role of climate, catchment and morphological variables and associated thresholds: *Journal of Hydrology*, v. 582, p. 124533, doi:<https://doi.org/10.1016/j.jhydrol.2019.124533>.

- Veettil, A.V., and Mishra, A.K., 2023, Quantifying thresholds for advancing impact-based drought assessment using classification and regression tree (CART) models: *Journal of Hydrology*, v. 625, p. 129966, doi:<https://doi.org/10.1016/j.jhydrol.2023.129966>.
- Visser, E.J.W., Voesenek, L.A.C.J., Vartapetian, B.B., and Jackson, M.B., 2003, Flooding and Plant Growth: *Annals of Botany*, v. 91, p. 107–109, doi:[10.1093/aob/mcg014](https://doi.org/10.1093/aob/mcg014).
- Western Regional Climate Center, 2024, Station Summary for Gila Bend, Arizona:, <https://wrcc.dri.edu/cgi-bin/cliMAIN.pl?azgila> (accessed January 2024).
- Western Regional Climate Center, 2023a, Station Summary for Overton, Nevada:, https://cemp.dri.edu/cgi-bin/cemp_stations.pl?stn=over (accessed October 2023).
- Western Regional Climate Center, 2023b, Station Summary for Pahrump Nevada:, https://cemp.dri.edu/cgi-bin/cemp_stations.pl?stn=pahr (accessed October 2023).
- Williams, A.P., Abatzoglou, J.T., Gershunov, A., Guzman-Morales, J., Bishop, D.A., Balch, J.K., and Lettenmaier, D.P., 2019, Observed Impacts of Anthropogenic Climate Change on Wildfire in California: *Earth's Future*, v. 7, p. 892–910, doi:<https://doi.org/10.1029/2019EF001210>.
- Williams, C.A., and Cooper, D.J., 2005, Mechanisms of Riparian Cottonwood Decline Along Regulated Rivers: *Ecosystems*, v. 8, p. 382–395, doi:[10.1007/s10021-003-0072-9](https://doi.org/10.1007/s10021-003-0072-9).
- Williams, J., Stella, J.C., Voelker, S.L., Lambert, A.M., Pelletier, L.M., Drake, J.E., Friedman, J.M., Roberts, D.A., and Singer, M.B., 2022, Local groundwater decline exacerbates response of dryland riparian woodlands to climatic drought: *Global Change Biology*, v. 28, p. 6771–6788, doi:<https://doi.org/10.1111/gcb.16376>.
- Zdon, A., 2014, 2014 State of the Basin Report Amargosa River Basin, Inyo and San Bernardino Counties, California & Nye County, Nevada: The Nature Conservancy.

3.8 Supplementary materials

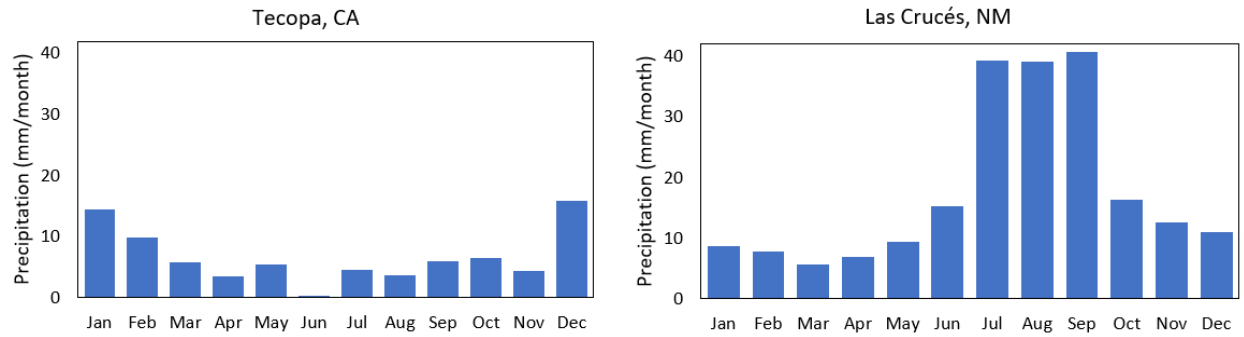


Figure S3.1. Monthly precipitation for **a.** Southern California (Tecopa, CA), with a winter-storm dominated climate, and **b.** New Mexico (Las Cruces), with a monsoon dominated climate.



Figure S3.2. Experimental setup to study the root distribution of three screwbean mesquite seedlings under different groundwater level scenarios.

Table S3.1. Summary statistics and trend for NDVI of all study locations calculated for 1993-2023.

Location	Name	Coordinates	Mean ± SD	Min-max	Trend (p-value)	Slope (NDVI/year)
Ash Meadows	Ash1*	36.4205N, -116.3336E	0.30 ± 0.055	0.19 – 0.38	1.82E-04	-0.0044
	Ash2*	36.4191N, -116.3333E	0.40 ± 0.075	0.26 – 0.52	4.59E-04	-0.0056
	Ash3*	36.4186N, -116.3353E	0.41 ± 0.082	0.28 – 0.59	0.0063	-0.0060
	Ash4*	36.4200N, -116.3326E	0.35 ± 0.037	0.27 – 0.45	2.14E-04	-0.0025
	Ash5	36.4010N, -116.2743E	0.32 ± 0.034	0.25 – 0.38	0.14	-0.0013
	Ash6*	36.3638N, -116.3010E	0.18 ± 0.046	0.13 – 0.29	6.39E-05	-0.0037
	Ash7*	36.3644N, -116.3016E	0.14 ± 0.024	0.11 - 0.19	2.54E-04	-0.0017
	Ash8*	36.4009N, -116.2997E	0.24 ± 0.065	0.14 – 0.35	0.023	-0.0043
	Ash9*	36.4019N, -116.2993E	0.23 ± 0.065	0.15 – 0.35	0.0079	-0.0040
	Ash10*	36.4274N, -116.3047E	0.27 ± 0.073	0.19 – 0.41	4.19E-08	-0.0067
Shoshone	Sho1*	35.9814N, -116.2678E	0.34 ± 0.056	0.23 – 0.42	0.0012	-0.0036
	Sho2*	35.9809N, -116.2675E	0.29 ± 0.069	0.17 – 0.39	3.25E-05	-0.0061
	Sho3*	35.9798N, -116.2668E	0.28 ± 0.056	0.20 – 0.37	2.69E-04	-0.0047
	Sho4*	35.9747N, -116.2662E	0.32 ± 0.073	0.21 – 0.46	1.52E-07	-0.0070
	Sho5*	35.9703N, -116.2602E	0.26 ± 0.034	0.18 – 0.32	1.42E-06	-0.0031
	Sho6	35.9662N, -116.2575E	0.19 ± 0.025	0.11 – 0.23	0.10	5.88e-04
	Sho7*	35.9682N, -116.2602E	0.23 ± 0.057	0.14 – 0.32	2.83E-07	-0.0054
Tecopa	Tec1*	35.8489N, -116.2191E	0.27 ± 0.035	0.21 – 0.35	7.40E-04	-0.0027
	Tec2*	35.8532N, -116.2214E	0.36 ± 0.034	0.27 – 0.42	0.0024	-0.0024
	Tec3*	35.8543N, -116.2248E	0.15 ± 0.023	0.11 – 0.19	1.38E-04	-0.0018
	Tec4*	35.8538N, -116.2234E	0.34 ± 0.050	0.25 -0.45	1.06E-07	-0.0050
Virgin River	VR1*	36.7410N, -114.2133E	0.42 ± 0.124	0.24 – 0.59	1.31E-06	-0.012
	VR2*	36.7222N, -114.2375E	0.42 ± 0.182	0.13 – 0.63	1.79E-08	-0.015
	VR3*	36.6517N, -114.3092E	0.42 ± 0.182	0.17 – 0.64	1.35E-04	-0.015
	VR4*	36.6233N, -114.3244E	0.44 ± 0.156	0.20 – 0.63	0.020	-0.012
	VR5*	36.6077N, -114.3267E	0.45 ± 0.159	0.18 – 0.61	1.53E-05	-0.014
	VR6*	36.5731N, -114.3294E	0.44 ± 0.213	0.14 – 0.65	1.75E-05	-0.019
	VR7*	36.5464N, -114.3346E	0.39 ± 0.191	0.11 – 0.60	1.16E-06	-0.018
	VR8	36.5027N, -114.3426E	0.18 – 0.380	-0.43 – 0.72	0.19	0.015
Muddy River	MR1	36.7155N, -114.7006E	0.39 ± 0.084	0.24 – 0.62	0.91	0
	MR2*	36.6587N, -114.6473E	0.50 ± 0.063	0.36 – 0.61	9.46E-05	-0.0042
	MR3*	36.6570N, -114.6121E	0.28 ± 0.061	0.17 – 0.35	2.19E-05	-0.0044
	MR4*	36.6556N, -114.6023E	0.48 – 0.110	0.26 – 0.61	3.23E-05	-0.0090
	MR5*	36.6559N, -114.5967E	0.50 ± 0.072	0.36 – 0.60	8.99E-06	-0.0057
	MR6*	36.6581N, -114.5876E	0.46 ± 0.056	0.33 – 0.56	0.0022	-0.0025
	MR7*	36.6295N, -114.4870E	0.37 ± 0.064	0.25 – 0.46	1.93E-07	-0.0063
	MR8*	36.6284N, -114.4832E	0.35 ± 0.069	0.21 – 0.43	1.50E-04	-0.0050
	MR9*	36.5378N, -114.4276E	0.39 ± 0.118	0.22 – 0.56	1.57E-05	-0.011
	MR10*	36.5221N, -114.4148E	0.51 ± 0.125	0.32 – 0.66	1.64E-07	-0.011

Arizona	AZ1**	33.9374N, -112.7012E	0.57 ± 0.065	0.40 – 0.67	8.19E-09	0.0060
	AZ2	33.2684N, -112.1945E	0.58 ± 0.057	0.46 – 0.67	0.69	-4.76e-04
	AZ3	33.2642N, -112.1928E	0.60 ± 0.048	0.50 – 0.66	0.12	0.0015
	AZ4**	33.0424N, -112.9215E	0.36 ± 0.194	-0.18 – 0.61	0.043	0.0010
New Mexico	NM1*	33.7903N, -106.8798E	0.39 ± 0.058	0.31 – 0.55	6.99E-05	-0.0044
	NM2**	34.6703N, -106.7480E	0.56 ± 0.068	0.30 – 0.66	0.0024	0.0038
	NM3*	34.6715N, -106.7443E	0.49 ± 0.052	0.35 – 0.58	0.019	-0.0029
	NM4**	32.8713N, -107.3004E	0.46 ± 0.057	0.36 – 0.60	4.58E-06	0.0056
	NM5**	32.8783N, -107.3002E	0.52 ± 0.047	0.43 – 0.61	7.46E-05	0.0038

* Indicates a significant negative trend in growing season NDVI between 1993-2023 at a significance level of 0.05.

** Indicates a significant positive trend in growing season NDVI between 1993-2023 at a significance level of 0.05.

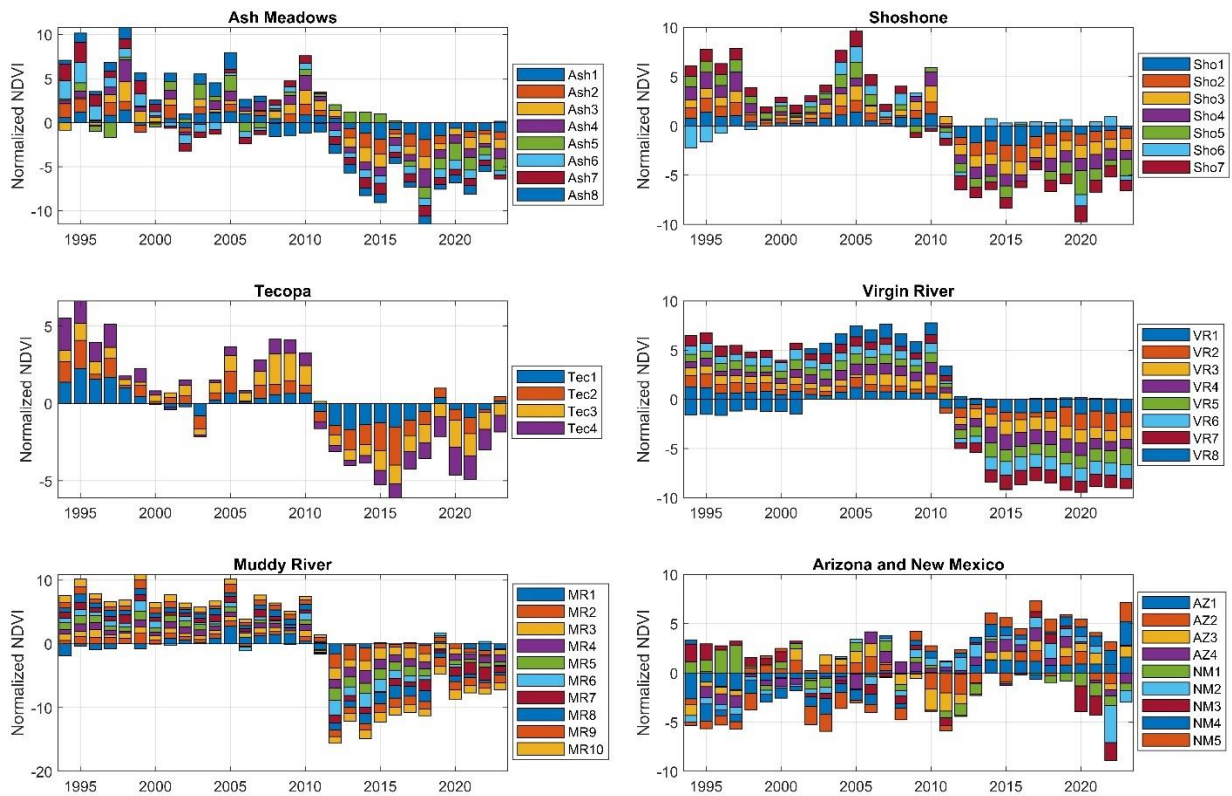


Figure S3.3. Stacked bars of annual average normalized NDVI during the growing season (Apr 1-Oct 30) for all studied sites in regions experiencing woodland mortality in winter storm dominated climate systems for riparian vegetation along the Amargosa River in **a.** Ash Meadows, **b.** Shoshone, and **c.** Tecopa, and along the **d.** Virgin, and **e.** Muddy Rivers, compared to vegetation sites along the **f.** Gila River in New Mexico. Sites in Nevada and Arizona (a-e) show rapid decrease in NDVI values between 2011-2012, which was absent from the Rio Grande.

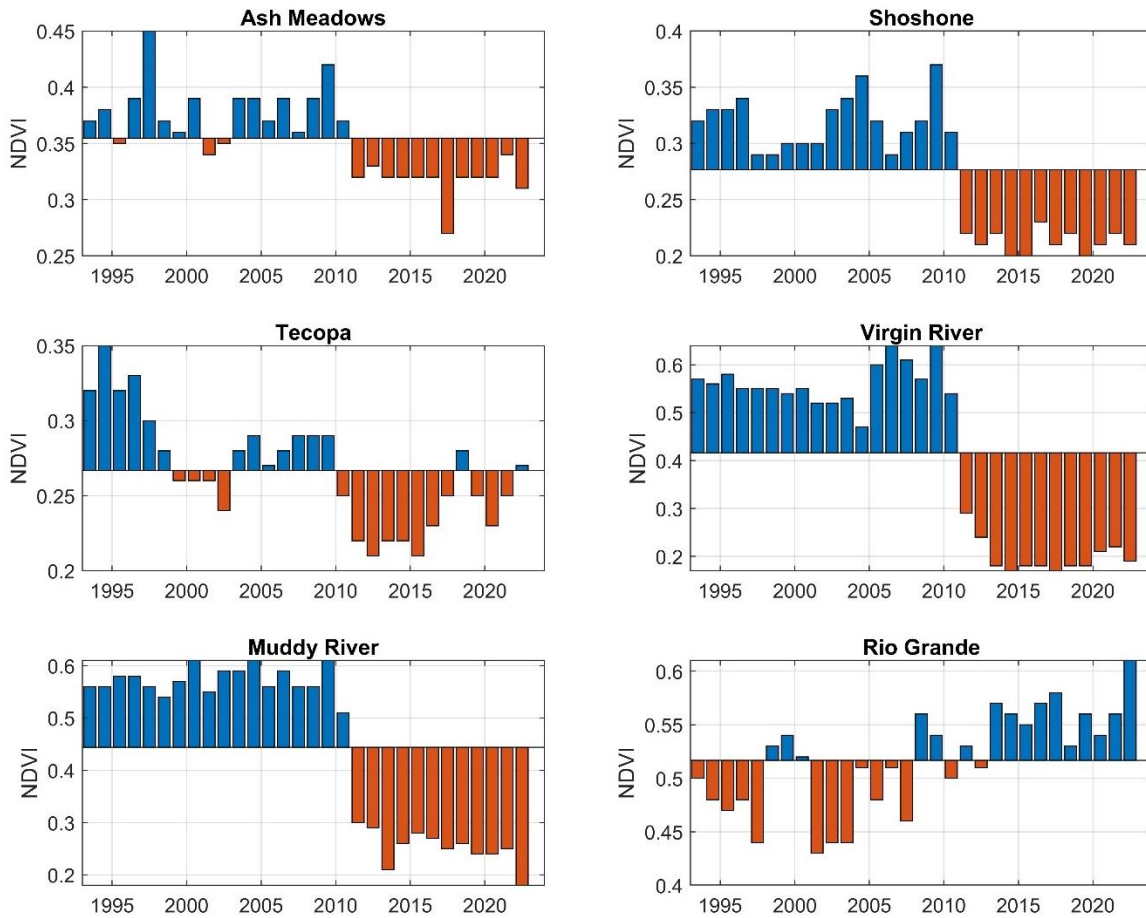


Figure S3.4. Annual average NDVI during the growing season (Apr 1-Oct 31) for areas experiencing riparian woodland mortality along the Amargosa River in **a.** Ash Meadows, **b.** Shoshone, and **c.** Tecopa, and along the **d.** Virgin, and **e.** Muddy Rivers, compared to vegetation along the **f.** Gila River in New Mexico. Sites in Nevada and Arizona (a-e) show rapid decrease in NDVI values between 2011-2012, which was absent from the Rio Grande. Sites a-c were dominated with screwbean mesquite, sites d-f with tamarisk.

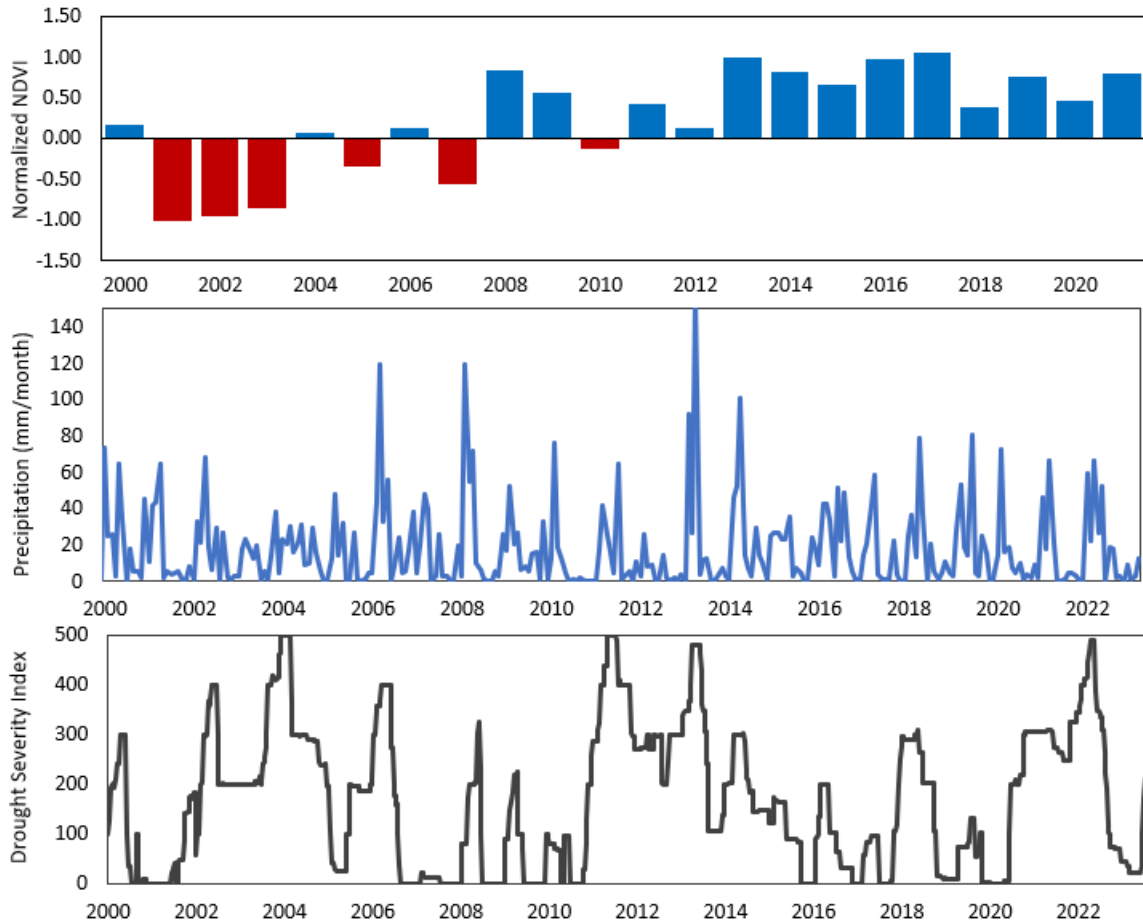


Figure S3.5. Climatic variables for a riparian woodland along the Gila River, AZ. **a.** Average annual normalized NDVI for the growing season (Apr-Oct). **b.** Monthly precipitation showing frequent peaks representing monsoonal precipitation, **c.** Drought severity and coverage index, where 0 means none of the area is experiencing drought, and 500 means the entire area is in exceptional drought, source = US drought monitor.

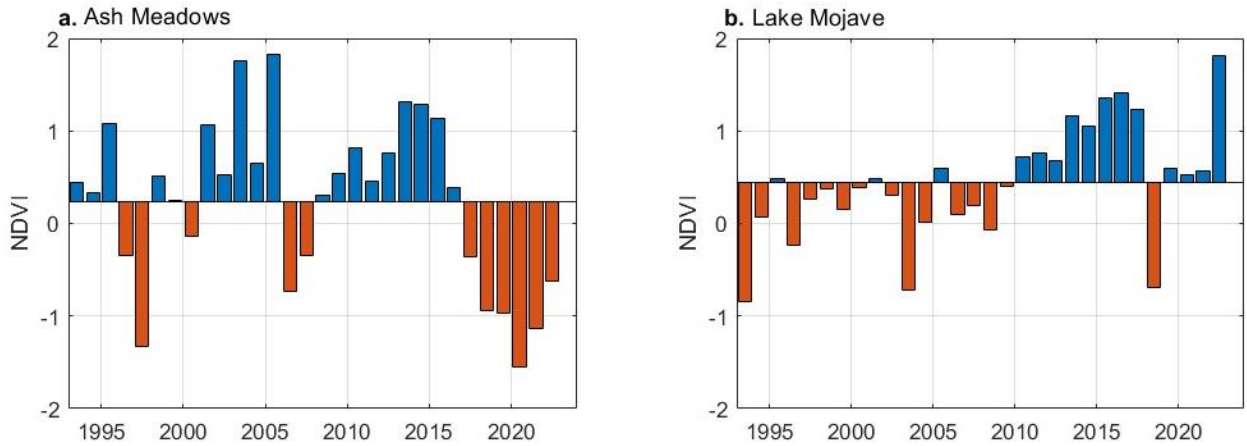


Figure S3.6. Average annual NDVI during the growing season (Apr-Oct) for riparian woodlands in **a.** Ash Meadows, California, showing die-off between 2015-2017, and **b.** Lake Mojave, Nevada/Arizona, showing no signs of mortality between 2011-2012.

Table S3.2. Drought and precipitation values associated with node 5 in the regression tree model, showing most years with large decreases in NDVI are accompanied by above average precipitation (110 mm).

NDVI change	Drought	Precipitation	Node number
3.0	226.8	83.6	5
-21.4	226.8	83.6	5
-5.6	226.8	83.6	5
-6.3	226.8	83.6	5
-4.8	226.8	83.6	5
-17.6	226.8	83.6	5
-22.6	226.8	83.6	5
-29.0	226.8	83.6	5
0	226.8	83.6	5
-12.0	226.8	83.6	5
0	226.8	83.6	5
-13.3	226.8	83.6	5
-3.1	226.8	110.0	5
-17.6	226.8	110.0	5
-28.6	226.8	110.0	5
-42.9	226.8	110.0	5
-46.4	226.8	110.0	5
-26.5	226.8	110.0	5
-34.0	226.8	110.0	5

-26.5	226.8	110.0	5
-29.8	226.8	110.0	5
-16.6	226.8	110.0	5
-33.3	226.8	110.0	5

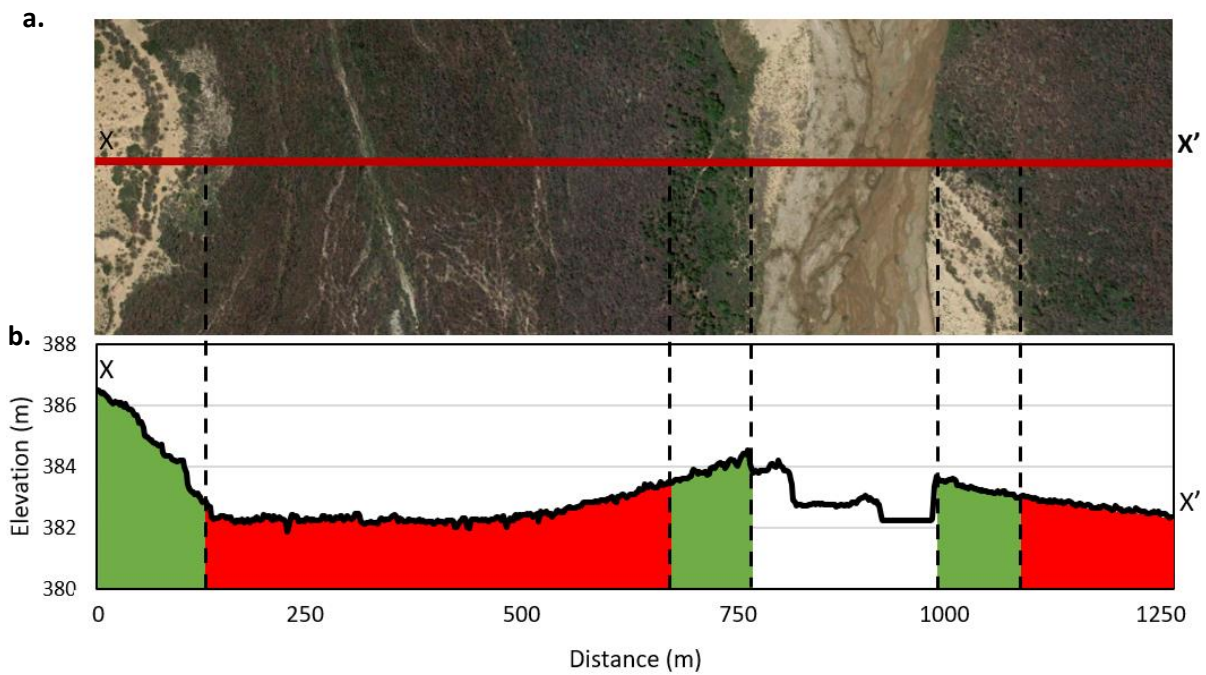


Figure S3.7. a. Mortality of riparian trees in the lower Virgin River showing patches of surviving trees near the river. **b.** Elevation transect showing die-off is focused in topographic lows, where flood water accumulates.



Figure S3.8. Root structure of screwbean mesquite from a field excavation, showing lateral surface roots and a taproot splitting off and moving laterally.

CHAPTER 4 – DRYLAND ECOSYSTEMS

Soil moisture as driver for vegetation patterns created by the Western Harvester ant,
Pogonomyrmex occidentalis

4.1 Abstract

Dryland ecosystems contain vegetation patterns ranging from stripes to gaps and spots. Patterns concentrate resources such as precipitation, allowing plants and insects to occupy environments where existence otherwise would not be possible. Previous research indicates vegetation patterns emerge prior to the ecosystem reaching its tipping point, at which abrupt and potentially irreversible shifts in ecosystem states may occur. Patterns can be created through various mechanisms including self-organization and vegetation clearing behavior of social insects. Understanding the driver of pattern formation is essential to predict how the ecosystem responds to change. Here, I studied soil moisture as driver for creation of a vegetation gap pattern created by the Western Harvester ant, *Pogonomyrmex occidentalis*. Harvester ants create and maintain a 1-4 m barren circle, i.e., ant circle, around their nest. I hypothesize circle creation is driven to meet moisture requirements for ant colony survival, by reducing moisture lost from the nest through transpiration. I show this hypothesis is consistent with soil moisture differences between ant circles and natural vegetation gaps, local circle occurrences on valley floors following drainage patterns, regional occurrence of ant circles in the Great Basin but not Mojave Desert, as well as the presence of abandoned circles in more arid regions. Increased aridity can lower soil moisture levels below the threshold moisture requirement for harvester ants, causing the ants and their barren circles to disappear. This can result in loss of plant and animal diversity, making the ecosystem more vulnerable to rapid state change.

4.2 Introduction

Vegetation patterns including stripes, gaps, and spots are a common phenomenon in dryland ecosystems (Hardenberg et al., 2001; Deblauwe et al., 2008). Patterns concentrate resources, allowing sensitive organisms such as plants and insects to exist in more arid environments than would be possible on homogeneous vegetation (Klausmeier, 1999; Rietkerk et al., 2002; Van De Koppel and Rietkerk, 2004; Sherratt and Lord, 2007). Drylands in the southwestern and western United States contain insect-created vegetation patterns. These patterns consist of vegetation gaps constructed by the Western Harvester ant, *Pogonomyrmex occidentalis*. Harvester ants are known ecosystem engineers who actively clear vegetation around their nest, creating barren vegetation gaps of 1-4 m in diameter, hereafter ant circles (Sharp and Barr, 1960; Clark and Comanor, 1975; Wu, 1990; Soule and Knapp, 1996; Viles et al., 2021). As they are created by insects, ant circles differ from patterned vegetation where shrubs and other vascular plants self-organize through positive feedback loops between plant growth and available water (Aguilar and Sala, 1999; Klausmeier, 1999; Rietkerk et al., 2002). Previous studies suggest patterned vegetation can indicate an imminent ecosystem shift and sensitivity to climate change (Scheffer et al., 2001; Rietkerk et al., 2004).

Ant circles serve as an extension of the ant nest. The nest consists of two parts, a system of underground tunnels and galleries, and an aboveground mound. The underground part extends on average to 1.4 m depth (Rogers and Lavigne, 1974) and contains granaries and nurseries. Ants overwinter in the deeper parts of the nest when temperatures are low (Willard and Crowell, 1965), while the queen lives in chambers at the bottom of the nest most of the year (Lavigne, 1969; Cole, 1994). The aboveground mound is a conical structure with multiple chambers. Ant workers and the brood occupy the mound and shallow chambers in summer (Lavigne, 1969), when higher temperatures aid brood development (Cole, 1994). While the exact functioning of the ant circle surrounding the mound remains unknown, previous studies have indicated two main hypotheses for ant circle creation: to create a more favorable temperature or soil moisture environment. Circles increase soil temperature by allowing unobstructed access to solar

insolation warming of the nest (Wheeler, 1960; Wu, 1990; Bucy and Breed, 2006). Circles also promote higher soil moisture levels by reducing transpiration from the circle (Wight and Nichols, 1966; Laundre, 1990).

Understanding driving forces behind ant circle creation is necessary to predict how the pattern and ecosystem may respond to environmental change. Vegetation patterns can indicate an ecosystem is approaching its tipping point (Scheffer et al., 2009). A tipping point is a threshold after which abrupt and often irreversible change may occur, where an ecosystem shifts to an alternative stable state (Scheffer et al., 2001; Rietkerk et al., 2004). For example, in semi-arid ecosystems, drought and land use change can increase environmental stress until the tipping point is crossed, and the system shifts from a vegetated state to a desert state (Reynolds et al., 2007; D'Odorico et al., 2013).

Below, I elaborate the moisture hypothesis as driver for vegetation patterns created by the Western Harvester ant. Ant colonies are sensitive to low soil moisture levels as ant brood is desiccation sensitive (Wheeler and Wheeler, 1976). Queen survival, health, and brood production are also positively linked to higher soil moisture (Johnson, 2021). At the same time, plants inhabiting xeric regions can be highly desiccation tolerant. By the end of the growing season, soil moisture around their roots reaches extreme low levels (Drivas and Everett, 1988; Kolb and Sperry, 1999). I hypothesize that 1) vegetation clearing around the ant nest reduces root area and root water uptake from within the ant circle, leading to higher soil moisture in the circle, 2) this higher moisture environment will be sustained throughout the growing season, 3) ant circles will not occur in regions where soil moisture is too low, and 4) increased aridity may lead to empty, hereafter abandoned, ant circles due to colony mortality. To test these hypotheses, I studied soil moisture and root density differences between ant circles and naturally occurring vegetation gaps, local occurrence of ant circles in watersheds, regional occurrence of ant circles in the Great Basin and Mojave Desert, and the occurrence and spatial pattern of abandoned ant circles in more arid regions.

4.3 Methods

I studied the driving force behind ant circle creation and its response to climate change through a combination of field measurements, numerical simulations, and remote sensing.

4.3.1 Study area

Physical measurements on active ant circles were made in the Muleshoe Valley in eastern Nevada, United States (Fig. 4.1; 38°12'38.7"N 114°48'54.4"W). This site is located at an elevation of 1637 m within the Great Basin Desert, approximately 44 km northwest of Pioche, Nevada. The main vegetation is Big sagebrush, *Artemisia tridentata*, a woody shrub (approximately 1 x 1 m), and an annual ragweed, *Ambrosia* sp. (approximately 0.3 x 0.3 m). Soils consist of silty to sandy loam (Soil Survey Staff, 2024), with circles located on alluvium of basin floors and along washes. Colonies of the Western Harvester ant, *Pogonomyrmex occidentalis*, are responsible for ant circle creation at this site (Wheeler and Wheeler, 1986). The climate is classified as cool semi-arid (Köppen, 1936; Peel et al., 2007), with mean annual precipitation of 224 mm (Western Regional Climate Center, 2023c). Winters are cold, with most precipitation falling as snowfall, whereas summers are generally hot and dry (Comstock and Ehleringer, 1992; Petersky and Harpold, 2018) (Fig. S4.1).

Ant circles at the study site were compared to circles at 160 locations throughout the western United States using satellite imagery (Fig. S4.2). Locations were selected based on resemblance to the study site to 1) contain the Western Harvester ant, based on the species distribution and reported occurrences in the western and southwestern United States (Cole, 1932, 1994; Sharp and Barr, 1960; Lavigne, 1969; Nagel and Rettenmeyer, 1973; Rogers and Lavigne, 1974; Clark and Comanor, 1975; Wheeler and Wheeler, 1986; Carlson and Whitford, 1991; Cole and Wiernasz, 2000), 2) match the vegetation type at the study type, based on the distribution of sagebrush (Kartesz, 2015), 3) contain similar geomorphological structures, 4) a similar climate, based on a drought index < 0.5 (Zomer et al., 2022), and 5) contain circular vegetation gaps.

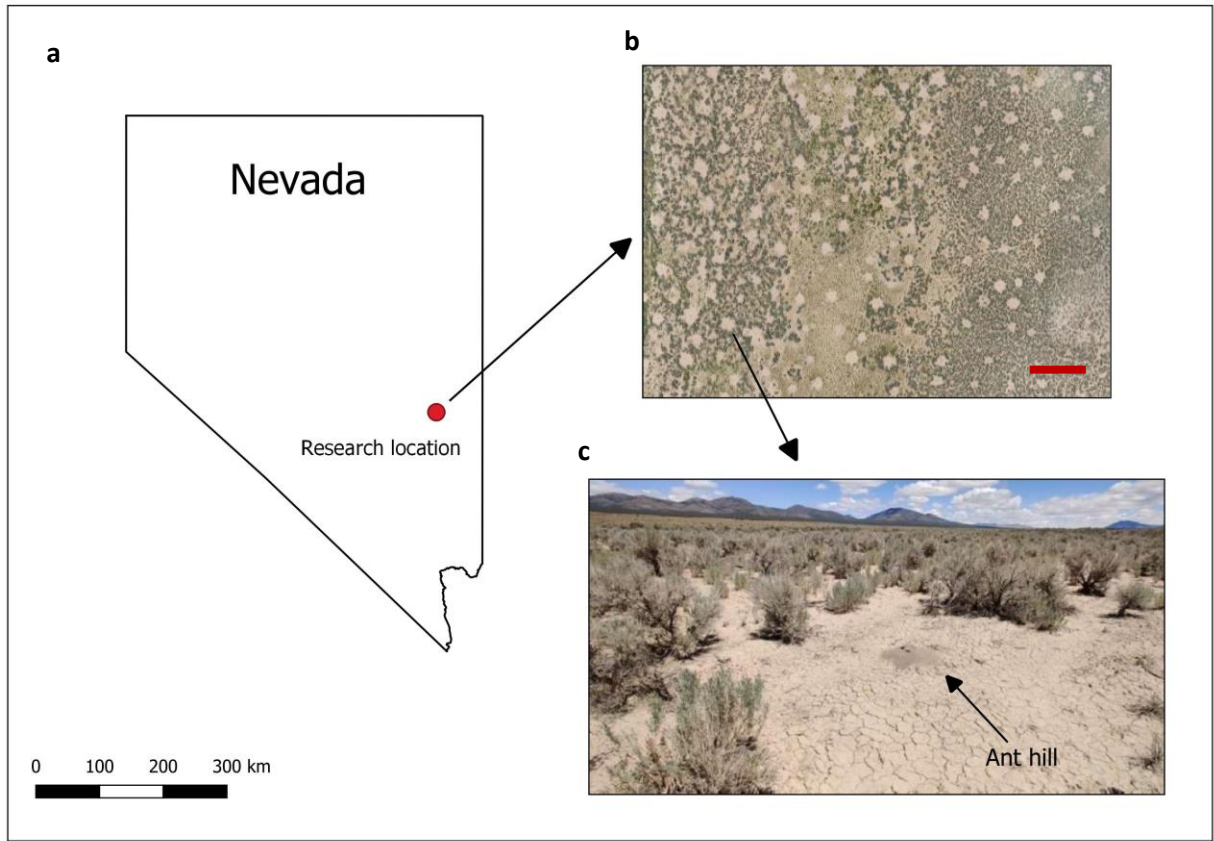


Figure 4.1. **a.** Location of the field study site in Nevada, United States, **b.** Drone image showing the distribution of ant circles in both annual vegetation (light green) and sagebrush (dark green); the scale bar represents 40 m. **c.** Ant circle surrounded by sagebrush, including a central nest approximately 0.3m in height.

4.3.2 Field measurements

Soil texture, moisture, temperature, and root area were measured in and around ant circles at the study site in Nevada.

4.3.2.1 Soil texture

Soil texture was measured to verify the texture class indicated by the Soil Survey Geographic Database (silt loam to sandy loam ((Soil Survey Staff, 2024))). Four soil samples were collected from 0.1-

0.2 m depth in October 2019: one from an ant circle and one from a natural vegetation gap, in annual and shrub-dominated vegetation. Soil samples were pretreated using a 1% surfactant solution. Soil texture was measured using laser particle size analysis (Malvern Mastersizer 3000), according to ASTM C1070. Analysis was carried out by the Soil Characterization and Quaternary Pedology Laboratory (Desert Research Institute, Reno).

4.3.2.2 Soil moisture and temperature

Soil moisture was measured inside ant circles, along vegetated circle margins, and in natural vegetation gaps. Gravimetric soil moisture was measured for 14 samples at a depth of 0.1-0.2 m inside ant circles and natural vegetation gaps in shrub and annual dominated vegetation during field trips in May, August, and October 2019. Three samples were collected from each circle and natural vegetation gap during August and October, one sample was collected from each site during May. For ant circles, samples were collected at the halfway point between the circle margin and ant nest. For natural vegetation gaps, samples were collected from the gap center.

Volumetric soil moisture was measured in two ant circles, one in shrub and one in annual dominated vegetation during the growing season from May 15 to July 10, 2019, using time-domain reflectometry (TDR) soil moisture sensors (Pico Soil Moisture Probe, MESA Systems Co, Stonington, CT 06378, USA), with a rod length of 0.16 m and rod spacing of 0.04 m. Sensors were buried at 0.4-0.6 m and 0.8-1.0 m depth inside each ant circle, at the midpoint between the circle edge and ant mound, and under the canopy of vegetation on the circle margin. Sensors were vertically inserted at the bottom of 0.8m and 0.4m dug holes. Data collection was started immediately after sensor installation; therefore, soil disturbance will have occurred during the installation process and will have impacted results. Soil temperature was measured through a temperature sensor on the probe body of each TDR sensor. Statistical differences between soil moisture and temperature at 0.5 m and 1 m depth in ant circles and under vegetated margins were tested using the non-parametric, two-sided Wilcoxon rank sum test.

4.3.2.3 Root area

To test the hypothesis that ant circle creation reduces root area, I calculated total root area in ant circles, natural vegetation gaps, and near vegetation. The results of this analysis will show how ant circles impact total root area and how this differs with natural vegetation gaps. Root area was calculated near the soil surface, for these roots impact moisture in the upper part of the ant nest during summer. 24 Soil samples were collected from in and around three ant circles in November 2023. Samples were collected from 0.1-0.2 m depth after removing the top 0.05 m of soil to prevent debris from entering samples. Roots were separated from the soil using a 2mm sieve to obtain medium root biomass (e.g., Levillain et al., 2011). Root samples were spread out and photographed against a white background. Resulting images were binarized and scaled to estimate the area covered by roots per kg of dry soil. Significance of differences in root area was evaluated using unpaired t-tests.

4.3.3 Numerical simulations

To test the hypothesis that elevated soil moisture levels are maintained inside ant circles through the end of the growing season, I modeled the spatial-temporal distribution of soil moisture in ant circles and natural vegetation gaps using HYDRUS 3D (Šimůnek et al., 2016; v.5.02). This finite element model solves Richard's equation for water flow in variably saturated porous media (Eq. 4.1),

$$\frac{\partial \theta}{\partial t} = \frac{\partial}{\partial x} \left[K_h(\theta) \left(\frac{\partial h(\theta)}{\partial x} \right) \right] + \frac{\partial}{\partial y} \left[K_h(\theta) \left(\frac{\partial h(\theta)}{\partial y} \right) \right] + \frac{\partial}{\partial z} \left[K_h(\theta) \left(\frac{\partial h(\theta)}{\partial z} + 1 \right) \right] - S \quad (\text{Equation 4.1})$$

where θ represents volumetric soil moisture ($\text{m}^3 \text{m}^{-3}$), t is time (s), z is depth (m), K_h is the unsaturated hydraulic conductivity (m s^{-1}), h is the pressure head (m), xyz are the spatial coordinates (m) and S is a sink term that accounts for root water uptake (RWU) ($\text{m}^3 \text{m}^{-3} \text{s}^{-1}$). RWU was simulated as a function of

potential transpiration, root distribution and pressure head (Feddes, 1982; Šimůnek and Hopmans, 2009) (Eq. 4.2),

$$s(h, x, y, z, t) = \alpha(h, x, y, z, t)b(x, y, z, t) L_t T_p \quad (\text{Equation 4.2})$$

where s is the potential root water uptake at pressure head h (s^{-1}), at location (x,y,z) , at time t , α is the dimensionless stress response function of the pressure head h ($0 \leq \alpha \leq 1$) accounting for reduced potential root water uptake due to moisture stress, $b(x,y,z,t)$ is the normalized root water uptake distribution to account for a root system with an arbitrary shape (m^{-3}), L_t the soil surface associated with transpiration (m^2), and T_p the potential transpiration rate (m s^{-1}).

Numerical simulations were performed for a 1 m deep, three-dimensional angular segment of an ant circle and surrounding vegetation with a 4 m radius (Fig. S4.3). The soil domain was discretized into elements of 0.05 m, leading to a total of 40,434 elements and 10,440 nodes. Soil hydraulic properties in the non-hysteretic van Genuchten equation were parameterized from field data. Residual, θ_r , and saturated, θ_s , soil water contents were estimated from grain size distributions of soil samples collected at 20cm depth inside ant circles, using the Neural Network Prediction tool in HYDRUS, based on pedo-transfer functions of the Rosetta model. Parameters α and n in the soil water retention function were optimized using TDR volumetric soil moisture from 0.5 m depth through inverse modeling in HYDRUS 1D (Šimůnek et al., 2013) using the Levenberg-Marquardt algorithm. HYDRUS 1D in the vertical direction was used for parameter optimization as TDR data was collected vertically from two depths and vertical soil moisture movement was assumed dominant over horizontal movement.

The upper surface of the model was defined as a time-variable atmospheric boundary and the lower boundary was set to free drainage (deep water table). The outside of the soil segment was defined as no flux boundary, assuming processes at this boundary minimally impact soil moisture inside the ant circle. Assuming radial symmetry allows the vertical sides of the slice to be set as no flux boundaries. The

atmospheric boundary condition (precipitation, evapotranspiration) was estimated from meteorological data collected at a weather station in Pioche, Nevada, at an elevation of 1806 m (Western Regional Climate Center, 2023c) (Table 4.1; Fig. S4.4). This station is located 44 km from the research location and separated by a mountain range with highest elevation of 2,722 m. Potential evapotranspiration was calculated according to the FAO 56 method (Allan et al., 1998) (Eq. 4.3),

$$ET_c = ET_o * K_c \quad (\text{Equation 4.3})$$

where ET_c is crop evapotranspiration (mm day^{-1}), K_c is the crop coefficient [-], taken as 0.3 to reflect sagebrush (Pereira et al., 2023), and ET_o is reference evapotranspiration (mm day^{-1}) (Eq. 4.4),

$$ET_o = \frac{0.408 \Delta (R_n - G) + \gamma \frac{900}{T+273} u_2 (e_s - e_a)}{\Delta + \gamma (1 + 0.34 u_2)} \quad (\text{Equation 4.4})$$

where R_n is net radiation ($\text{MJ m}^{-2} \text{d}^{-1}$), G the soil heat flux ($\text{MJ m}^{-2} \text{d}^{-1}$), γ the psychrometric constant ($\text{kPa } ^\circ\text{C}^{-1}$), T is mean daily air temperature at 2 m height ($^\circ\text{C}$), u_2 is wind speed at 2 m height (m s^{-1}), e_s is saturation vapor pressure (kPa), e_a is actual vapor pressure (kPa), and Δ the slope of the vapor pressure curve ($\text{kPa } ^\circ\text{C}^{-1}$), calculated as (Eq. 4.5) (Zotarelli et al., 2015).

$$\Delta = \frac{4098 [0.6108 \exp\left(\frac{17.27 * T}{T+273.3}\right)]}{(T+273.3)^2} \quad (\text{Equation 4.5})$$

Potential evaporation for barren soil inside the ant circle was simulated using HYDRUS 1D and site-specific parameters (Table 4.1;S4.2). Potential evaporation was then subtracted from the crop potential evapotranspiration to obtain potential transpiration. The numerical model was constructed from 03/01/2019 to 09/30/2019, with the first two months used as burn-in time to establish representative spatial distributions of soil moisture in and around the ant circle. Model performance was evaluated by calculating the R-squared and mean absolute error (MAE) of measured and modeled soil moisture during the period of measured TDR soil moisture data (05/15/2019 – 07/10/2019). Modeled soil moisture was obtained from observation nodes at 0.5 m depth at the halfway point between the ant mound and circle edge, and one node 0.15 m from the modeled vegetation. A more detailed description of the specific settings used for the HYDRUS model is available in the supplementary information.

Table 4.1. Summary of meteorological data and soil hydraulic properties, listed in units as required by HYDRUS software.

Parameter	Unit	Range (min-max)	Mean ± SD	Source
Temperature max	°C	6.1-31.7	23.2 ± 6.7	WRCC, 2023c
Temperature min	°C	-0.6-16.7	9.4 ± 5.2	WRCC, 2023c
Precipitation	cm/d	0 -3.2	0.2 ± 0.5	WRCC, 2023c
Wind	km/d	108.1-332.2	193.0 ± 63.2	WRCC, 2023c
Radiation	MJ/m ² /d	4.6-31.5	24.6 ± 6.7	WRCC, 2023c
Humidity	%	15-90	39.8 ± 21.1	WRCC, 2023c
Residual soil water content	-		0.03	Šimůnek et al., 2016
Saturated soil water content	-		0.4	Šimůnek et al., 2016
α	1/cm		0.03*	
n	-		3*	
Saturated hydraulic conductivity	cm/d		52.6	Li et al., 2004
Tortuosity parameter	-		0.5	Šimůnek et al., 2016

* Value was parameterized through inverse modeling.

4.3.4 Remote sensing

To test the hypothesis that soil moisture is an important driver for ant circle occurrence, I analyzed the regional and local distribution of ant circles using Google Earth Pro. The results will show how climatic differences impact regional ant circle distribution, and how topography and geomorphic features impact local ant circle distribution. Ant circles or barren circular structures were analyzed in 160 locations throughout the western and southwestern United States. Locations were selected to match the study site based on species distribution of the Western Harvester ant, vegetation type, geomorphology, drought index, and presence of ant circles or circular barren gaps, as observed through satellite imagery (Fig. S4.6).

To test the hypothesis that increased aridity can lead to abandoned ant circles, I analyzed the spatial patterns of ant circles and abandoned circles using the Pair Correlation Function (PCF). The results of this analysis inform how the spatial pattern of abandoned circles matches the pattern of active circles. Abandoned circles were defined as barren circles similar in size and circular to elliptical shape as ant circles, but without a central ant mound.

The PCF quantifies the probability of finding points separated by a specific distance, r (Satoh, 2003). This test calculates the most common distance between ant circles (Eq.4.4) (Baddeley et al., 2015),

$$g(r) = \frac{K'(r)}{2\pi r} \quad (\text{Equation 4.4})$$

where r is the search radius and K' is the derivative of $K(r)$, also known as Ripley's K function to estimate the number of points in an area surrounding a selected point, calculated as (Eq. 4.5),

$$K(r) = \frac{a}{n(n-1)} \sum_i \sum_j I(d_{ij} < r) e_{ij} \quad (\text{Equation 4.5})$$

where a is the area of the search window, n the number of data points in the search window, d_{ij} the distance between the i^{th} and j^{th} point, with $I(d_{ij} < r)$ an indicator that equals 1 if $d_{ij} < r$, and e_{ij} the edge correction for when part of the search window falls outside the study area (Dixon, 2001). $G(r)$ of 0 indicates no points are separated by the specific distance r ; at large distances, $G(r)$ moves towards 1. PCF analysis was carried out using the *pcf* and *envelope* functions in the Spatstat Package in RStudio (v4.2.2; R Core Team, 2022). The *envelope* function creates simulation envelopes (mean \pm standard deviation) to test spatial pattern against 5000 randomly created point patterns, generated of similar number of points as the original point pattern (Baddeley et al., 2015; v2.3-4). Ant circles and abandoned circles were geospatially marked on plots of minimally 400 x 400 m in QGIS and imported into RStudio as spatial point patterns.

4.4 Results

In this study, I studied soil moisture as driver for ant circle creation by the Western Harvester ant through field measurements, numerical simulations, and remote sensing. First, I used field measurements to compare soil moisture, soil temperature, and root density between ant circles, natural vegetation gaps, and vegetated circle margins. Second, I constructed a numerical model to study the fate of soil moisture in ant circles during the growing season. Last, I used remote sensing to study the regional and local distribution of ant circles, and the effect of increased aridity.

4.4.1 Field measurements

4.4.1.1 Soil texture

All measured soils were classified as sandy loams (Table S4.1). Within that classification, soils within the ant circles consistently showed more fines (silt, clay) than those in the vegetation gaps.

4.4.1.2 Soil moisture and soil temperature

Average gravimetric soil moisture at 0.2 m depth inside ant circles was significantly higher than soil moisture in naturally occurring vegetation gaps for shrubland ($p = 0.002$, $n = 7$, unpaired t-test) (Fig. 4.2a; Table S4.2), and annual vegetation ($p = 0.03$, $n = 7$, unpaired t-test) (Fig. 4.2b; Table S4.2). At the end of summer and the growing season (August 18 and October 3), soil moisture inside ant circles averaged 7-8%, compared to 4-5% inside natural vegetation gaps. For shrubland, this difference was statistically significant ($p = 0.009$, $n = 3$ for August and $p = 0.02$, $n = 3$ for October), for annual vegetation, the difference was not statistically significant ($p = 0.13$, $n = 3$ for August and $p = 0.07$, $n = 3$ for October).

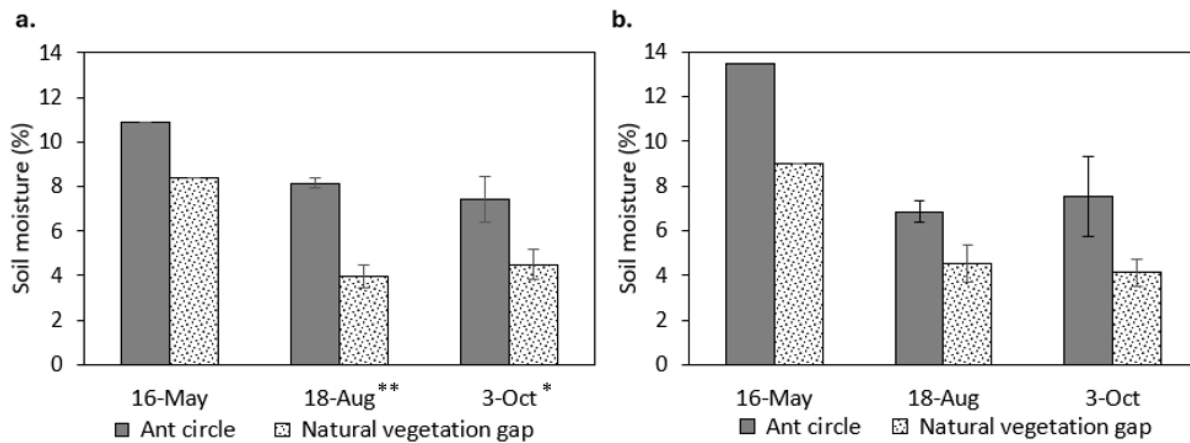


Figure 4.2. Gravimetric soil moisture from 0.1-0.2 m depth for ant circles and natural vegetation gaps in **a.** sagebrush dominated vegetation, and **b.** annual dominated vegetation. Error bars display standard deviation with $n = 3$ for August and October, and $n = 1$ for May. * Represents a significant difference between samples at a confidence level of 0.05, ** at a confidence level of 0.01.

Daily averaged volumetric soil moisture at 0.5 m and 1 m depth inside the ant circle, halfway between the mound and circle edge, was significantly higher than soil moisture underneath vegetation at the circle margin for most of the measured timeframe, with means at 0.5 m depth of 9.3% and 8.1%, and minimum soil moisture of 8.0% and 6.8%, respectively ($p = 4.8 \times 10^{-9}$ for 0.5 m depth, $p = 3.5 \times 10^{-20}$ for 1 m depth, Wilcoxon signed-rank test) (Fig. 4.3, Fig. S4.7). The highest soil moisture levels of 10% volumetric soil moisture were reached at the end of spring, after multiple precipitation events. Through summer, precipitation was low and soil temperature increased, following air temperature increases (Fig. 4.3ab). Soil temperature inside the ant circle was significantly higher than underneath the vegetated margin, with mean temperatures of 19.4 °C and 16.1 °C, respectively ($p = 6.7 \times 10^{-5}$ for 0.5 depth, $p = 0.0073$ for 1 m depth, Wilcoxon signed-rank test) (Fig. 4.3b; Fig. S4.7). Soil moisture on the circle margin decreased in two phases; an initial fast decrease followed by a gradual decrease (Fig. 4.3c). Soil moisture decrease in the circle was slow and gradual throughout summer. By mid-summer, soil moisture levels at 0.5 m depth in the ant circle remained 1.4% higher relative to those near vegetation.

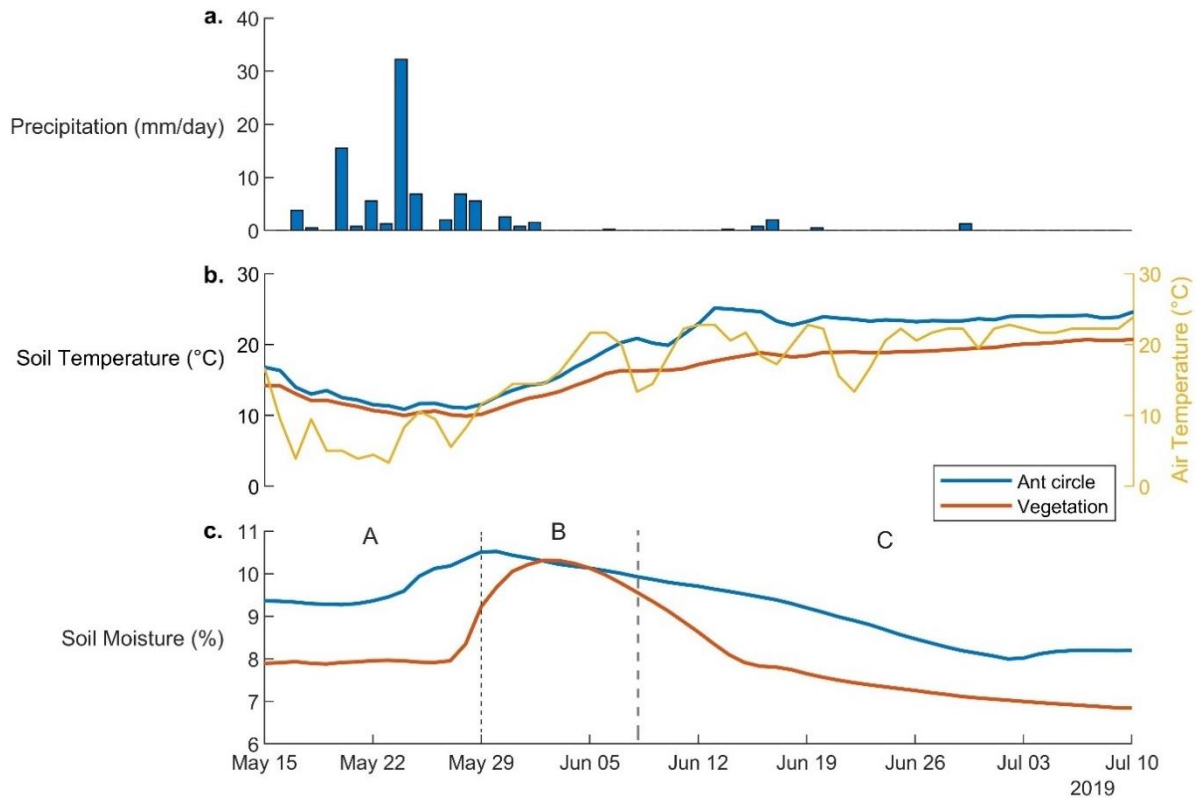


Figure 4.3. Precipitation, air temperature, and daily TDR averages from 5/15/2019 to 7/10/2019. **a.** Daily precipitation from a weather station in Pioche, NV (Western Regional Climate Center, 2023c). **b.** Daily averaged soil temperature at 0.5 m depth inside the ant circle and under vegetation canopy near the circle (left axis) and air temperature (right axis) from a weather station in Pioche, NV (Western Regional Climate Center, 2023c). **c.** Daily averaged volumetric soil moisture at 0.5 m depth inside the ant circle and under vegetation canopy near the circle, with soil moisture significantly different in timeframes A and C ($p < 0.05$), and not significantly different in B (May 29 – June 08) ($p = 0.06$).

4.4.1.3 Root area

Roots were present throughout natural vegetation gaps, ant circles, and underneath the ant mound (Fig. 4.4). Root area varied between 10.0 – 72.9 cm²/kg soil, with highest values occurring closest to vegetation, and lowest values occurring inside the ant circle. Root area decreased moving away from the vegetation into either the natural or ant created gap, with root area significantly different between sampling locations ($p = 0.003$, one-way ANOVA test). Root area underneath vegetation was significantly

higher in the ant circle ($p = 0.0005$, $n = 15$ when comparing groups a and b in Fig. 4.4), but not significantly different from natural vegetation gaps ($p = 0.07$, $n = 3$). In all three sampled ant circles, root area directly underneath the ant mound was higher than the soil directly next to the mound.

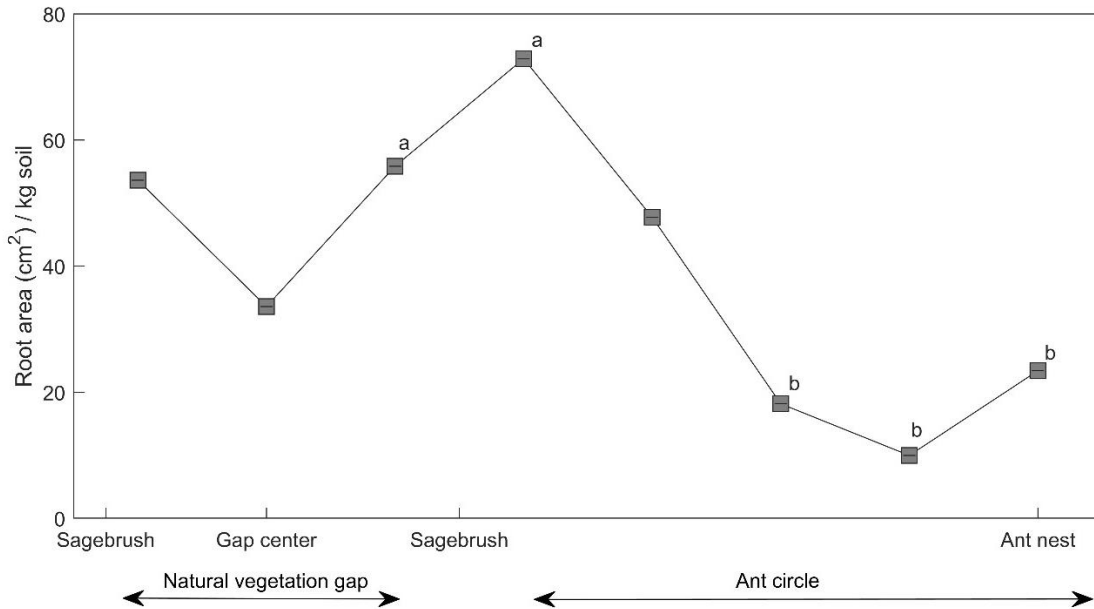


Figure 4.4. Distribution of root area per 1kg of soil from 0.2 m depth in a natural vegetation gap and an ant circle. Root area was highest closest to the sagebrush surrounding the natural vegetation gap and ant circle. Root area decreased when moving away from the vegetation, with the largest decrease in root area occurring right before the ant nest. Each datapoint is the average of 3 samples. Group a represents vegetation, group b the inside of the ant circle, with statistically different root area ($p = 0.0005$, $n = 15$).

4.4.2 Numerical simulations

Soil moisture inside ant circles and natural vegetation gaps was numerically simulated to study the fate of soil moisture during the growing season. Daily averaged soil moisture was obtained from

observation nodes at 0.5 m depth inside an ant circle (halfway point between the ant mound and circle margin), a vegetated circle margin (0.15 m from the simulated plant), and inside a natural vegetation gap (center). The constructed model simulated moisture patterns as observed by TDR data, with R-squared values of 0.60 and 0.75 for the inside of the circle and vegetated circle margin, respectively. The model generally predicted soil moisture around 8% correctly, but overpredicted soil moisture levels higher than 8-10% and underpredicted values lower than 7-8%, with a mean absolute error of 0.36% inside the circle and 0.45% on the vegetated circle margin (Fig. 4.5).

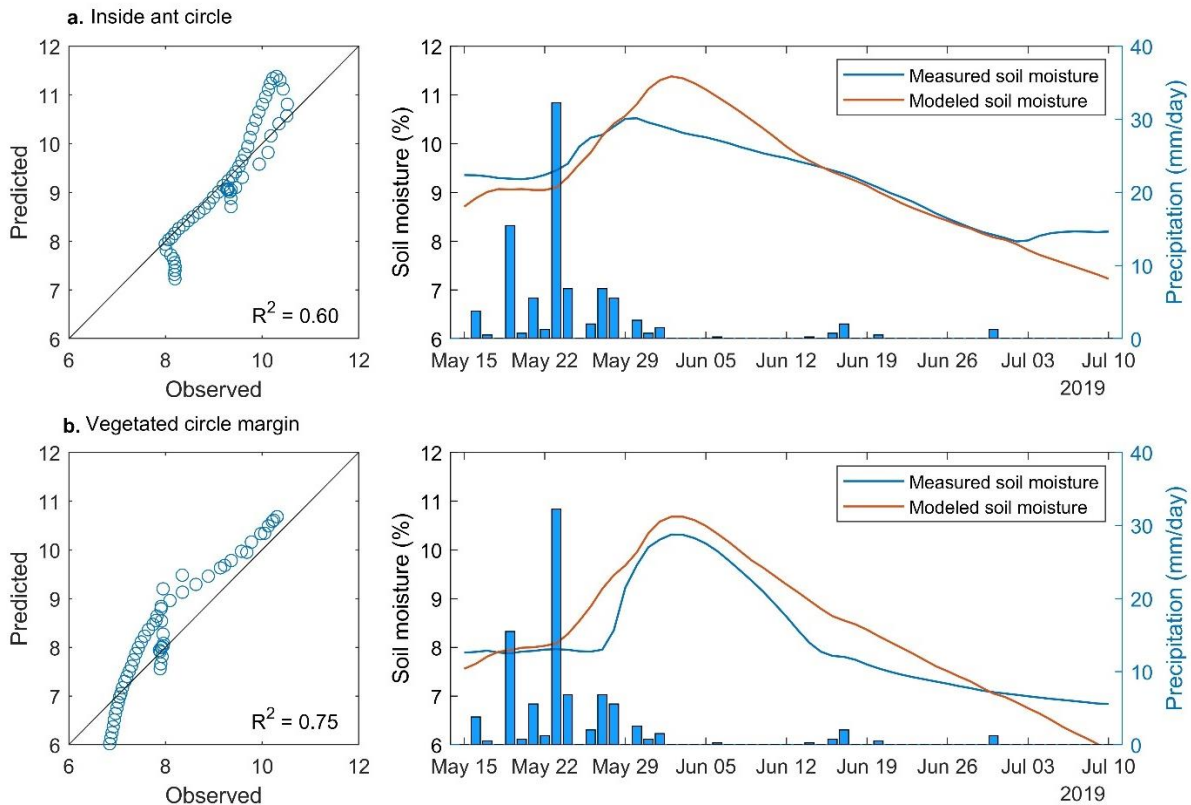


Figure 4.5. Model performance for simulating soil moisture **a.** inside an ant circle and **b.** on the vegetated circle margin at 0.5 m depth using HYDRUS 2D, from May 15, 2019 to July 10, 2019. Model data is compared to volumetric soil moisture measured at 0.5 m depth inside and outside the circle, yielding

mean absolute error of 0.36% for inside the ant circle, and 0.45% for on the circle margin. Precipitation data added for reference from a weather station in Pioche, NV (Western Regional Climate Center, 2023c).

Simulated soil moisture of the entire model domain ranged from 4.0-14.5% between 5/1/2019 and 9/30/2019. Soil moisture was highest in spring, with similar surface soil moisture inside the ant circle and natural vegetation gap following precipitation events (Fig. 4.6a; Fig. 4.7a). Progressing into summer, soil moisture rapidly declined around vegetation to 5.5-6.0% at 0.5 m depth directly underneath vegetation, following high evaporation and RWU (Fig. 4.7bc). Soil moisture was higher inside the ant circle and natural vegetation gap, with levels up to 9.2% and 6.6% at 0.5 m depth, respectively (Fig. 4.6b). At the end of the growing season, soil moisture levels up to 7.1% were still present underneath the ant circle at 0.5 m depth, whereas soil moisture in the natural vegetation gap was reduced to 4.0% (Fig. 4.6c), and water movement across system boundaries had been greatly reduced (Fig. 4.7). Pore-water velocity also rapidly decreased as soil moisture decreased (Fig. S4.8). Horizontal water movement was orders of magnitude lower than vertical water movement, with maximum velocities of 3.3×10^{-3} cm day⁻¹ in July and 9.3×10^{-4} cm day⁻¹ in September.

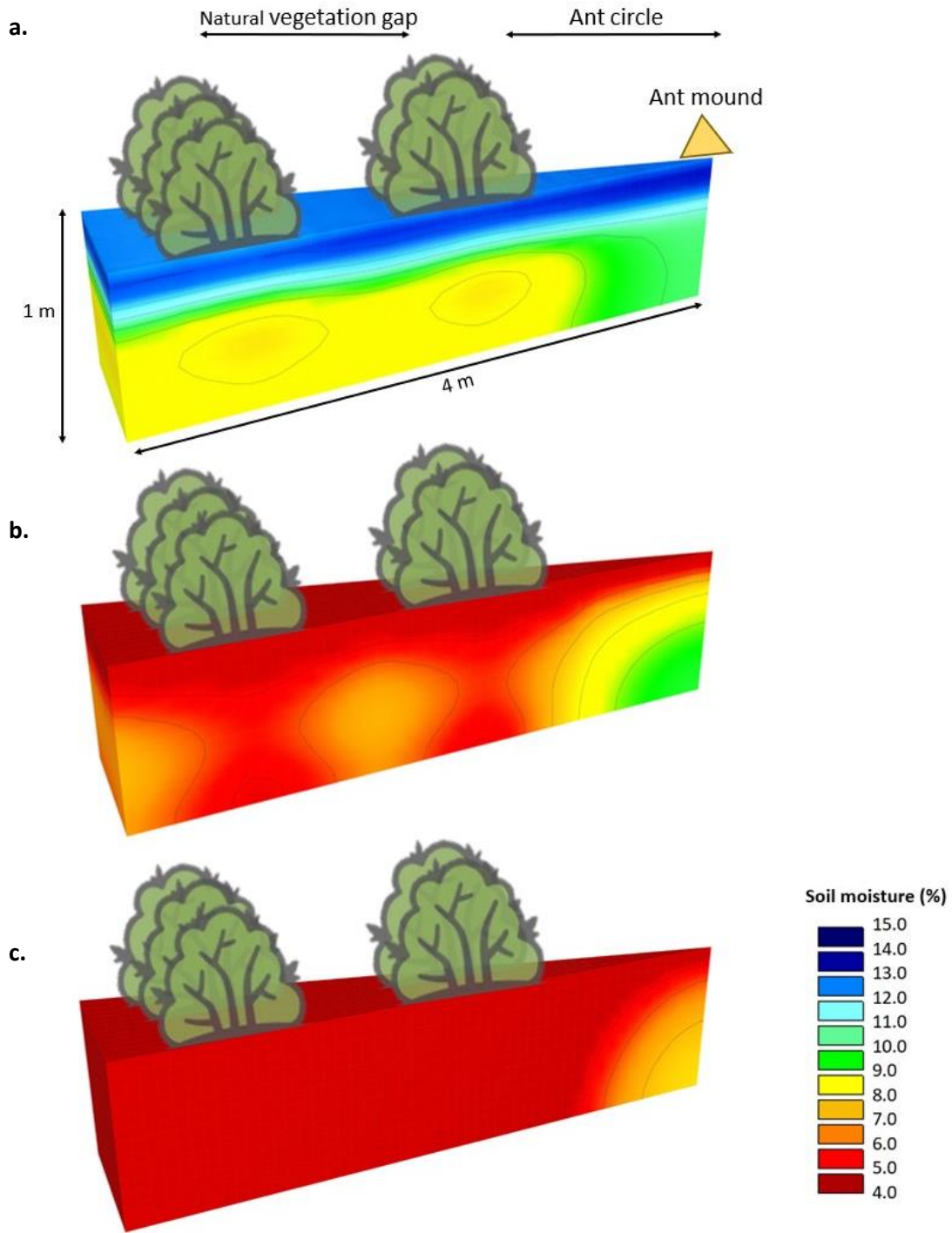


Figure 4.6. Simulated soil moisture levels through the growing season, showing faster moisture loss from vegetated areas and natural vegetation gaps compared to the ant circle. **a.** Day 83 (5/22/2019), **b.** Day 132 (7/10/2019), and **c.** day 214 (9/30/2019). Locations of vegetation and ant mound added for reference.

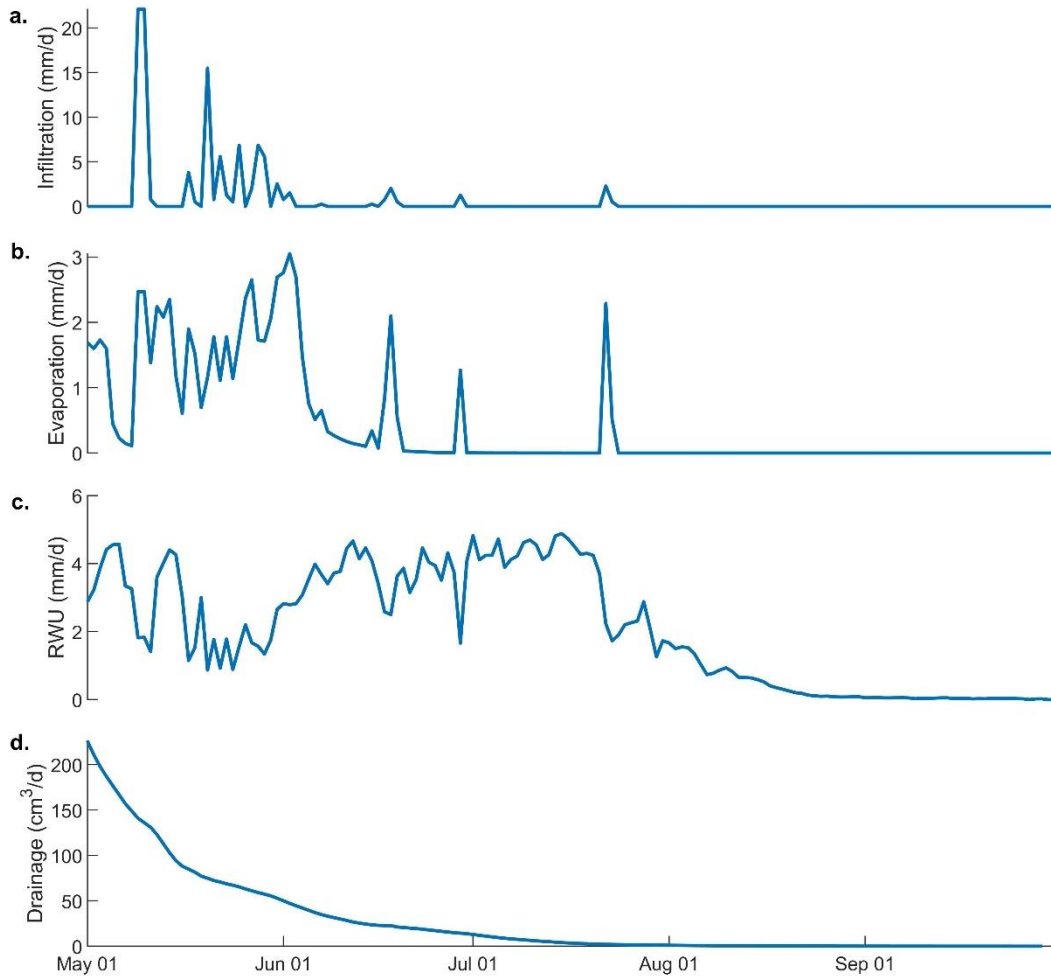


Figure 4.7. Daily averaged mass movement across system boundaries, showing high **a.** infiltration, **b.** evaporation, **c.** root water uptake (RWU), and **d.** drainage in spring and early summer, which all decline rapidly throughout the progression of summer.

4.4.3 Remote sensing

Remote sensing was used to study the regional and local distribution of ant circles, and the effect of increased aridity. At the regional scale, ant circles were found in high density on valley floors of the Great Basin but were absent to the south in the Mojave Desert (Fig. S4.9). At the local scale, ant circles

populated valley floors, but were absent from higher elevations. The circles tended to concentrate along drainage paths, despite the apparent homogeneity in vegetation (Fig. 4.8; Fig. S4.10).

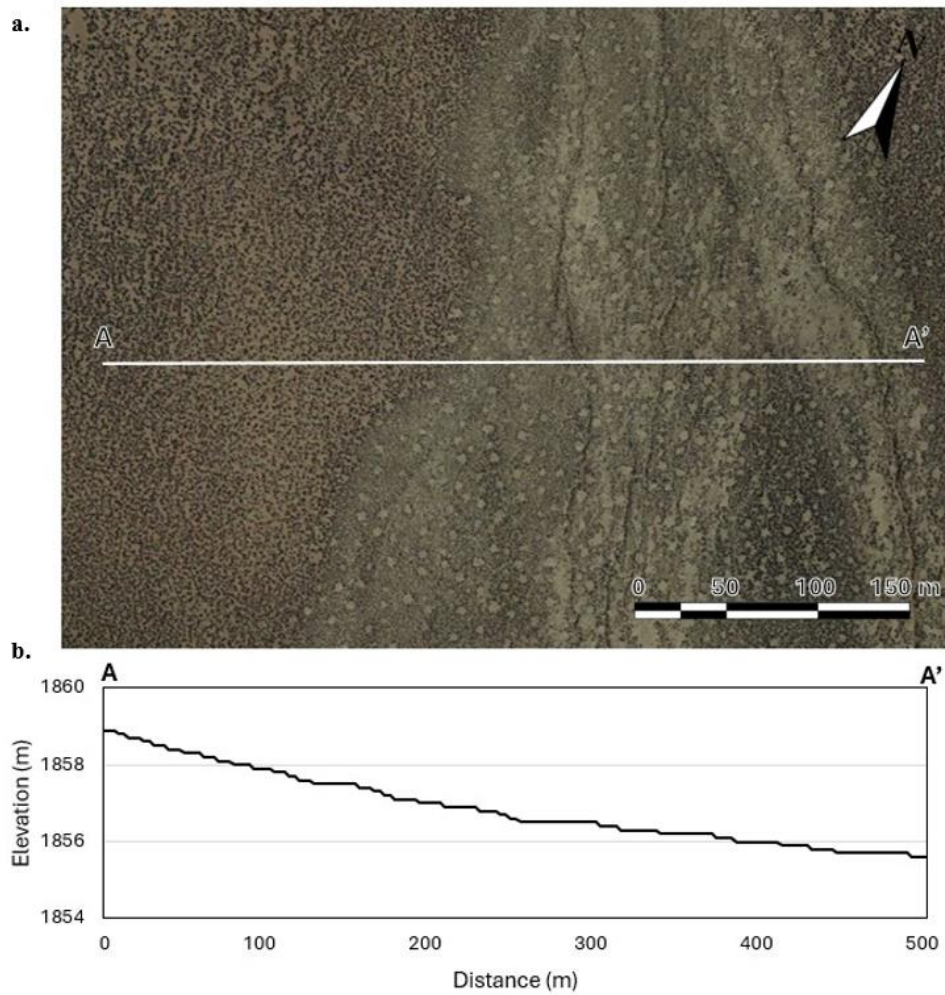


Figure 4.8. Example of distribution of ant circles linked to drainage features in the landscape (location = 38.69511, -116.0231), where a continuously vegetated area (left) is intersected by a drainage feature (right). Ant circle occurrence is closely related to the drainage feature, and **b.** generally occupies the lower parts of the landscape.

Vegetation gaps similar to ant circles but without harvester ants were identified near the southern border of the Great Basin (Fig. S4.9). Near the study site, vegetation gaps were identified without harvester ants or mound structure; however, gravels were present in the center of vegetation gaps (Fig. 4.9a). Further south, circles were starting to get revegetated by annual vegetation (Fig. 4.9b). Circles vegetated with shrubs were also identified, which were still recognizable from satellite imagery (Fig. 4.9c).

The spatial pattern of active circles was compared to potentially abandoned circles using the pair correlation function. If a barren circle was previously an active circle, then the spatial pattern of abandoned circles will be similar to that of active circles, as the distribution of nests of social insects is determined by colony competition for resources and territoriality (Levings and Traniello, 1981; Rytí and Case, 1992; Barton et al., 2009; Grohmann et al., 2010). The spatial signal of active ant circles differed between locations (Fig. 4.10). Most distinct peaks in the pair correlation function were found at sites on valley floors with constant topography. For these sites, the highest probability for distance between ant circles was 15-17 m (Fig. 4.10 a-b; Table 4.2), consistent with Tarnita et al. (2017) for *Pogonmyrmex barbatus* nests. However, site characteristics were rarely homogenous, and the spatial pattern of circles in landscapes with drainage features ranged between 20-40m (Fig. 4.10 c-d), with peaks occurring around 30 m. Vegetation gaps that could be abandoned ant circles showed a similar range in the spatial pattern between 20-40m (Fig. 4.10 e-f), with peaks at 30 m (Table 4.2). Potentially abandoned circles were located within the elevation range observed for active ant circles and similar vegetation density, as observed through satellite imagery and fieldwork.

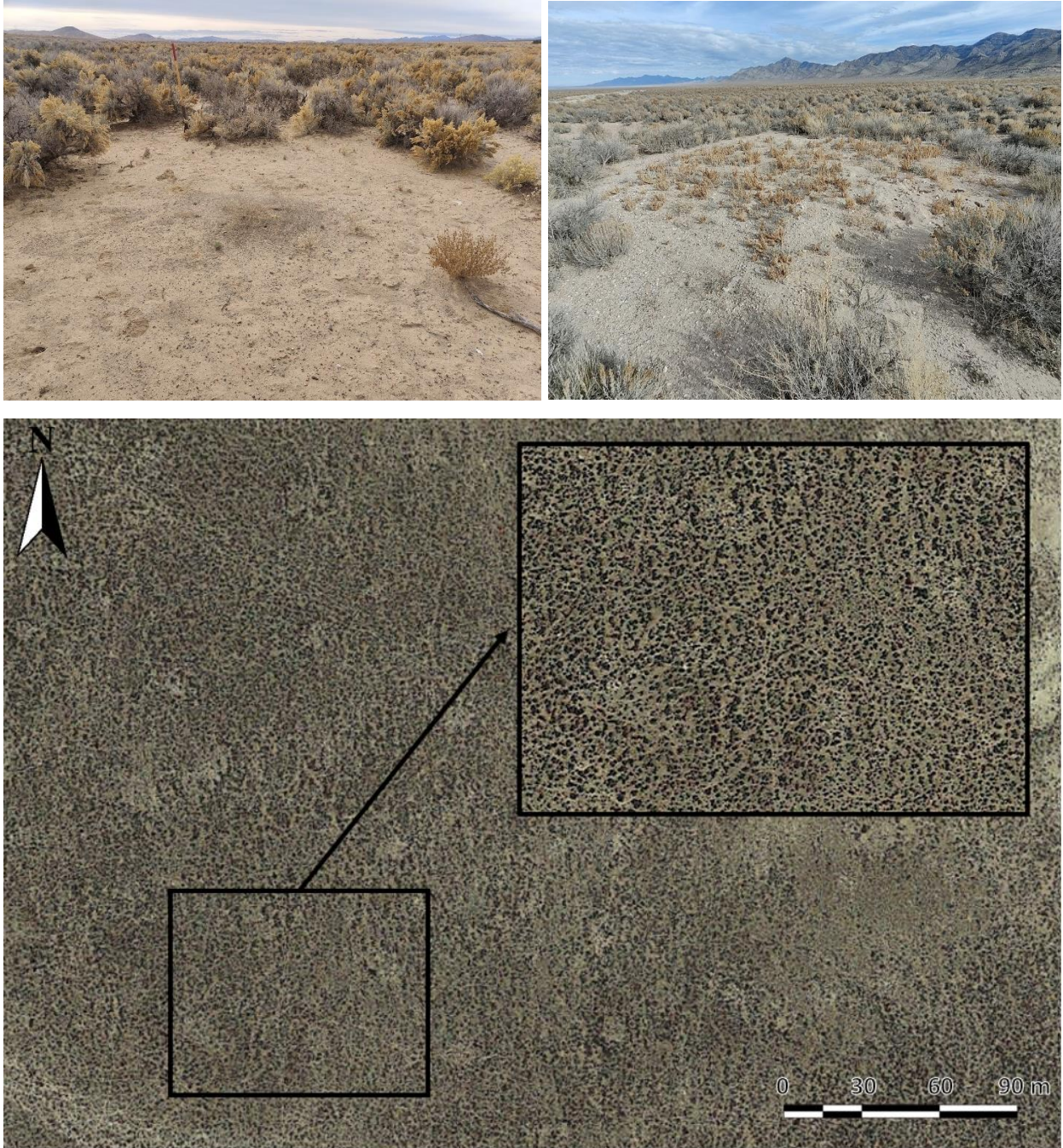


Figure 4.9. **a.** Abandoned circle near the study site that still contains pebbles that used to make up the ant mound (location = 38.33210, -115.0552), **b.** circles revegetated with annuals (location = 38.31905, -115.0667), **c.** circles revegetated with shrubs. While circles are hard to distinguish from a closeup view, an aerial view still shows the general distribution of circles (location = 38.7820804419, -114.541231585).

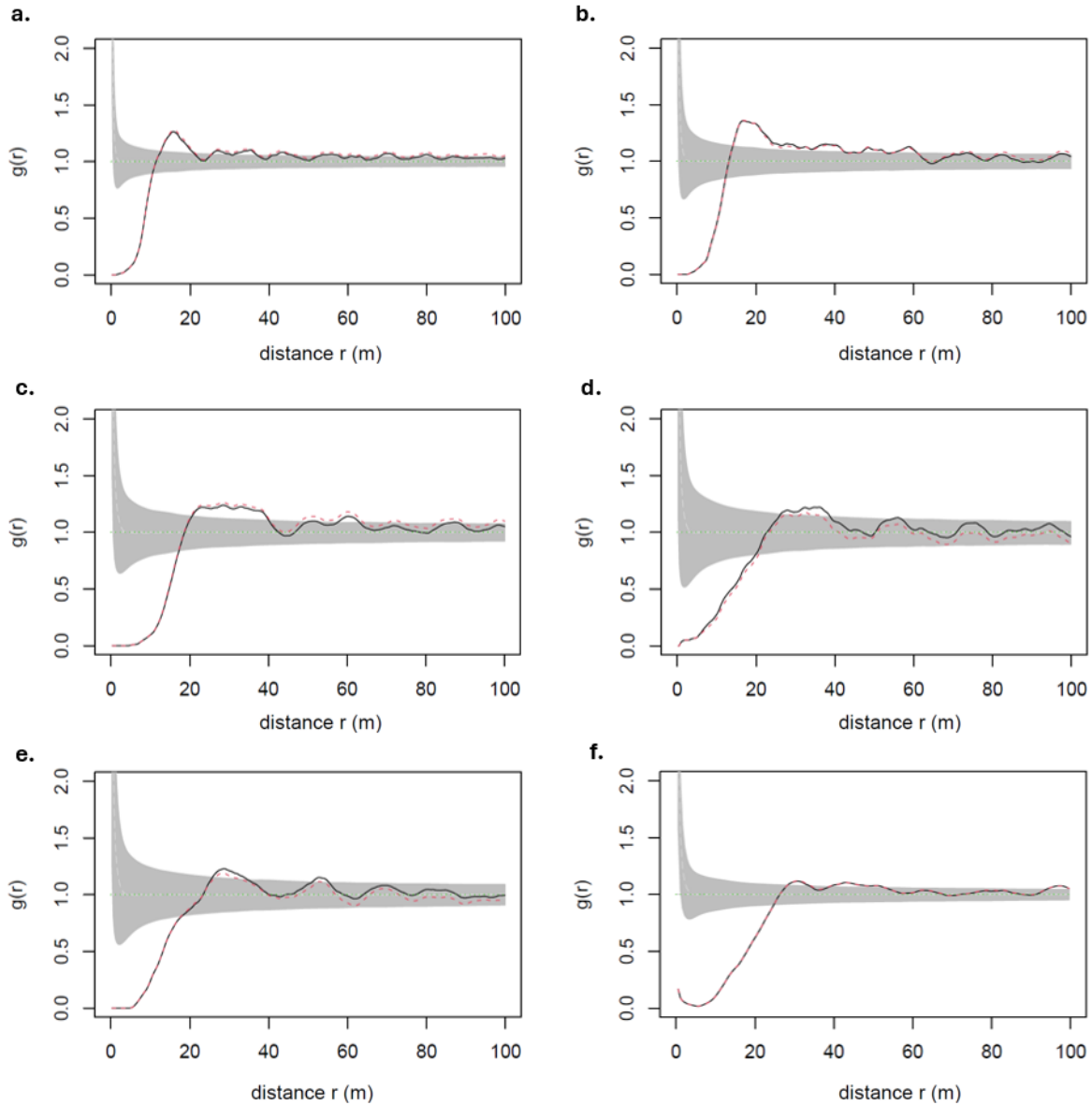


Figure 4.10. Pair correlation function showing the spatial pattern of active ant circles (a-d) and abandoned circles (e-f), with peaks representing the most frequent distance between circles. Peaks of abandoned circles (e-f) and active circles on heterogeneous landscape (c-d) were found at 30 m. The shaded area represents the area associated with complete spatial randomness for each point pattern. Locations = a = 38.5204414411, -115.208540217, b= 38.1891740069, -114.818573473, c = 41.5811214203, -115.864845316, d = 38.5120280337, -115.215266479, e = 38.2675611111, -115.047262095, f = 38.3227895738, -115.056146503.

Table 4.2. Spatial pattern analysis of active and abandoned circles.

Number	Circle type	Plot size (m)	Number of circles	Elevation (m)	g(r) max (m)
1 (a)	Active	450 x 450	864	1,625	15.8
2 (b)	Active	400 x 400	476	1,619	16.6
3 (c)	Active	500 x 500	407	1,967	28.6
4 (d)	Active	420 x 420	256	1,634	32.4
5 (e)	Empty	500 x 500	309	1,745	28.7
6 (f)	Empty	900 x 900	1037	1,659	31.2

4.5 Discussion

Evidence presented in this study supports the soil moisture hypothesis of ant circle creation where higher moisture levels are maintained in the ant circle by removing nearby vegetation. Soil moisture as driver for circle creation affects the climatological response of the vegetation pattern, where increased aridity may lead to regional wide circle abandonment and pattern disappearance following ant colony mortality.

4.5.1 Threshold for vegetation gaps created by harvester ants

Soil moisture is an important driver for vegetation patterns created by harvester ants. As such, the threshold for this pattern is impacted by the minimum soil moisture required for ant colony survival. This moisture minimum is reached at the end of the plant growing season after months of high rates of evapotranspiration and little precipitation. Low soil moisture levels can be lethal to ant larvae as their cuticle is not yet fully developed (Wheeler and Wheeler, 1976). Additionally, queen survival and brood production are also positively correlated to higher soil moisture levels (R. A. Johnson, 2021 for *Veromessor pergandei*) and queens are often located in the lowest and wettest parts of the nest (Cole, 1994).

Soil moisture levels inside ant circles were significantly higher compared to natural vegetation gaps ($p = 0.002$ for shrubland, $p = 0.03$ for annual vegetation) (Fig.4.2). The minimum soil moisture at 0.1-0.2 m depth inside the ant circle was 8% compared to 4% in natural vegetation gaps. While harvester ant nests can reach depths of 1.4 m (Rogers and Lavigne, 1974), during spring and summer, ant brood is frequently placed in the mound, which is used as incubator (Cole, 1994). Although the threshold moisture for western harvester ant colony survival is currently unknown, it is met at 8%, but not at 4% soil moisture. This is supported by Johnson (1998; 2000) who found higher mortality of brood, workers, and alate females of *P. rugosus* and *P. barbatus* under desiccating conditions.

While plants on ant circle margins were further apart compared to natural vegetation gaps, roots were found through the entire radius of the ant circle (Fig. 4.4). Total root area at 0.1-0.2 m depth was highest near vegetation and decreased when moving away into an ant circle and natural vegetation gap, with lowest root area measured inside ant circles. Counterintuitively, root area directly underneath the ant mound was higher than the soil sample taken next to the mound. This was likely caused by seed germination during spring, before seedlings are killed by ants.

Reduced root water uptake inside ant circles limits soil moisture loss through plant transpiration. Additionally, textural differences between ant circles and natural vegetation gaps can impact soil moisture levels. Fine grained soils are characterized by higher water retention leading to higher soil moisture than coarse grained soils (e.g., Fernandez-Illescas et al., 2001). Ant circles contained slightly higher silt and clay contents than natural vegetation gaps (Table S4.1). Added effects of soil texture on ant circle microenvironments and local distribution patterns likely occur but were not tested in this study. Reduced root water uptake combined with increased water retention caused soil moisture levels inside ant circles to be consistently higher than soil moisture near vegetation and in naturally occurring vegetation gaps during the growing season (Fig. 4.11).

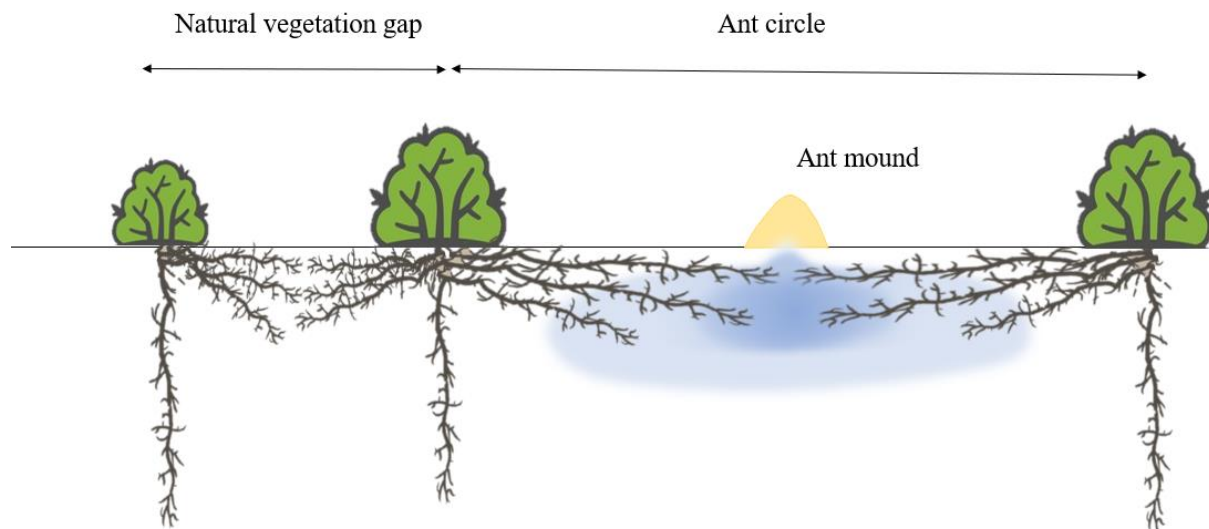


Figure 4.11. The effect of an ant circle on soil moisture and root density. Spacing in vegetation created by the ant circle significantly reduces root density inside the circle, therefore reducing root water uptake causing elevated soil moisture levels, as shown by blue shading. Roots modified from Schroeder and Johnson, 2018.

4.5.2. Numerical modeling of moisture dynamics in ant circles

Numerical modeling highlighted the importance of the ant circle to create favorable moisture conditions for harvester ants. The model confirmed elevated soil moisture levels were maintained inside ant circles through the end of the growing season. While elevated soil moisture conditions were initially also present in the natural vegetation gap, soil moisture at 0.5 m depth was reduced to 4% by the end of the growing season, compared to soil moisture levels up to 7% inside the ant circle (Fig. 4.6). The three-dimensional triangular model domain allowed for evaluation of root water uptake from neighboring vegetation while accounting for increased horizontal pore-water flow velocity near the center of the ant circle. Construction of the HYDRUS model allowed for model calibration during the period of available continuous soil moisture data, to evaluate moisture dynamics through the end of the growing season. Overall, the model aided in understanding moisture dynamics inside and surrounding ant circles during

the growing season, yet there are limitations to the model as several assumptions were made regarding the soil pore structure, hydraulic model and meteorological data used.

Soil hydraulic material properties were assumed to be vertically and horizontally homogenous. However, large spatial heterogeneity exists in soil pore structures. This affects parameterization of hydraulic material properties for the soil moisture retention curve and the unsaturated hydraulic conductivity, and therefore water movement and soil moisture levels (Vereecken et al., 2007; Vogel, 2019). Soil hydraulic properties are expected to vary with depth; using surface layer soil hydraulic properties could therefore have inaccurately simulated soil moisture in deeper soil layers. Additionally, saturated hydraulic conductivity and soil hydraulic parameters were estimated from the grain size distribution using the built-in HYDRUS neural network tool, based on pedo-transfer functions of the Rosetta model. This model estimates soil hydraulic parameters using neural networks and soil parameters from various databases and reference soils (Schaap et al., 1998). Uncertainty in the estimated parameters will have occurred as only grain size distribution was included as input, as opposed to also including bulk density and soil organic matter, which has been identified to yield most accurate parameters (Schaap et al., 2001).

Soil water movement was described through the Richard's equation using the unimodal van Genuchten model to describe the shape of the water retention curve. This method does not consider macropores and preferential flow during saturated conditions (Van Genuchten, 1980; Durner, 1994). Macropores can be created by soil fauna, plant roots, and cracks and fissures in for example clay rich soils (Beven and Germann, 1982). Such structures can cause non-uniform flow with faster infiltration rates than predicted by the Richard's equation (Beven and Germann, 2013). Higher infiltration rates could have occurred near sagebrush and below the ant mound, as the tunnels and dug up soil can create preferential flow paths and reduce bulk density (Laundre, 1990). Preferential flow paths would increase soil moisture heterogeneity.

Meteorological data used in the model was obtained from a weather station in Pioche, Nevada, 44 km from the study site. The weather station and study site are separated by a mountain range with highest elevation of 2,722 m. As mountainous landscapes can create spatial variability in precipitation, the data obtained from Pioche might not have accurately represented precipitation at the study site. Input of precipitation values exceeding actual precipitation at the study site could have overpredicted soil moisture in late-May and early-June (Fig. 4.5).

4.5.3 Soil temperature as alternative hypothesis for circle creation

Soil temperature has been suggested as alternative hypothesis to drive ant circle creation. Elevated soil temperature maximizes worker activity by increasing the foraging window (Bucy and Breed, 2006), and helps incubate the brood (Wheeler, 1960; Cole, 1994). Indeed, soil temperatures inside ant circles continuously exceeded temperatures underneath vegetation, as open areas had no canopy light interception (Fig. 4.3b). However, observations in regional and local ant circle occurrences indicate that the higher soil temperature is an incidental benefit, but not the driver for circle creation.

On a regional scale, the ant habitat did not extend to the warmer and drier Mojave Desert; rather it stopped at the southern edge of the Great Basin (Fig. S4.9). Previous studies have located ant circles in the Mojave Desert, but occurrences were localized to moist microsites (Rissing, 1988; Wagner et al., 2004). I suggest such microsites are suitable for ant circle creation as soil moisture levels after circle creation can sustain ant colonies. Additionally, Dibner et al. (2015) found precipitation was the only abiotic factor significantly affecting ant circle density on a regional scale.

On a local scale, ant circle occurrence is largely confined to drainage patterns on a temperature-wise homogenous landscape (Fig. 4.8). Drainage patterns not only provide better suited sediment for ant nest development, but also concentrate runoff and might contain higher silt and clay contents. Sharp boundaries in circle distribution across such landscapes as seen in Figure 4.9 could not be explained with

the temperature hypothesis, as this area would have similar temperatures. Additionally, on the ant circle scale, three observations were inconsistent with the temperature hypothesis. First, the benefits of increased soil surface temperatures are also found in natural vegetation gaps, as these gaps also have no canopy light interception and are exposed to solar heating. However, ant colonies do not occupy natural vegetation gaps. Second, the benefit of increased soil temperature for workers only applies to the ant circle, yet workers forage outside the ant circle (Bucy and Breed, 2006). Third, ant circles increase the period ground temperatures are above the maximum thermal tolerance of harvester ants (Bucy and Breed, 2006).

4.5.4 Pattern persistence through vegetation change

Harvester ants are expected to be present on a landscape if two conditions are met. First, appropriate soil moisture levels for colony survival must be sustained. Second, the vegetation must produce suitable seeds for ants to harvest. Once they are established, ant circles can withstand vegetation changes. Ants can continue to maintain their circles by killing seedlings that try to establish in the circle, regardless of the vegetation type. Alternatively, new circles can be created following fire, allowing harvester ants to populate landscapes that were previously vegetated by vegetation such as shrubs and trees that are too large to kill (Porter and Jorgensen, 1988). Consequently, ant circles exist on forests and shrublands as well as on annuals and grasslands (Sharp and Barr, 1960; Clark and Comanor, 1975; Wu, 1990; Carlson and Whitford, 1991; Soulé and Knapp, 1996; Dibner et al., 2015).

4.5.5 Effects of threshold crossing and climate change

Ant circles are a global phenomenon of dryland environments, occurring not only in North America, but also in Africa (Picker et al., 2012), and the Middle East (Ginzburg et al., 2008; Brown et al., 2012). Climate change can increase aridity in these ecosystems. Ants will cease to exist once soil moisture

falls below their threshold. At that point, revegetation of the circle begins, first by annual vegetation, and eventually by shrubs (Fig. 4.9). Disappearance of ant circles can negatively impact dryland ecosystems. Ant circles increase ecosystem resiliency by promoting higher biodiversity. They function as refugia during dry periods and accelerate post-drought recovery (Nicolai et al., 2008). Additionally, harvester ants constitute an important part of the food chain. Ants are consumed by the horned lizard, *Phrynosoma coronatum* (Suarez et al., 2000), which in turn is consumed by many large animals, including rodents, birds, coyotes, and snakes (Munger, 1986; Sherbrooke, 2003). Ants are also food for chicks of the endangered greater sage-grouse, *Centrocercus urophasianus* (Johnson and Boyce, 1990).

Climate change is expected to cause ant colony mortality if it reduces soil moisture levels. Climate change in the southwestern United States over the past century shows an overall drying trend, which is predicted to continue through the 21st century. Following this trend, the Mojave Desert is predicted to extend northward (Archer and Predick, 2008; Rehfeldt et al., 2012; Bradley et al., 2016). This will push the ant habitat range northward, leaving abandoned circles in its wake. Indeed, empty circles and revegetated circles to varying degrees were detected in the transition zone between the Mojave Desert and the Great Basin (Fig. 4.9). Based on the spatial pattern similarity to active circles, the empty circles could have previously been active ant circles (Fig. 4.10). This finding is consistent with the poleward shift in range boundaries of many species (Thomas, 2010).

Abandoned ant circles can be seen as an initial sign of ecosystem change. Initial change occurs as a reduction in ecosystem biodiversity and loss of part of the food chain. However, loss of the vegetation pattern does not cause rapid phase change as predicted by mathematic modeling (e.g., Sherratt and Lord, 2007). Instead, when ant circles disappear, the landscape is reverted to a homogeneous vegetation cover. The minimum soil moisture needed by the vegetation is therefore lower than that of ant circles. This allows vegetation to survive while ant colonies die. This contrasts with patterned vegetation, where the pattern is dependent on the vegetation moisture requirements and therefore followed by potential desertification if the threshold is passed. Additionally, the vegetation pattern is sometimes persevered as a

new ecosystem engineer takes over. For example, kangaroo rat burrows were frequently encountered in abandoned circles. If circles are maintained by another organism, the threshold value for circle occurrence will now be determined by this organism. Understanding what drives pattern thresholds thus allows for a better prediction of when environmental change may occur.

4.6 Conclusion

Vegetation patterns in semi-arid regions can indicate imminent ecosystem change as the system approaches its tipping point. Understanding driving forces behind pattern formation aids in predicting ecosystem change. Here, I showed soil moisture as a major driving force behind formation of ant circles, a vegetation gap pattern, by the Western Harvester ant, *Pogonomyrmex occidentalis*. My results showed ant circle creation increases soil moisture inside circles throughout the growing season by clearing vegetation around the ant nest. Ant circle distribution confirmed the link to moisture patterns by being restrained to drainage features and valleys floors, as well as regional occurrences of ant circles in the Great Basin but not in the drier Mojave Desert. Other factors such as the effect of grain size and sediment sorting also impact soil moisture and are presumed to be important for ant circle distribution but were not tested. If climate change increases aridity, soil moisture levels can drop below the threshold for ant colony survival, leading to circle abandonment. Abandoned ant circles were observed near the southern limit of the harvester ant habitat, indicating a northward shift in habitat. Ecosystems can be negatively impacted when harvester ants disappear by reduced biodiversity and ecosystem resilience. However, loss of vegetation patterns created by harvester ants did not result in rapid desertification, as predicted by mathematical models.

4.7 References

- Aguiar, M.R., and Sala, O.E., 1999, Patch structure, dynamics and implications for the functioning of arid ecosystems: *Trends in Ecology & Evolution*, v. 14, p. 273–277, doi:[https://doi.org/10.1016/S0169-5347\(99\)01612-2](https://doi.org/10.1016/S0169-5347(99)01612-2).
- Allan, R., Pereira, L., and Smith, M., 1998, Crop evapotranspiration-Guidelines for computing crop water requirements-FAO Irrigation and drainage paper 56: v. 56.
- Archer, S.R., and Predick, K.I., 2008, Climate Change and Ecosystems of the Southwestern United States: *Rangelands*, v. 30, p. 23–28, doi:[10.2111/1551-501X\(2008\)30\[23:CCAEOT\]2.0.CO;2](https://doi.org/10.2111/1551-501X(2008)30[23:CCAEOT]2.0.CO;2).
- Baddeley, A., Rubak, E., and Turner, R., 2015, *Spatial Point Patterns: Methodology and Applications with R*: Chapman and Hall/CRC Press, 225–230 p.
- Barton, K., Sanders, N., and Gordon, D., 2009, The Effects of Proximity and Colony Age on Interspecific Interference Competition between the Desert Ants *Pogonomyrmex barbatus* and *Aphaenogaster cockerelli*: *The American Midland Naturalist*, v. 148, p. 376–382, doi:[10.1674/0003-0031\(2002\)148\[0376:TEOPAC\]2.0.CO;2](https://doi.org/10.1674/0003-0031(2002)148[0376:TEOPAC]2.0.CO;2).
- Beven, K., and Germann, P., 1982, Macropores and water flow in soils: *Water Resources Research*, v. 18, p. 1311–1325, doi:<https://doi.org/10.1029/WR018i005p01311>.
- Beven, K., and Germann, P., 2013, Macropores and water flow in soils revisited: *Water Resources Research*, v. 49, p. 3071–3092, doi:<https://doi.org/10.1002/wrcr.20156>.
- Bradley, B.A., Curtis, C.A., and Chambers, J.C., 2016, Bromus Response to Climate and Projected Changes with Climate Change, *in* Germino, M.J., Chambers, J.C., and Brown, C.S. eds., *Exotic Brome-Grasses in Arid and Semiarid Ecosystems of the Western US: Causes, Consequences, and Management Implications*, Cham, Springer International Publishing, p. 257–274, doi:[10.1007/978-3-319-24930-8_9](https://doi.org/10.1007/978-3-319-24930-8_9).
- Brown, G., Scherber, C., Ramos, P., and Ebrahim, E.K., 2012, The effects of harvester ant (*Messor ebeninus* Forel) nests on vegetation and soil properties in a desert dwarf shrub community in north-eastern Arabia: *Flora - Morphology, Distribution, Functional Ecology of Plants*, v. 207, p. 503–511, doi:[10.1016/J.FLORA.2012.06.009](https://doi.org/10.1016/J.FLORA.2012.06.009).
- Bucy, A.M., and Breed, M.D., 2006, Thermoregulatory trade-offs result from vegetation removal by a harvester ant: *Ecological Entomology*, v. 31, p. 423–429, doi:[10.1111/J.1365-2311.2006.00803.X](https://doi.org/10.1111/J.1365-2311.2006.00803.X).
- Carlson, S.R., and Whitford, W.G., 1991, Ant Mound Influence on Vegetation and Soils in a Semiarid Mountain Ecosystem: *American Midland Naturalist*, v. 126, p. 125–139, doi:[10.2307/2426157](https://doi.org/10.2307/2426157).
- Clark, W.H., and Comanor, P.L., 1975, Removal of Annual Plants from the Desert Ecosystem by Western Harvester Ants, *Pogonomyrmex occidentalis*: *Environmental Entomology*, v. 4, p. 52–56, doi:[10.1093/ee/4.1.52](https://doi.org/10.1093/ee/4.1.52).
- Cole, B.J., 1994, Nest architecture in the western harvester ant, *Pogonomyrmex occidentalis* (Cresson): *Insectes Sociaux*, v. 41, p. 401–410, doi:[10.1007/BF01240643](https://doi.org/10.1007/BF01240643).

- Cole, A.C., Jr., 1932, The Relation of the Ant, *Pogonomyrmex Occidentalis* Cr., to its Habitat: The Ohio Journal of Science, v. 32, <https://kb.osu.edu/handle/1811/2557> (accessed November 2021).
- Cole, B.J., and Wiernasz, D.C., 2000, Colony size and reproduction in the western harvester ant, *Pogonomyrmex occidentalis*: *Insectes Sociaux*, v. 47, p. 249–255, doi:10.1007/PL00001711.
- Comstock, J.P., and Ehleringer, J.R., 1992, Plant adaptation in the Great Basin and Colorado Plateau: The Great Basin Naturalist, v. 52, p. 195–215, <http://www.jstor.org/stable/41712719>.
- Deblauwe, V., Barbier, N., Couteron, P., Lejeune, O., and Bogaert, J., 2008, The global biogeography of semi-arid periodic vegetation patterns: *Global Ecology and Biogeography*, v. 17, p. 715–723, doi:<https://doi.org/10.1111/j.1466-8238.2008.00413.x>.
- Dibner, R., Doak, D., and Lombardi, E., 2015, An ecological engineer maintains consistent spatial patterning, with implications for community-wide effects: *Ecosphere*, v. 6, p. art151, doi:10.1890/ES14-00415.1.
- Dixon, P., 2001, Ripley's K function: *Encyclopedia of Environmetrics*, doi: <https://doi.org/10.1002/9780470057339.var046.pub2>.
- D'Odorico, P., Bhattachan, A., Davis, K.F., Ravi, S., and Runyan, C.W., 2013, Global desertification: Drivers and feedbacks: *Advances in Water Resources*, v. 51, p. 326–344, doi:<https://doi.org/10.1016/j.advwatres.2012.01.013>.
- Drivas, E.P., and Everett, R.L., 1988, Water relations characteristics of competing singleleaf pinyon seedlings and sagebrush nurse plants: *Forest Ecology and Management*, v. 23, p. 27–37, doi:[https://doi.org/10.1016/0378-1127\(88\)90011-4](https://doi.org/10.1016/0378-1127(88)90011-4).
- Durner, W., 1994, Hydraulic conductivity estimation for soils with heterogeneous pore structure: *Water resources research*, v. 30, p. 211–223.
- Feddes, R.A., 1982, Simulation of field water use and crop yield, *in* Simulation of plant growth and crop production, Pudoc, p. 194–209.
- Fernandez-Illescas, C.P., Porporato, A., Laio, F., and Rodriguez-Iturbe, I., 2001, The ecohydrological role of soil texture in a water-limited ecosystem: *Water Resources Research*, v. 37, p. 2863–2872, doi:<https://doi.org/10.1029/2000WR000121>.
- Van Genuchten, M.T., 1980, A closed-form equation for predicting the hydraulic conductivity of unsaturated soils: *Soil science society of America journal*, v. 44, p. 892–898.
- Ginzburg, O., Whitford, W.G., and Steinberger, Y., 2008, Effects of harvester ant (*Messor* spp.) activity on soil properties and microbial communities in a Negev Desert ecosystem: *Biology and Fertility of Soils*, v. 45, p. 165–173, doi:10.1007/s00374-008-0309-z.
- Grohmann, C., Oldeland, J., Stoyan, D., and Linsenmair, K.E., 2010, Multi-scale pattern analysis of a mound-building termite species: *Insectes Sociaux*, v. 57, p. 477–486, doi:10.1007/s00040-010-0107-0.
- Hardenberg, J., Meron, E., Shachak, M., and Zarmi, Y., 2001, Diversity of Vegetation Patterns and Desertification: *Physical review letters*, v. 87, p. 198101, doi:10.1103/PhysRevLett.87.198101.

- Johnson, R.A., 2021, Desiccation limits recruitment in the pleometrotic desert seed-harvester ant *Veromessor pergandei*: *Ecology and Evolution*, v. 11, p. 294–308, doi:<https://doi.org/10.1002/ece3.7039>.
- Johnson, R.A., 2000, Habitat segregation based on soil texture and body size in the seed-harvester ants *Pogonomyrmex rugosus* and *P. barbatus*: *Ecological Entomology*, v. 25, p. 403–412, doi:<https://doi.org/10.1046/j.1365-2311.2000.00286.x>.
- Johnson, G.D., and Boyce, M.S., 1990, Feeding Trials with Insects in the Diet of Sage Grouse Chicks: *The Journal of Wildlife Management*, v. 54, p. 89–91, doi:10.2307/3808906.
- Kartesz, J.T., 2015, The biota of North America program (BONAP), North American Plant Atlas, 412, 413, <https://bonap.net/Napa/TaxonMaps/Genus/County/Artemisia>.
- Klausmeier, C.A., 1999, Regular and Irregular Patterns in Semiarid Vegetation: *Science*, v. 284, p. 1826–1828, doi:10.1126/science.284.5421.1826.
- Kolb, K., and Sperry, J., 1999, Transport constraints on water use by the Great Basin shrub, *Artemisia tridentata*: *Plant, Cell & Environment*, v. 22, p. 925–935, doi:<https://doi.org/10.1046/j.1365-3040.1999.00458.x>.
- Van De Koppel, J., and Rietkerk, M., 2004, Spatial Interactions and Resilience in Arid Ecosystems: *American Naturalist*, v. 163, p. 113–121, doi:10.1086/380571/ASSET/IMAGES/LARGE/FG4.JPEG.
- Köppen, W., 1936, *Handbuch der Klimatologie in fünf Bänden Das geographische System der Klimate*, www.borntraeger-cramer.com.
- Laundre, J., 1990, Soil Moisture Patterns below Mounds of Harvester Ants: *Journal of Range Management*, v. 43, p. 10–12, doi:10.2307/3899111.
- Lavigne, R.J., 1969, Bionomics and Nest Structure of *Pogonomyrmex occidentalis* (Hymenoptera: Formicidae): *Annals of the Entomological Society of America*, v. 62, p. 1166–1175, doi:10.1093/aesa/62.5.1166.
- Levillain, J., Thongo M’Bou, A., Deleporte, P., Saint-André, L., and Jourdan, C., 2011, Is the simple auger coring method reliable for below-ground standing biomass estimation in Eucalyptus forest plantations? *Annals of Botany*, v. 108, p. 221–230, doi:10.1093/aob/mcr102.
- Levings, S.C., and Traniello, J.F.A., 1981, Territoriality, nest dispersion, and community structure in ants: *Psyche: A Journal of Entomology*, v. 88, p. 265–319.
- Munger, J.C., 1986, Rate of Death Due to Predation for Two Species of Horned Lizard, *Phrynosoma cornutum* and *P. modestum*: *Copeia*, v. 1986, p. 820–824, doi:10.2307/1444970.
- Nagel, H.G., and Rettenmeyer, C.W., 1973, Nuptial Flights, Reproductive Behavior and Colony Founding of the Western Harvester Ant, *Pogonomyrmex occidentalis* (Hymenoptera: Formicidae): *Journal of the Kansas Entomological Society*, v. 46, p. 82–101, <http://www.jstor.org/stable/25082548>.
- Nicolai, N., Smeins, F.E., and Cook, J.L., 2008, Harvester Ant Nests Improve Recovery Performance of Drought Impacted Vegetation in Grazing Regimes of Semiarid Savanna, Texas: *The American Midland Naturalist*, v. 160, p. 29–40, <http://www.jstor.org/stable/20491363>.

- Peel, M.C., Finlayson, B.L., and McMahon, T.A., 2007, Updated world map of the Köppen-Geiger climate classification: *Hydrology and Earth System Sciences*, v. 11, p. 1633–1644, doi:10.5194/HESS-11-1633-2007.
- Pereira, L.S., Paredes, P., Espírito-Santo, D., and Salman, M., 2023, Actual and standard crop coefficients for semi-natural and planted grasslands and grasses: a review aimed at supporting water management to improve production and ecosystem services: *Irrigation Science*, doi:10.1007/s00271-023-00867-6.
- Petersky, R., and Harpold, A., 2018, Now you see it, now you don't: a case study of ephemeral snowpacks and soil moisture response in the Great Basin, USA: *Hydrol. Earth Syst. Sci.*, v. 22, p. 4891–4906, doi:10.5194/hess-22-4891-2018.
- Picker, M.D., Ross-Gillespie, V., Vlieghe, K., and Moll, E., 2012, Ants and the enigmatic Namibian fairy circles - cause and effect? *Ecological Entomology*, v. 37, p. 33–42, doi:10.1111/j.1365-2311.2011.01332.x.
- Porter, S.D., and Jorgensen, C.D., 1988, Longevity of Harvester Ant Colonies in Southern Idaho: *Journal of Range Management*, v. 41, p. 104–107, doi:10.2307/3898942.
- R Core Team, 2022, R: A Language and Environment for Statistical Computing: <https://www.R-project.org/> (accessed January 2024).
- Rehfeldt, G.E., Crookston, N.L., Sáenz-Romero, C., and Campbell, E.M., 2012, North American vegetation model for land-use planning in a changing climate: a solution to large classification problems: *Ecological Applications*, v. 22, p. 119–141, doi:10.1890/11-0495.1.
- Reynolds, J.F. et al., 2007, Global Desertification: Building a Science for Dryland Development: *Science*, v. 316, p. 847–851, doi:10.1126/science.1131634.
- Rietkerk, M., Boerlijst, M.C., Van Langevelde, F., Hillerislambers, R., Van De Koppel, J., Kumar, L., Prins, H.H.T., and De Roos, A.M., 2002, Self-Organization of Vegetation in Arid Ecosystems: *Couleron and Lejeune*, v. 160, p. 524–530.
- Rietkerk, M., Dekker, S.C., de Ruiter, P.C., and van de Koppel, J., 2004, Self-Organized Patchiness and Catastrophic Shifts in Ecosystems: *Science*, v. 305, p. 1926–1929, doi:10.1126/science.1101867.
- Rissing, S.W., 1988, Seed-Harvester Ant Association with Shrubs: Competition for Water in the Mohave Desert?: *Ecology*, v. 69, p. 809–813, doi:10.2307/1941030.
- Rogers, L.E., and Lavigne, R.J., 1974, Environmental Effects of Western Harvester Ants on the Shortgrass Plains Ecosystem: *Environmental Entomology*, v. 3, p. 994–997, doi:10.1093/ee/3.6.994.
- Ryti, R.T., and Case, T.J., 1992, The Role of Neighborhood Competition in the Spacing and Diversity of Ant Communities: *The American Naturalist*, v. 139, p. 355–374, <http://www.jstor.org/stable/2462416>.
- Satoh, A., 2003, Chapter 10 - Typical Properties of Colloidal Dispersions Calculable by Molecular-Microsimulations, *in* Satoh, A. ed., *Studies in Interface Science*, Elsevier, v. 17, p. 153–159, doi:[https://doi.org/10.1016/S1383-7303\(03\)80038-8](https://doi.org/10.1016/S1383-7303(03)80038-8).

- Schaap, M.G., Leij, F.J., and van Genuchten, M.Th., 1998, Neural Network Analysis for Hierarchical Prediction of Soil Hydraulic Properties: *Soil Science Society of America Journal*, v. 62, p. 847–855, doi:<https://doi.org/10.2136/sssaj1998.03615995006200040001x>.
- Schaap, M.G., Leij, F.J., and van Genuchten, M.Th., 2001, rosetta: a computer program for estimating soil hydraulic parameters with hierarchical pedotransfer functions: *Journal of Hydrology*, v. 251, p. 163–176, doi:[https://doi.org/10.1016/S0022-1694\(01\)00466-8](https://doi.org/10.1016/S0022-1694(01)00466-8).
- Scheffer, M., Bascompte, J., Brock, W.A., Brovkin, V., Carpenter, S.R., Dakos, V., Held, H., van Nes, E.H., Rietkerk, M., and Sugihara, G., 2009, Early-warning signals for critical transitions: *Nature*, v. 461, p. 53–59, doi:[10.1038/nature08227](https://doi.org/10.1038/nature08227).
- Scheffer, M., Carpenter, S., Foley, J.A., Folke, C., and Walker, B., 2001, Catastrophic shifts in ecosystems: *Nature*, v. 413, p. 591–596, doi:[10.1038/35098000](https://doi.org/10.1038/35098000).
- Schroeder, V., and Johnson, D., 2018, *Western Roots: Diving into a sagebrush sea of diversity.*
- Sharp, L.A., and Barr, W.F., 1960, Preliminary Investigations of Harvester Ants on Southern Idaho Rangelands: *Rangeland Ecology & Management*, p. 131–134.
- Sherbrooke, W., 2003, *Introduction to Horned Lizards of North America*: Berkeley, University of California Press.
- Sherratt, J.A., and Lord, G.J., 2007, Nonlinear dynamics and pattern bifurcations in a model for vegetation stripes in semi-arid environments: *Theoretical Population Biology*, v. 71, p. 1–11, doi:[10.1016/J.TPB.2006.07.009](https://doi.org/10.1016/J.TPB.2006.07.009).
- Šimůnek, J., van Genuchten, M.Th., and Šejna, M., 2016, Recent Developments and Applications of the HYDRUS Computer Software Packages: *Vadose Zone Journal*, v. 15, p. v. 15, p. vzj2016.04.0033, doi:<https://doi.org/10.2136/vzj2016.04.0033>.
- Šimůnek, J., and Hopmans, J.W., 2009, Modeling compensated root water and nutrient uptake: *Ecological Modelling*, v. 220, p. 505–521, doi:<https://doi.org/10.1016/j.ecolmodel.2008.11.004>.
- Simunek Jirka, J., Šejna, M., Saito, H., Sakai, M., and Van Genuchten, M., 2013, *The Hydrus-1D Software Package for Simulating the Movement of Water, Heat, and Multiple Solutes in Variably Saturated Media, Version 4.17*, HYDRUS Software Series 3, Department of Environmental Sciences, University of California Riverside, Riverside, California: USA,.
- Soil Survey Staff, 2024, *Web Soil Survey*: Natural Resources Conservation Service, United States Department of Agriculture. Available online at <https://websoilsurvey.nrcs.usda.gov/> (accessed 05/13/2024)
- Soulé, P.T., and Knapp, P.A., 1996, *Pogonomyx owyheeii* nest site density and size on a minimally impacted site in central Oregon: *The Great Basin Naturalist*, v. 56, p. 162–166, <http://www.jstor.org/stable/41716185>.
- Soule, P.T., and Knapp, P.A., 1996, The Influence of Vegetation Removal by Western Harvester Ants (*Pogonomyrmex owyheeii*) in a Relict Area of Sagebrush-steppe in Central Oregon: *The American Midland Naturalist*, v. 136, p. 336–345, doi:[10.2307/2426737](https://doi.org/10.2307/2426737).

- Suarez, A. v, Richmond, J.Q., and Case, T.J., 2000, Prey selection in horned lizards following the invasion of Argentine ants in Southern California: *Ecological Applications*, v. 10, p. 711–725, doi:[https://doi.org/10.1890/1051-0761\(2000\)010\[0711:PSIHLF\]2.0.CO;2](https://doi.org/10.1890/1051-0761(2000)010[0711:PSIHLF]2.0.CO;2).
- Tarnita, C.E., Bonachela, J.A., Sheffer, E., Guyton, J.A., Coverdale, T.C., Long, R.A., and Pringle, R.M., 2017, A theoretical foundation for multi-scale regular vegetation patterns: *Nature*, v. 541, p. 398–401, doi:[10.1038/nature20801](https://doi.org/10.1038/nature20801).
- Thomas, C.D., 2010, Climate, climate change and range boundaries: *Diversity and Distributions*, v. 16, p. 488–495, doi:<https://doi.org/10.1111/j.1472-4642.2010.00642.x>.
- Vereecken, H., Kasteel, R., Vanderborght, J., and Harter, T., 2007, Upscaling Hydraulic Properties and Soil Water Flow Processes in Heterogeneous Soils: A Review: *Vadose Zone Journal*, v. 6, p. 1–28, doi:<https://doi.org/10.2136/vzj2006.0055>.
- Viles, H.A., Goudie, A.S., and Goudie, A.M., 2021, Ants as geomorphological agents: A global assessment: *Earth-Science Reviews*, v. 213, p. 103469, doi:<https://doi.org/10.1016/j.earscirev.2020.103469>.
- Vogel, H.-J., 2019, Scale Issues in Soil Hydrology: *Vadose Zone Journal*, v. 18, p. 190001, doi:<https://doi.org/10.2136/vzj2019.01.0001>.
- Wagner, D., Jones, J.B., and Gordon, D.M., 2004, Development of harvester ant colonies alters soil chemistry: *Soil Biology and Biochemistry*, v. 36, p. 797–804, doi:[10.1016/J.SOILBIO.2004.01.009](https://doi.org/10.1016/J.SOILBIO.2004.01.009).
- Western Regional Climate Center, 2023, Station Summary for Pioche, Nevada:, https://cemp.dri.edu/cgi-bin/cemp_stations.pl?stn=pioc (accessed October 2023).
- Wheeler, W.M., 1960, *Ants: Their Structure, Development and Behavior*: Columbia University Press, Columbia University biological series, <https://books.google.com/books?id=KjHRuG5nfs4C>.
- Wheeler, G.C., and Wheeler, J., 1976, Ant larvae: review and synthesis: *Memoirs of the Entomological Society of Washington*, Volume: 7, Pages: 1-108.
- Wheeler, G., and Wheeler, J., 1986, *Ants of Nevada*: Natural History Museum of Los Angeles County.
- Wight, J.R., and Nichols, J.T., 1966, Effects of Harvester Ants on Production of a Saltbush Community: *Journal of Range Management*, v. 19, p. 68–71.
- Willard, J.R., and Crowell, H.H., 1965, Biological Activities of the Harvester Ant, *Pogonomyrmex owyheeii*, in Central Oregon: *Journal of Economic Entomology*, v. 58, p. 484–489, doi:[10.1093/JEE/58.3.484](https://doi.org/10.1093/JEE/58.3.484).
- Wu, R.-L., 1990, Disk clearing behavior of the red harvester ant, *Pogonomyrmex barbatus* Smith.: *Bulletin of the Institute of Zoology, Academia Sinica*, v. 29, p. 153–164.
- Zomer, R.J., Xu, J., and Trabucco, A., 2022, Version 3 of the Global Aridity Index and Potential Evapotranspiration Database: *Scientific Data*, v. 9, p. 409, doi:[10.1038/s41597-022-01493-1](https://doi.org/10.1038/s41597-022-01493-1).
- Zotarelli, L., Dukes, M., Romero, C., Migliaccio, K., and Morgan, K., 2015, Step by Step Calculation of the Penman-Monteith Evapotranspiration (FAO-56 Method) 1: *Agricultural and Food Sciences*,.

4.8 Supplementary materials

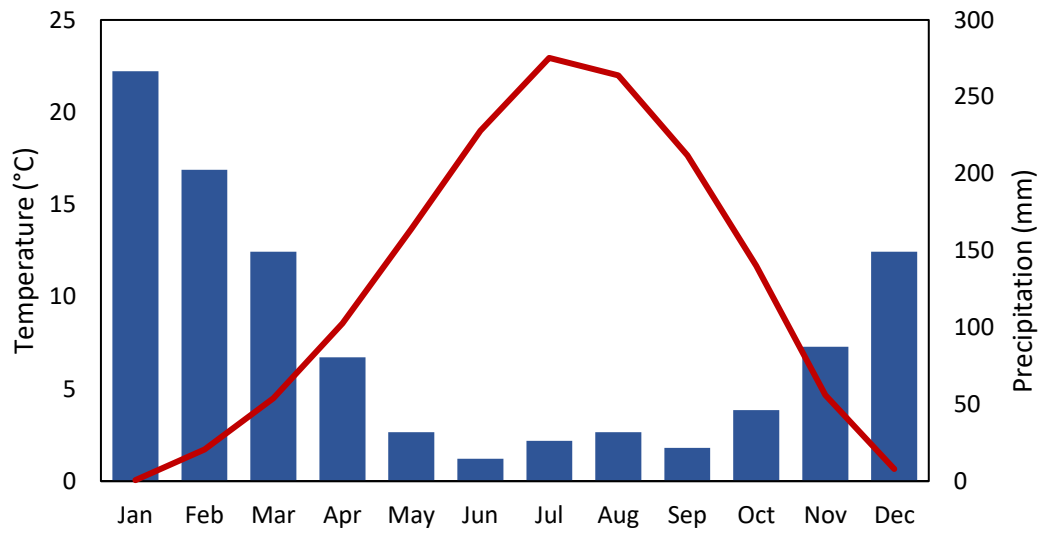


Figure S4.1. Average monthly temperature and precipitation at Pioche, NV (Western Regional Climate Center, 2023c).

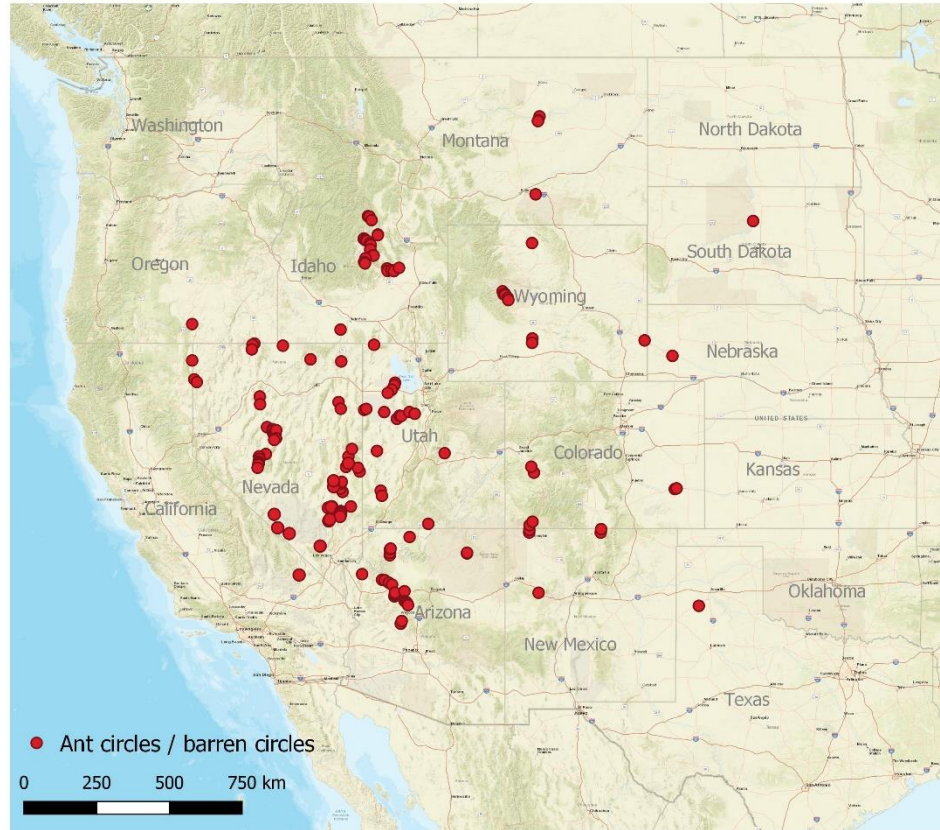


Figure S4.2. Range of ant circle and barren areas of similar dimensions and shape as ant circles in the southwestern and western United States.

Table S4.1. Average grain size distribution for an ant circle and natural vegetation gap in annual and shrub dominated vegetation at the research site.

Vegetation type	Location	Sand (%)	Silt (%)	Clay (%)	Soil Texture
Shrub	Ant circle	55.79	36.69	7.51	Sandy Loam
Shrub	Vegetation gap	64.62	31.39	3.99	Sandy Loam
Annual	Ant circle	47.22	46.06	6.70	Sandy Loam
Annual	Vegetation gap	55.88	39.56	4.58	Sandy Loam

Table S4.2. Gravimetric soil moisture during the growing season inside ant circles and natural vegetation gaps on shrub and annual dominated vegetation.

Date	Vegetation type	Soil moisture ant circle (%)	Soil moisture natural vegetation gap (%)
May 16, 2019	Shrub	10.9	8.4
May 16, 2019	Annual	13.5	9.0
Aug 18, 2019	Shrub	8.6	5.0
Aug 18, 2019	Shrub	8.1	3.0
Aug 18, 2019	Shrub	7.7	3.9
Aug 18, 2019	Annual	6.7	3.3
Aug 18, 2019	Annual	7.9	3.9
Aug 18, 2019	Annual	6.0	6.5
Oct 3, 2019	Shrub	6.6	4.0
Oct 3, 2019	Shrub	8.6	5.2
Oct 3, 2019	Shrub	7.1	4.2
Oct 3, 2019	Annual	5.5	4.6
Oct 3, 2019	Annual	8.7	3.4
Oct 3, 2019	Annual	8.4	4.3

HYDRUS set-up

Soil moisture conditions inside and outside an ant circle were simulated using the water flow and root water uptake modules on a general three-dimensional domain to represent a triangular soil section of 4 x 1 x 1 m in *xyz*-dimensions. The soil domain was discretized into elements of 5 cm, leading to a total of 40,434 elements and 10,440 nodes, with the upper surface defined as meteorological boundary and the lower surface defined as free drainage boundary (Fig. S4.3). A free drainage boundary was selected as lower boundary as the groundwater level is located far below the domain bottom. For the upper boundary, a value of -100,000 cm was used as *hCritA*, which defines the minimum pressure head allowed at the soil surface, consistent with (Turkeltaub and Bel, 2022).

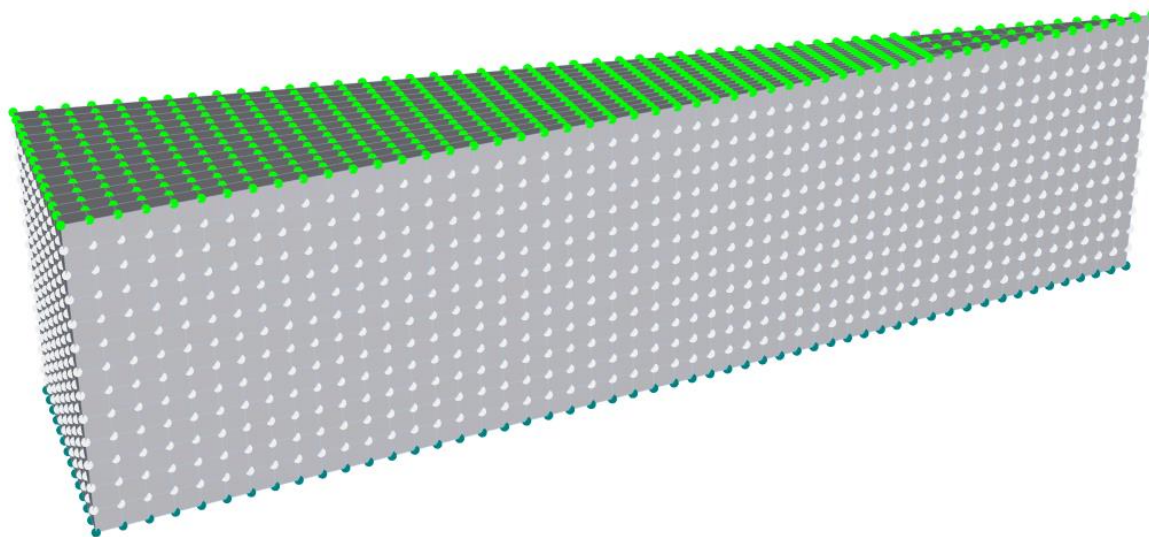


Figure S4.3. Model domain of a three-dimensional soil slice of 400*100*100 cm in xyz -dimensions with atmospheric boundary as upper boundary and free drainage as lower drainage.

The simulation was run with daily boundary conditions from 03/01/2019 – 09/30/2019, a total of 214 days and time variable boundary conditions. The initial model condition was measured in water content of 14%, representing elevated soil moisture levels following snowmelt in early spring. The single-porosity model of van Genuchten-Mualem (Van Genuchten, 1980) without hysteresis was used as hydraulic model as the drying and wetting curves in the retention function were unknown. Soil hydraulic parameters were either predicted using the pedo-transfer functions of the Rosetta model (Q_r and Q_s), through literature search for similar soil textures with presence of soil crusts (K_s ; Li et al., 2005), or optimized through inverse modeling in HYDRUS 1D (α and n). HYDRUS 1D was also used to calculate potential evaporation using the build-in Penman-Monteith equation. Settings for the one-dimensional model were similar to the 3D model, except for the vertical one-dimensional domain and simulation of only water flow. Additional meteorological parameters used as input into the model were a latitude of 38.2107, altitude (m) of 1637, measurement height of wind speed and temperature of 2 m and albedo of

0.36. All other parameters were kept at default values. The precipitation event of day 84 (May 23, 2019) was reduced from 32.3 mm to 5.6 mm to match the observed peak in soil moisture in the TDR data. Time-variable meteorological data for the 1D and 3D models were obtained from a nearby weather station (Fig. S4.4).

Table S4.3. Summary of meteorological data and vegetation and site-specific parameters, listed in units as required by HYDRUS software.

Parameter	Unit	Range (min-max)	Mean \pm SD	Source
Albedo inside circle	-		0.35	Tetzlaff, 1983
Albedo outside circle	-		0.14	(Dirnhirn and Belt, 1971; Hanson and Clayton Hanson, 2001)
Latitude	degree, N		38.2107	
Altitude	m		1637	
P50*	cm		-26500	Kolb & Sperry, 1999
Crop height	cm		100	
LAI	-		0.34	Olsoy et al., 2016
Max. rooting depth	cm		200	(Richards and Caldwell, 1987; Reynolds and Fraley, 1989)
Interception	mm		1.5	(West and Gifford, 1976)
hCritA**	cm		-100000	(Turkeltaub and Bel, 2022)

* Pressure head at which root water uptake is reduced by 50%

** Minimum pressure head allowed at the soil surface

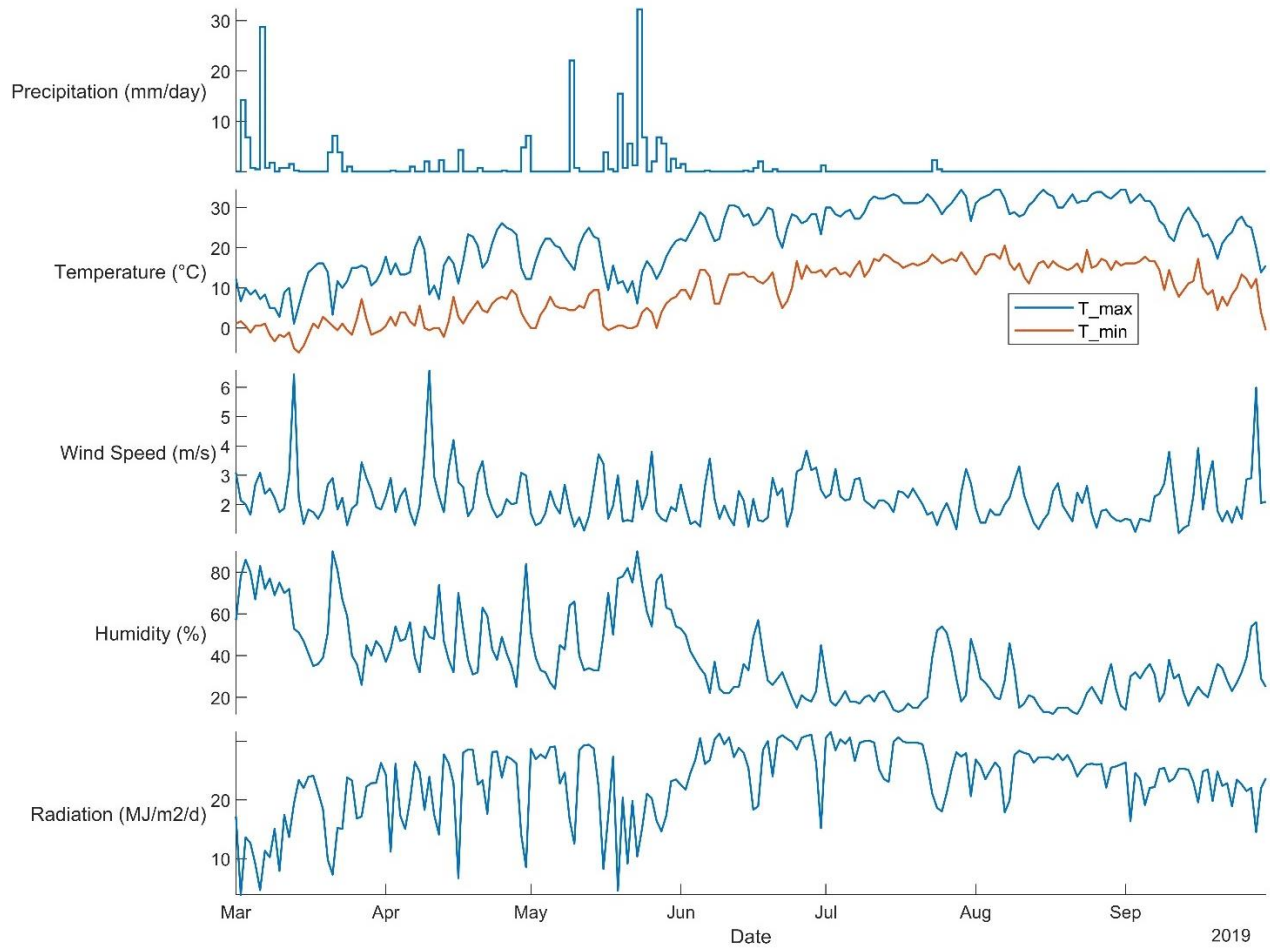


Figure S4.4. Meteorological input data used for the HYDRUS model including precipitation, minimum and maximum temperature, wind speed, humidity, and radiation from March 1, 2019, to September 30, 2019, obtained from a weather station in Pioche, Nevada (Western Regional Climate Center, 2023c).

Soil moisture timeseries were obtained from observation nodes at locations corresponding to the TDR sensors. The observation node inside the ant circle was placed at 0.5 m depth halfway between the ant nest and the circle margin. The second observation node was placed at 0.5 m depth and 0.15 m from the simulated plant. Ant circle and natural vegetation gap size were determined using the average gap sizes at the research site using Google Earth Pro.

Root water uptake was simulated through the Feddes water uptake reduction model with a critical stress index of 0.8 to account for compensatory root water uptake. Root growth was not simulated. Feddes' parameters were obtained through the values listed in the database in HYDRUS for more drought tolerant crop species, combined with literature values for sagebrush (Table S4.2). Root distribution parameters were fitted to field observations (Table S4.2) to yield the root system of two plants (Fig. S4.5). Horizontal root distribution in the Y-dimension was not specified. HYDRUS normalizes root water uptake values prior to running its simulation and uses these values in combination with hydraulic head and potential transpiration to calculate actual transpiration rates.

Table S4.4. Parameters for the Feddes water uptake reduction model and root distribution.

Parameter	Value	Notes
P0 (cm)	-15	
Popt (cm)	-25	
P2H (cm)	-1000	
P2L (cm)	-1000	
P3 (cm)	-26,500	(Kolb and Sperry, 1999)
R2H (cm day ⁻¹)	0.5	(Šimůnek et al., 2016)
R2L (cm day ⁻¹)	0.1	(Šimůnek et al., 2016)
Maximum Rooting depth (cm)	400	Vertical Distribution
Depth of maximum intensity (cm)	10	Vertical Distribution
Parameter Pz	20	Vertical Distribution
Maximum Rooting Radius	200	Horizontal distribution
Radius of Maximum intensity	150	Horizontal distribution
Parameter Px	0	Horizontal distribution
Center coordinate	75	Horizontal distribution

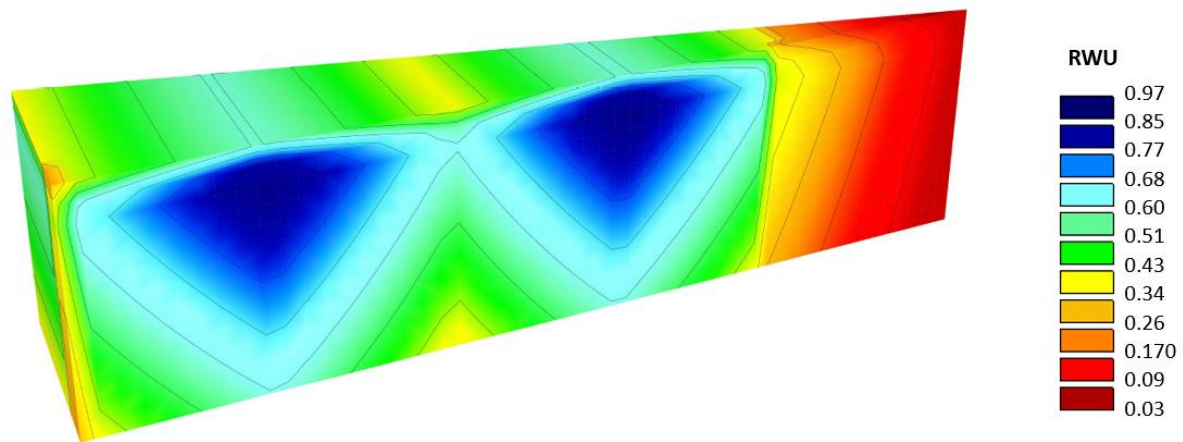


Figure S4.5. Distribution of root water uptake (RWU) in the model domain, fit to match the root distribution of two plants.



Figure S4.6. Satellite view of ant circles in western Utah. Individual vegetation clearings are clearly visible, as well as ant mounds in the center of each clearing. Location = 40.002458, -112.836855.

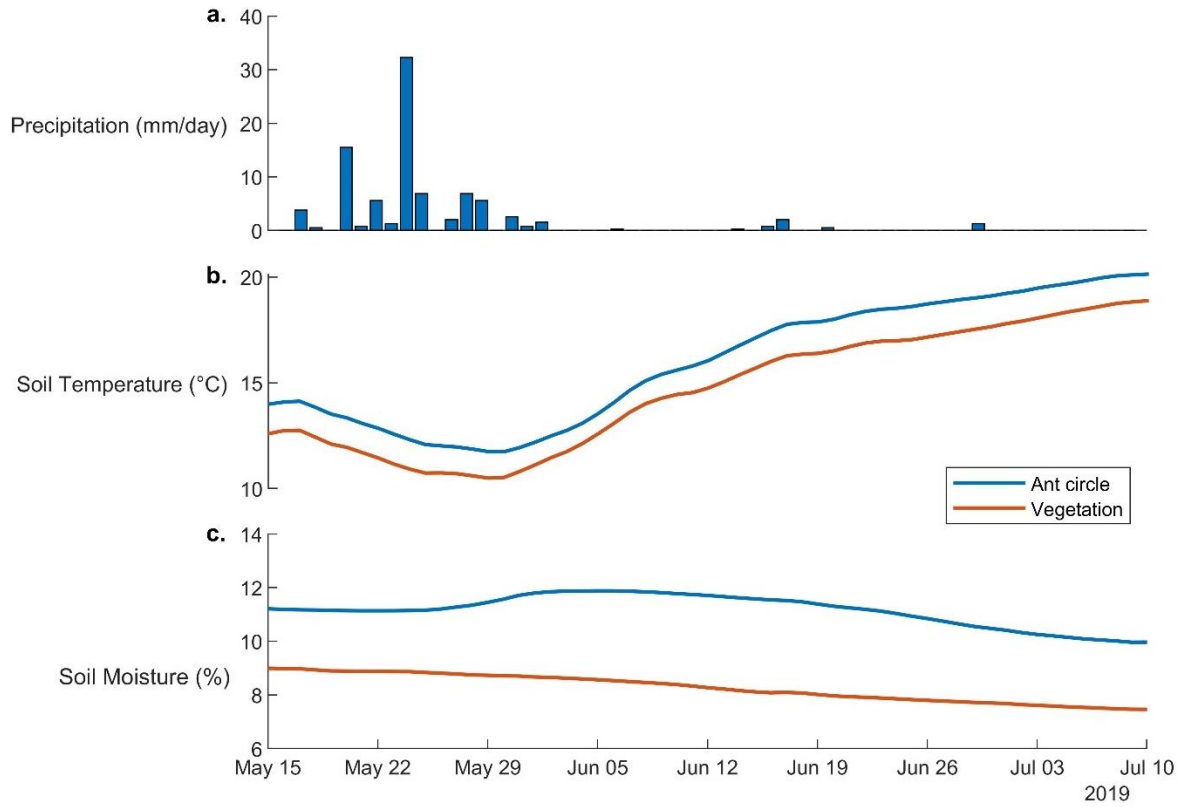


Figure S4.7. Precipitation and TDR readings from 5/15/2019 to 7/10/2019. **a.** Daily precipitation from a weather station in Pioche, NV (Western Regional Climate Center, 2023c). **b.** Soil temperature at 1m depth inside the ant circle and under vegetation on the circle margin, **c.** Volumetric soil moisture at 1m depth inside the ant circle and under vegetation on the circle margin.

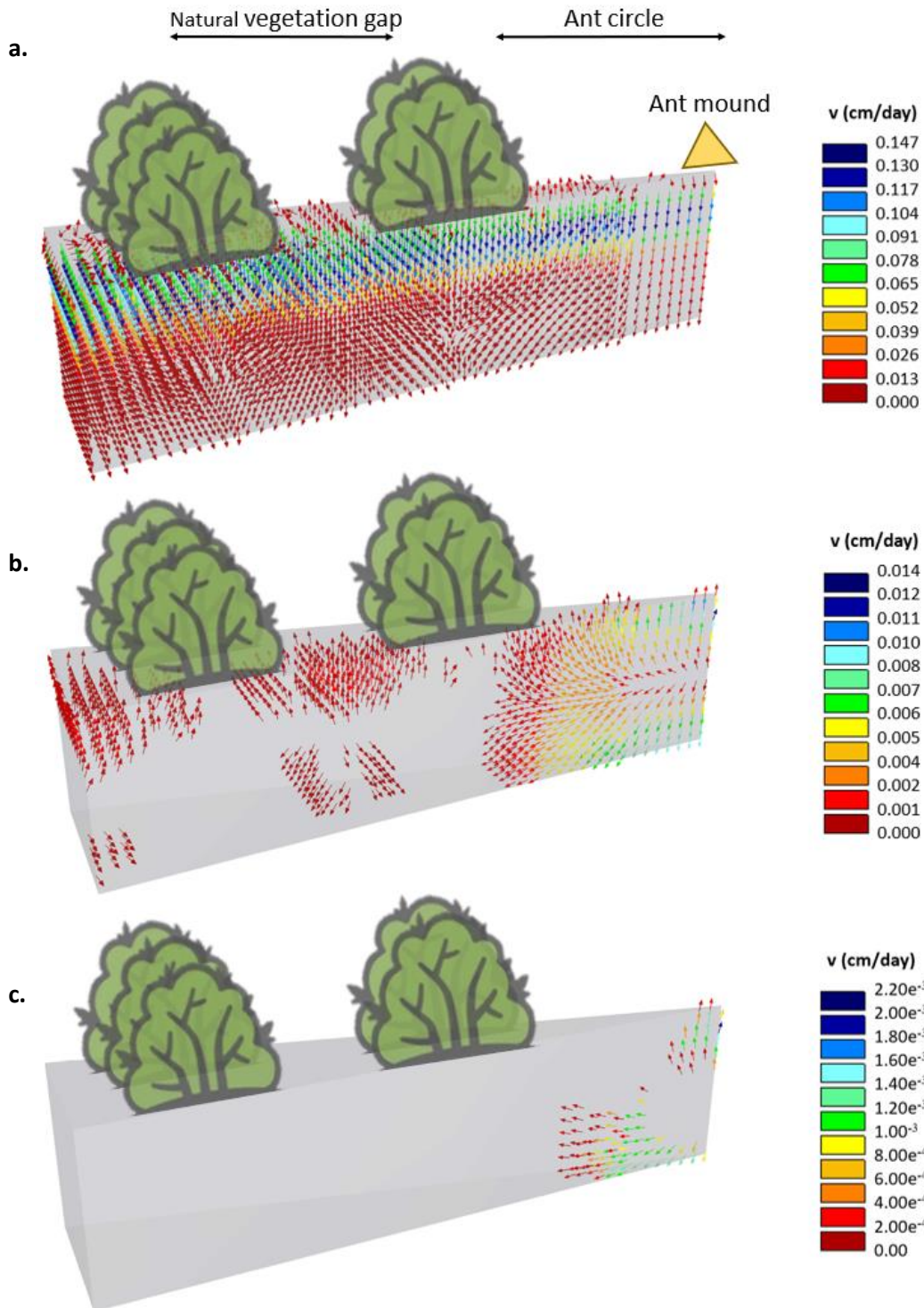


Figure S4.8. Velocity vectors (water flow velocity) in the ant circle and natural vegetation gap for **a.** Day 83 (5/22/2019), **b.** Day 132 (7/10/2019), and **c.** day 214 (9/30/2019), showing largely reduced velocity vectors through the progression of summer and the growing season. Locations of vegetation and ant mound added for reference.

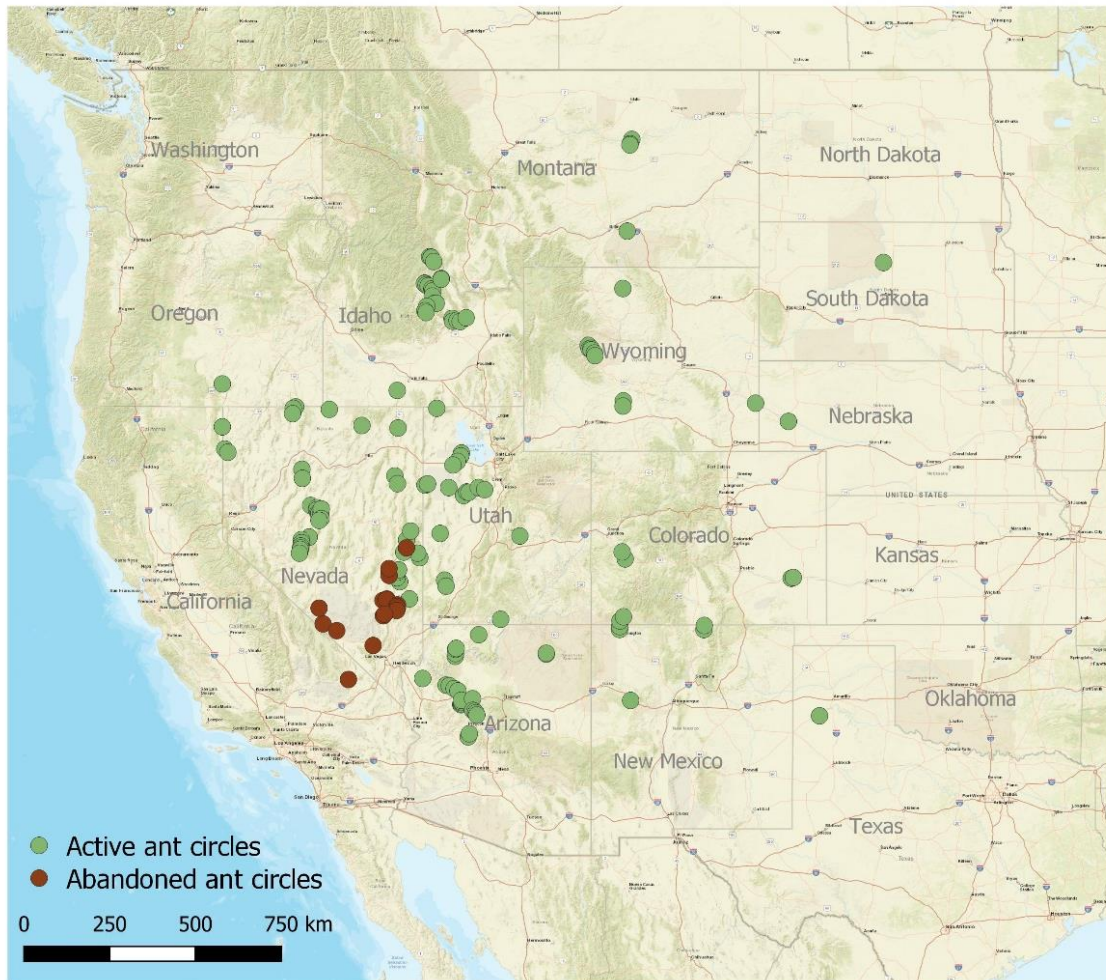


Figure S4.9. Distribution of ant circles through the western United States, showing the range in circle distribution from Arizona and New Mexico to Montana.

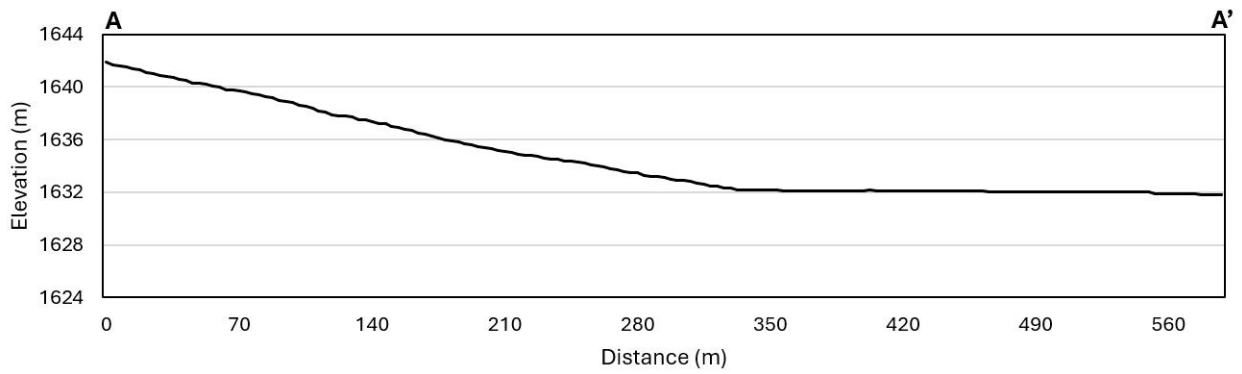
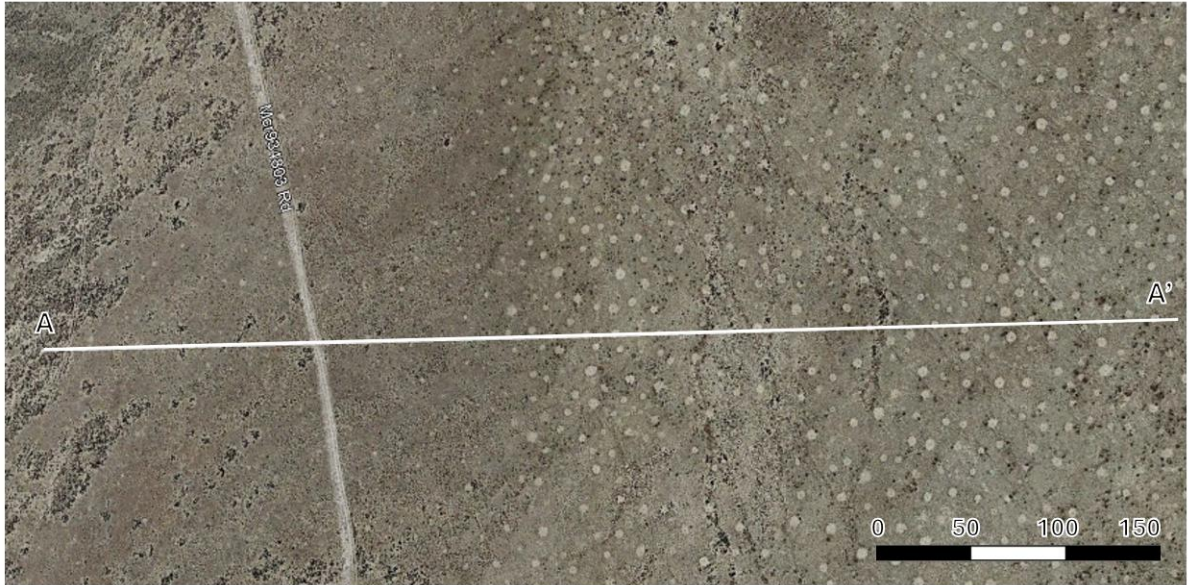


Figure S4.10 a. Example of distribution of ant circles linked to drainage features in the landscape, where a continuously vegetated area (left) is intersected by a drainage feature (right). Ant circle occurrence is closely related to the drainage feature, and **b.** generally occupies the lower parts of the landscape.

CHAPTER 5 - CONCLUSION

The desert is a complex system containing a variety of ecosystems. Ecosystems are similar regarding potential evapotranspiration rates far exceeding precipitation. However, responses to climate change might differ. In my dissertation, I studied the effects of climate change on three different ecosystems in the (semi)-arid southwestern United States that are considered amongst the most vulnerable ecosystems to climate change: lacustrine, riparian, and dryland ecosystems. This approach allowed for comparison of the sensitivity to climate change in (semi)-arid ecosystems.

Ecosystems contain tipping points at which environmental stress passes a threshold, and the system rapidly shifts to an alternative stable state. The responses of three (semi)-arid ecosystems to climate change differed. Lacustrine ecosystems of large volume and inflow of high-quality water, such as Lake Mead, showed minimum responses to climate change. Water quality parameters such as temperature and nutrients, and phytoplankton community structures did not significantly change since the early 2000s. This chapter highlighted the buffering capacity of large, oligotrophic reservoirs to maintain stable water quality. Changes in phytoplankton structures did occur once this buffering capacity was passed, most noticeable in shallow areas near river inflows where water temperature or nutrients had increased.

Dryland ecosystems containing vegetation patterns created by the harvester ant, *Pogonomyrmex occidentalis*, showed intermediate sensitivity to climate change. In this chapter, I studied soil moisture as driver for pattern creation, which is needed to meet the minimum moisture requirements for ant colony survival. Increased aridity caused by climate change can drop minimum soil moisture levels below the threshold moisture required for harvester ants. I showed evidence of a northward shift in harvester ant distribution, evident from abandoned ant circles in the southern part of their distribution. While loss of ant circles reduced biodiversity and ecosystem resilience to change, ecosystem response differed from responses predicted from mathematical models. After circle abandonment, vegetation gaps slowly got

revegetated, instead of a total ecosystem collapse leading to desertification. Understanding the driver of vegetation pattern formation thus allows for better prediction of ecosystem change and severity of change.

Riparian ecosystems in the southwestern United States were most sensitive to climate change. In this chapter, I introduced a mechanism of how a sequence of extreme hydrological events, intense drought and flooding, caused riparian woodland mortality at sites in Nevada and California. Intensified drought conditions can reduce shallow root activity, affecting the ability of riparian trees to deal with high groundwater levels in wet years. Riparian woodland mortality is expected to occur globally in areas experiencing increases in drought intensity. Loss of riparian tree species can negatively impact riparian ecosystems as riparian woodlands harbor large biodiversity, improve water quality, and aid in erosion and flood control.

The work presented in this dissertation has shown how responses to climate change can be highly ecosystem dependent. Ecosystems in similar climatic zones can respond vastly different to environmental change owing to intrinsic differences in ecosystems, such as the presence of vegetation patterns or reservoir volume.

CURRICULUM VITAE

Charlotte van der Nagel

Charlotte.van.der.nagel@gmail.com

EDUCATION

Ph.D. Geoscience, University of Nevada, Las Vegas, 2024

Dissertation: The effects of climate change on semi-arid ecosystems in the Southwestern United States.

Ph.D. Advisor – Dr. Henry Sun

M.S. Hydrology, VU Amsterdam, Netherlands, 2020

Thesis: Understanding soil moisture mechanisms of ant circles in Nevada, USA, using HYDRUS-1D.

M.S. Advisor – Dr. Jorien Vonk

B.S. Earth Science, VU Amsterdam, Netherlands, 2018

Thesis: Effects of climate change on permafrost degradation in northwestern Canada.

B.S. Advisor – Dr. Jorien Vonk

WORK EXPERIENCE

Graduate Intern Regional Water Quality, Southern Nevada Water Authority, 2022-current

- Project water quality of a complex reservoir using 3D-hydrodynamical modeling (AEM3D).
- Apply statistical analyses including trend detection, hypothesis testing, and clustering on multidecadal phytoplankton and water quality datasets.
- Construct machine learning models with hyperparameter optimization and uncertainty analysis to create water quality forecasting models.
- Prepare manuscripts for publication in peer-reviewed journals.

Graduate Research Assistant, Desert Research Institute, 2021-current

- Conduct multi-disciplinary research involving hydrology, geology, biology, and ecology.
- Collect and analyze soil moisture and root distribution data.
- Simulate soil moisture dynamics using HYDRUS 2D and 3D.
- Use remote sensing to study regional wide vegetation health.
- Communicate results to stakeholders, write proposals, reports, and prepare manuscript for publication in peer-reviewed journals.

Graduate Teaching Assistant, University of Nevada, Las Vegas, 2022

- Teach the lab component of Geology 101, including topics on minerals and rock identification, groundwater, topographic maps, and structural geology.
- Provide guidance for students.

Research Intern, Desert Research Institute, 2020

- Conduct fieldwork to study soil moisture in central Nevada.
- Simulate soil moisture using 1D-HYDRUS software.

PUBLICATIONS

van der Nagel, C., Hannoun, D., Tietjen, T. Stable phytoplankton community compositions in Lake Mead (Nevada-Arizona, USA) during two decades of severe drought, R&R in progress at *Environmental Science and Ecotechnology*.

PRESENTATIONS

van der Nagel, C., Hannoun, D., Tietjen, T. (2024, January). Projecting Recycled Water Concentrations in Lake Mead: Applications to Drinking Water Treatment and Microbial Risk. Oral presentation at the Nevada Water Resources Association Annual Conference, Las Vegas, NV.

Tietjen, T., Hannoun, D., **van der Nagel, C.** (2023, November). Lake Mead Water Quality During a Historic Drought: Data and Modeling Results. Oral presentation for the Associations of Environmental and Engineering Geologists Meeting, Las Vegas, NV.

van der Nagel, C., Hannoun, D., Tietjen, T. (2023, October). Dilution or Accumulation? Effects of drought on a highly-treated wastewater plume. Poster presentation at the North American Lake Management Society Annual Conference, Eerie, PA.

van der Nagel, C., Hannoun, D., Tietjen, T. (2023, October). Stability beside drought: phytoplankton and water quality in Lake Mead, NV. Oral presentation at the North American Lake Management Society Annual Conference, Eerie, PA.

van der Nagel, C., Hannoun, D., Tietjen, T. (2023, October). Effects of drought and reduced flow rates on water quality in Lake Mead: behavior of a highly-treated wastewater plume. Oral presentation at the California Lake Management Society Annual Conference, Lake Arrowhead, CA.

van der Nagel, C., Hannoun, D., Tietjen, T. (2023, April). Phytoplankton dynamics in a large, semi-arid reservoir. Oral presentation at the National Water Quality Monitoring Conference. Virginia Beach, VA.

van der Nagel, C., Hannoun, D., Tietjen, T. (2023, April). Phytoplankton dynamics in Lake Mead. Poster presentation at the UNLV Graduate & Professional Student Association Research Forum, Las Vegas, NV.

AWARDS AND SCHOLARSHIPS

- 2024 UNLV Research forum 2nd place poster presentation
- 2024 Nevada Water Reuse Association 1st place poster presentation
- 2024 Nevada Water Resources Association People's Choice Award
- 2024 Nevada Water Resources Association 1st place poster presentation
- 2024 Nevada Water Resources Association Clare Mahannah Memorial Scholarship
- 2023-2024 Geological Society of Nevada Scholarship
- 2023 Jody Connor Student Award 1st place oral presentation
- 2023 North American Lake Management Society Travel grant
- 2023 California Lake Management Society Scholarship
- 2023 UNLV Summer Session Scholarship

- 2023 UNLV Graduate & Professional Student Association Travel Grants
- 2023 UNLV Research forum 1st place poster presentation
- 2023 Nevada Water Resources Association Graduate Scholarship
- 2022-2023 Bernada French Scholarship

PROFESSIONAL INVOLVEMENT

Board of Trustees, Student Representative Southern Nevada

Nevada Water Resources Association, 2023-current, Las Vegas, NV